Temperature coefficients of multicrystalline compensated silicon solar cells

Charly Berthod

Temperature coefficients of multicrystalline compensated silicon solar cells

Doctoral dissertation for the degree Philosophiae Doctor (PhD) at the
Faculty of Engineering and Science, specialization in Renewable Energy

University of Agder

Faculty of Engineering and Science
2016

Doctoral Dissertation by the University of Agder 148
ISBN: 978-82-7117-842-0
ISSN: 1504-9272

Printed at the Printing Office, University of Agder
Kristiansand

Preface

This dissertation is based on experimental data obtained during the three year-period of the PhD. position. All the chapters are mainly based on previous work which are referenced. They give the state-of-the-art recommended to get a full understanding of the publications presented afterwards. The publications represent the main part of the research work carried out by the PhD. student.

Abstract

This thesis focuses on the bulk properties influencing the temperature coefficients of solar cells. The conversion efficiency of PV devices degrades with increasing temperature. The temperature coefficient of the open-circuit voltage can be improved by increasing the open-circuit voltage. Therefore with the continuous improvement of the conversion efficiencies over the last decades due to the global R&D efforts, the temperature sensitivity was continuously reduced. The major research question of this thesis is: are there other ways to improve the temperature sensitivity?

It had been shown prior to the present work, that solar cells made of silicon processed by upgraded metallurgical routes had beneficial temperature coefficients compared to cells made of polysilicon. This effect was studied in this work, and it is shown that no significant difference is observed between cells with distinct compensation levels. This was made on a relatively small compensation level range.

Another influencing parameter on the temperature coefficients is the height at which the wafer was picked in the ingot to be processed into a solar cell. The best temperature coefficients are most likely to be found at the top of the ingot. Yet the cell structure can change this result because of a larger variations of the cell parameters along the ingot height.

It is known that reducing the bulk resistivity can improve the temperature coefficients. In the present work, the role of reducing bulk resistivity is examined with a focus on the impact on each cell parameter. It is shown that using a cell structure with a lower series resistance for a given bulk resistivity, is beneficial for the temperature coefficient of the fill factor.

Light-induced degradation has a negative effect on the cell parameters, espe-

cially the open-circuit voltage. This degrades the temperature coefficients.

Additionally the dependence of the temperature coefficients with irradiance was investigated. It is shown that the temperature sensitivity is intensified at low irradiance due to the decrease of the open-circuit voltage.

In conclusion, it is shown that temperature sensitivity of solar cells can be controlled by adjusting various bulk parameters. The solidification step has a big impact on the temperature coefficients due to the cell parameters variations and the changes in recombination mechanisms. Moreover light-induced degradation deteriorates the temperature sensitivity.

Acknowledgements

Firstly, I would like to express my sincere gratitude to my advisor Prof. Tor Oskar Sætre for the continuous support of my Ph.D study and related research. I would also like to thank my co-supervisor Dr. Rune Strandberg for his excellent guidance, all the time he spent in valuable discussions, but also for the hard questions and comments that improved the quality of my research.

My sincere thanks also goes to Dr. Jan Ove Odden and Elkem Solar® for allowing me to study their material, and for the great support and advices he gave me. Without his precious support it would not have been possible to conduct this research.

I would like to express my gratitude to Dr. Muhammad Tayyib, who spent time showing me the lab equipment.

I would like to thank all my colleagues and friends at the university who: participated in the coffee breaks, discussed with me, supported me, encouraged me and all the fun we had. In short, they made these past three years a great time. Thank you Nazmin, Pål, Gunstein, Jesper (and for the help on LaTeX), Abhijit, Magnus, Jannik, Martin, Martin, and all those I forgot.

I would like to express my gratitude to my parents, who have always encouraged me in my education.

Last but not the least, a huge thanks to my amazing wife who followed me in this crazy adventure in Norway. She has been really supporting me spiritually throughout writing this thesis and in my life in general. I will never be enough grateful for what she did. And thank you my daughter for teaching me that I do not need full nights of sleep even when writing my thesis!

Charly Berthod
Grimstad, Norway
September 2016

Contents

Table of contents **ix**

List of abbreviations **xi**

List of symbols **xiii**

1 Introduction **1**

1.1 Background 1
1.2 Motivation 2
1.3 Contribution 3
1.4 Outline of dissertation 3
1.5 Publications 4

2 Theory of the temperature coefficients of a silicon solar cell **7**

2.1 Temperature coefficient of the short-circuit current 8
2.2 Temperature coefficient of the open-circuit voltage 9
2.3 Temperature coefficient of the fill factor 11
2.4 Temperature coefficient of the efficiency 12

3 Experimental setups **13**

3.1 Light-soaking bench 13
3.2 Sun simulator 14
3.3 Uncertainties of the temperature coefficient measurements 15
3.4 Studied silicon feedstocks 16

4 Solar grade silicon produced by metallurgical routes 19
4.1 Fundamentals of upgraded metallurgical grade silicon 20
4.2 Electronic properties 22
4.2.1 Compensation level 22
4.2.2 Mobility 23
4.2.3 Lifetime 26
4.2.4 Boron-Oxygen defect 27
4.3 Compensation engineering 29
4.3.1 Control of the majority carrier concentration 29
4.3.2 Addition of gallium 31
4.4 Impact of dopant compensation on the performances of solar cells 32

5 Temperature coefficients of compensated silicon solar cells 35
5.1 Review 35
5.2 Results 37
5.3 Reducing the temperature sensitivity by compensation engineering 39

6 Summary of papers 41

7 Conclusions and Outlook 45
7.1 Conclusions on the temperature coefficients in mc-Si 45
7.2 Future Work / Outlook 46

References 47

Appended papers 55

A Temperature coefficients of compensated silicon solar cells – influence of ingot position and blend-in-ratio 55

B Temperature dependent quantum efficiencies in multicrystalline silicon solar cells 63

C Reduced temperature sensitivity of multicrystalline silicon solar cells with low ingot resistivity 71

D Reduction of temperature coefficients in multicrystalline silicon solar cells after light-induced degradation **77**

E Temperature sensitivity of multicrystalline silicon solar cells **83**

F On the variability of the temperature coefficients of mc-Si solar cells with irradiance **97**

List of abbreviations

Abbreviation	*Full name*
AAA	Class type
Al-BSF	Aluminium-back surface field
AM	Air Mass
ASTM	American society for testing and materials
Cz-Si	Czochralski silicon
EG-Si	Electronic grade silicon
EQE	External quantum efficiency
ERE	External radiative efficiency
ESS®	Elkem Solar Silicon
FBR	Fluidized bed reactor
FF	Fill factor
GDMS	Glow discharge mass spectrometry
ICP-MS	Inductively coupled plasma mass spectrometry
ICP-OES	Inductively coupled plasma optical emission spectrometry
LCOE	Levelized cost of electricity
LID	Light-induced degradation
mc-Si	Multicrystalline silicon
MPP	Maximum power point
PERC	Passivated emitter and rear cell

PV	Photovoltaics
RT	Room temperature
SoG-Si	Solar grade silicon
SRH	Schockley-Read-Hall
STC	Standard test conditions
UMG-Si	Upgraded metallurgical grade silicon

List of symbols

Fundamental constants

k	Boltzmann constant, $k \approx 1.3806505 \times 10^{-23}$ J.K^{-1}
q	Electron charge, $q \approx 1.602 \times 10^{19}$ C

Symbols	*Meaning*
C_l	Compensation level
E_g	Bandgap Energy
E_g0	Bandgap Energy extrapolated linearly at 0K
f_c	Collection fraction
I_mpp	Current at maximum power point
I_sc	Short-circuit current
$I_\mathrm{sc,1sun}$	Ideal short-circuit current at 1 sun
n	Electron concentration
n	Ideality factor (if stated as such in the text)
n_0	Equilibrium electron concentration
N_A	Acceptor dopant concentration
N_A^-	Ionized acceptor dopant concentration
N_D	Donor dopant concentration
n_i	Intrinsic carrier concentration
n_maj	Equilibrium majority carrier concentration
Δn	Excess electron concentration

p	Hole concentration
p_0	Equilibrium hole concentration
R_s	Series resistance
R_sh	Shunt resistance
T	Temperature
T_c	Cell temperature
V_mpp	Voltage at maximum power point
V_oc	Open-circuit voltage
X	Concentration factor
β	Temperature coefficient
η	Efficiency
μ	Mobility
μ_min	Minority carrier mobility
τ	Lifetime
τ_eff	Effective lifetime
$\tau_\mathrm{intrisinc}$	Intrinsic lifetime
τ_SRH	SRH lifetime

Chapter 1

Introduction

1.1 Background

Crystalline silicon solar modules have been dominating the worldwide PV market for several decades. Multicrystalline silicon is the most used material for manufacturing solar cells because of a lower production cost than monocrystalline silicon, and because high efficiencies can be obtained [1]. Silicon produced for the solar industry is called solar-grade silicon (SoG-Si). The degree of purity of silicon for the solar industry can be slightly lower than for the electronic industry, where electronic-grade silicon (EG-Si) is used. The silicon produced by the Siemens process, which is a chemical purification route, for the electronics and photovoltaic industries can be referred to as polysilicon.

During the plummet of PV prices that happened from 2008 to 2012 because of a mismatch between demand and supply, many polysilicon producers went bankrupt. The polysilicon price has remained below $ 20/kg since 2012 and only the large and efficient players are surviving. On the other hand the growth of the PV market is expected to be steady for the next decade at least [2]. The incapacity of the SoG-Si producers to make short-term profits due to this low silicon price restrain them from investing in expanding their production capacity. This gave an increased opportunity for alternative routes to produce cheaper silicon. This low-cost SoG-Si made by metallurgical routes was expected to mainly be a blend in supply a few years ago. Yet recent studies have shown that efficiencies very close or equal to the efficiencies of cells made of polysilicon can be achieved [3, 4, 5].

SoG-Si obtained by metallurgical processes are often referred to in the literature as UMG-Si. The term UMG-Si will be used in the following to make the distinction between polysilicon and silicon purified by metallurgical processes. Obtaining comparable conversion efficiencies with UMG-Si is very important because the cost of silicon on a total solar module is rather small. This means that the efficiency cannot be significantly reduced otherwise the levelized-cost of electricity (LCOE) would be decreased [6]. In other words, alternative routes to the Siemens process to produce silicon must achieve a quality similar to the one of SoG-Si, so that any performance decrease is minimized, or not present on certain cell types.

Additionally, solar cells made of UMG-Si with improved temperature sensitivities were reported [7, 8, 9, 10]. This beneficial effect is shown, in all studies, to come from an advantageous increase of the short-circuit current (I_{sc}) with temperature. The influence of doping compensation on charge carrier mobility and lifetime is thought to be the cause of this larger increase of the current with temperature.

1.2 Motivation

If we assume that a solar cell made of UMG-Si possesses an almost equal efficiency (or slightly lower) to a cell made of polysilicon, and at the same time a reduced temperature sensitivity, then many questions arise. Can solar cells made of UMG-Si have superior efficiencies than cells made of polysilicon at high temperature? Or is the efficiency only converging to the one of polysilicon cells? Can a solar panel made of this feedstock have a better energy yield than modules made of polysilicon?

Silicon purified by metallurgical routes generally has a lower resistivity to obtain a good ingot yield during solidification. (The addition of gallium allows for a comparable resistivity, and it is explained in details in subsection 4.3.) And having a higher net doping is shown to improve the temperature coefficients [11, 12]. Therefore one can ask what were the resistivities used in the studies where UMG-Si cells were shown to have reduced temperature sensitivities? And what is the contribution of a lower resistivity if this was the case?

Generally there is a need to have a better understanding on the temperature coefficients; to know what are the most influential parameters, to what extent can they be manipulated, and can the temperature coefficients of all the cells from an

ingot be improved.

1.3 Contribution

The first objective of the author was to control the temperature coefficients by increasing the compensation level. It was shown that because the compensated silicon used in this work has low dopant concentrations, no influence was observed.

The second finding is temperature coefficients depend on the ingot height. Moreover different cell designs will show distinct trends. For instance the best temperature coefficients of Aluminium-back surface field (Al-BSF) cells are situated at the top of the ingot. This is explained by the variations of the cell parameters along the ingot height, combined with a change of recombination mechanisms impacting the temperature coefficients.

The effect of the bulk resistivity on the temperature coefficients is confirmed, and compensated silicon is proven to be the most suitable material to lower the resistivity and improve the temperature sensitivity.

Then the effect of light-induced degradation (LID) on the temperature coefficients is shown to results only from a deterioration of the cell parameters.

Finally, a discussion on the cell performances and temperature coefficients is made. The impact of the feedstock, if it is compensated or not, and the impurity concentration on these two parameters is discussed, as well as the relation between the cell parameters and the temperature coefficients.

1.4 Outline of dissertation

The dissertation is based on a collection of papers. The chapters give all the information needed to read and understand fully the publications in the appendices.

The first two chapters present the theory of temperature coefficients and the basics of compensated material. Then an overview of the temperature coefficients of compensated silicon solar cells is made, followed by a discussion on the advantages of using compensated silicon for tuning the temperature sensitivity.

Then a summary of the papers is made. This chapter shows also the red line between the different articles. This is followed by the conclusion where the main

findings are discussed, and put into perspective.

Finally the six papers are presented in the appendices and the list of these publications is found in the next subsection.

1.5 Publications

The following papers are appended and they will be referred to by the letters A-F. All papers were approved in peer-reviewed conferences except paper E which will be submitted in a journal. The conference papers are printed in their originally published state.

A) Berthod, C., Strandberg, R. and Odden, J.O., "Temperature coefficients of compensated silicon solar cells – influence of ingot position and blend-in-ratio", *5th International Conference on Silicon Photovoltaics, SiliconPV 2015* Konstanz, Germany.

B) Søndenå, R., Berthod, C., Odden, J.O., Søiland, A.K., Wiig, M.S. and Marstein, E.S., "Temperature dependent quantum efficiencies in multicrystalline silicon solar cells", *5th International Conference on Silicon Photovoltaics, SiliconPV 2015* Konstanz, Germany.

C) Berthod, C., Strandberg, R., Odden, J.O. and Saetre, T.O., "Reduced temperature sensitivity of multicrystalline silicon solar cells with low ingot resistivity", *Photovoltaic Specialist Conference (PVSC), 2016 IEEE 43rd* Portland, Oregon, USA.

D) Berthod, C., Strandberg, R., Odden, J.O. and Saetre, T.O., "Reduction of temperature coefficients in multicrystalline silicon solar cells after light-induced degradation", *Photovoltaic Specialist Conference (PVSC), 2015 IEEE 42nd* New Orleans, Louisiana, USA.

E) Berthod, C., Strandberg, R., Odden, J.O. and Saetre, T.O., "Temperature sensitivity of multicrystalline silicon solar cells", *To be submitted*

F) Berthod, C., Strandberg, R., Yordanov, G.H., Beyer, H.G. and Odden, J.O., "On the variability of the temperature coefficients of mc-Si solar cells with ir-

radiance", *6th International Conference on Silicon Photovoltaics, SiliconPV 2016* Chambery, France.

Chapter 2

Theory of the temperature coefficients of a silicon solar cell

Solar cells and PV modules are systematically characterized at standard test conditions (STC), that is 1000 $W \cdot m^{-2}$, 25°C and air mass (AM) 1.5. These correspond to the irradiance and spectrum of sunlight incident on a clear day upon a sun-facing 37°-tilted surface with the sun at an angle of 41.81° above the horizon. This condition approximately represents solar noon near the spring and autumn equinoxes in the northern countries with surface of the cell aimed directly at the sun.

Yet usual operating conditions deviate from STC. Solar modules can reach temperatures above 60°C. The efficiency varies with temperature and in order to take into account the temperature variations, the general parameter temperature coefficient is introduced to describe how the power output varies with temperature under maximum power point operation of a solar cell. In the case of crystalline silicon the efficiency decreases quasi-linearly with temperature as shown in [13]. Temperature coefficients for every cell parameter can be derived and they are often presented as relative temperature coefficients in order to compare different technologies. The relative temperature coefficient of a parameter X is defined as follows:

$$\beta_X = \frac{1}{X_{25°C}} \frac{\partial X}{\partial T_c} \tag{2.1}$$

where T_c is the cell temperature. The value is expressed in $ppm \cdot K^{-1}$ or in $\% \cdot °C^{-1}$ in the literature. Both units are equivalent and the author has chosen to use the

second one.

The first model of temperature coefficients using internal device physics without semi-empirical parameters was made by Green in [13]. In this paper he demonstrated that the temperature coefficient of a solar cell is mainly driven by the increase of the recombination rate which results from an increased carrier concentrations.

First, a general expression for the relative temperature coefficient of the short-circuit current (I_{sc}) derived by Green will be presented in the next section. Second, an improved version of the relative temperature coefficient of the open-circuit voltage (V_{oc}) made by Dupré et al. in [14] will be introduced in section 2.2. Third, Zhao et al. [15] included the series resistance effect in the original formulation of the relative temperature coefficient of the fill factor (FF) made by Green, which will be presented in section 2.3. Finally, the temperature sensitivity of a solar cell with the influence of each previous coefficient will be described.

2.1 Temperature coefficient of the short-circuit current

The bandgap of crystalline silicon decreases with temperature as is the case for most semiconductors. This causes the I_{sc} to increase as a function of temperature. We can write the I_{sc} as a function of an ideal current $I_{sc,1sun}$, a collection fraction f_c and a concentration factor X:

$$I_{sc} = I_{sc,1sun}\, f_c\, X. \tag{2.2}$$

The ideal current correspond to the current if all the photons with an energy above the bandgap are absorbed, and all the generated carriers are collected without any loss.

After differentiation of Eq. (2.2) the relative temperature coefficient of I_{sc} is obtained [13]:

$$\beta_{I_{sc}} = \frac{1}{I_{sc,1sun}} \frac{dI_{sc,1sun}}{dE_g} \frac{dE_g}{dT_c} + \frac{1}{f_c} \frac{df_c}{dT_c}. \tag{2.3}$$

The first right-hand term depends only on the bandgap of the semiconductor and on the spectrum. Landis et al. observed that the spectrum has a strong in-

fluence on this coefficient [16]. For instance, if a peak of intensity present in the lamp spectrum is situated at a wavelength right below the conduction band of an absorber, then when the temperature will rise these wavelengths will start being absorbed because of the bandgap reduction. This will cause a large increase in the current which doesn't correspond to the actual current increase with the sun spectrum. Moreover as a lamp spectrum changes when ageing, and diverse lamps are used, it is difficult to compare measurements done at different places. The second right-hand term is the relative temperature coefficient of the collection fraction. f_{c} is the ratio of useful photons (i.e that can be absorbed by the material) that get collected to the total number of useful photons. Thus it depends on the solar cell structure, the light trapping, and the recombination mechanisms.

2.2 Temperature coefficient of the open-circuit voltage

Green was the first to propose a model for the temperature coefficient of the V_{oc} based on device physics [13]. He defined the function ξ closely related to the product of the electron and hole concentrations np:

$$\xi = \frac{np}{n_{\mathrm{i}}} \exp \frac{-E_{\mathrm{g}}}{kT_{\mathrm{c}}}. \tag{2.4}$$

$\mathrm{n_i}$ is the intrinsic carrier concentration, $\mathrm{E_g}$ the band gap and k Boltzmann constant. With $\langle x \rangle$ the weighted value of the parameter x defined as:

$$\langle x \rangle = \frac{\sum_{i=1}^{N} x_i A_i T_{\mathrm{c}}^{\gamma_i} \xi_i (\mathrm{d}f_i/\mathrm{d}\xi_i)}{\sum_{i=1}^{N} A_i T_c^{\gamma_i} \xi_i (\mathrm{d}f_i/\mathrm{d}\xi_i)} \tag{2.5}$$

where there are N recombination processes depending respectively on ξ_i through the functions f_i, and A_i is a constant specific to each recombination mechanism. γ_i relates to the temperature dependence of the recombination mechanism. Then the relative temperature coefficient of the V_{oc} can be expressed after neglecting second-order terms as:

$$\beta_{V_{\mathrm{oc}}} = -\frac{1}{V_{\mathrm{oc}} T_{\mathrm{c}}} \left(\frac{\langle E_{\mathrm{g0}} \rangle}{q} - V_{\mathrm{oc}} + \frac{kT_{\mathrm{c}}}{q} \left\langle \gamma \frac{f}{\xi} \frac{\mathrm{d}\xi}{\mathrm{d}f} \right\rangle \right) \tag{2.6}$$

where E_{g0} is the extrapolated bandgap at 0K and q the electron charge.

This expression can be applied to any PV material. This coefficient is negative and reflects the increase of recombination rate with temperature. We can observe that improving the V_{oc}, by improving the passivation or the bulk mobility for example, will reduce the temperature coefficient. However a precise knowledge of the recombination mechanisms occuring in the solar cell is needed to calculate the term $\left\langle \gamma \frac{f}{\xi} \frac{\mathrm{d}\xi}{\mathrm{d}f} \right\rangle$.

Recently, Dupré et al. [14] derived an expression of this temperature coefficient based as well on internal device physics using the external radiative efficiency (ERE) defined by Green in [17] as the fraction of the total dark current recombination in the device that results in radiative emission from the PV device. The coefficient can be written as:

$$\beta_{V_{\mathrm{oc}}} = -\frac{1}{V_{\mathrm{oc}} T_{\mathrm{c}}} \left(\frac{E_{\mathrm{g0}}}{q} - V_{\mathrm{oc}} + \gamma \frac{kT_{\mathrm{c}}}{q}. \right) \tag{2.7}$$

where γ is a function of the ERE at open-circuit conditions:

$$\gamma = 1 - \frac{\mathrm{d}\ln ERE_{\mathrm{oc}}}{\mathrm{d}\ln T_{\mathrm{c}}} + \left(2 \frac{\mathrm{d}\ln E_{\mathrm{g}}}{\mathrm{d}\ln T_{\mathrm{c}}} - \frac{\mathrm{d}\ln J_{\mathrm{sc,1sun}}}{\mathrm{d}\ln T_{\mathrm{c}}} \right). \tag{2.8}$$

The parameter γ in Eq. (2.6) and (2.7) are the same. But Dupré et al. provided an expression of it based on device physics. Essentially γ describes the behavior of the recombination mechanisms with temperature.

The absolute value of the term in parenthesis in Eq. (2.8) is less than 0.5 according to Dupré et al. [14]. The term $\gamma \frac{kT_{\mathrm{c}}}{q}$ in Eq. (2.7) accounts for approximately 10% of the total relative temperature coefficient of the V_{oc}. Therefore for a given semiconductor V_{oc} is the main adjustable variable of its temperature coefficient. This explains why PV devices showing the best V_{oc} have as well the best cell temperature sensitivity [18, 19].

2.3 Temperature coefficient of the fill factor

The fill factor can be understood graphically as the "squareness" of an IV-curve. It is defined as:

$$FF = \frac{I_{\text{mpp}} \times V_{\text{mpp}}}{I_{\text{sc}} \times V_{\text{oc}}} \tag{2.9}$$

with I_{mpp} and V_{mpp} the current and voltage at maximum power point respectively.

FF is lowered by a large ideality factor (n), and series (R_{s}) and shunt (R_{sh}) resistances effects. The ideality factor depends on the recombinations. Typical values are 2/3 for Auger recombination, and between 1 and 2 for radiative recombination (depending on the injection level). A good approximation to calculate the fill factor free of parasitic resistance losses is [20]:

$$FF_0 = \frac{v_{\text{oc}} + \ln(v_{\text{oc}} + 0.72)}{v_{\text{oc}} + 1} \tag{2.10}$$

with v_{oc} the normalized open-circuit voltage defined as:

$$v_{\text{oc}} = \frac{V_{\text{oc}}}{nkT_{\text{c}}/q}. \tag{2.11}$$

Green derived an expression of the relative temperature coefficient of the FF as: [13]

$$\beta_{FF_0} = (1 - 1.02FF_0)\left(\beta_{V_{\text{oc}}} - \frac{1}{T_{\text{c}}}\right). \tag{2.12}$$

If we take into consideration the series resistance losses with this simple equation:

$$FF_{\text{s}} = FF_0\left(1 - \frac{R_{\text{s}}}{V_{\text{oc}}/I_{\text{sc}}}\right) \tag{2.13}$$

then we get the expression from [15]:

$$\beta_{FF_{\text{s}}} = (1 - 1.02FF_0)\left(\beta_{V_{\text{oc}}} - \frac{1}{T_{\text{c}}}\right) - \frac{R_{\text{s}}}{V_{\text{oc}}/I_{\text{sc}} - R_{\text{s}}}\,\beta_{R_{\text{s}}}. \tag{2.14}$$

The relative temperature coefficient of the *FF* is negative because both terms in Eq. (2.14) are negative in most type of cells. The first term can be reduced by increasing the V_{oc}. The term depending on the series resistance is negative for homojunction solar cells, however for heterojunction solar cells, carrier transport through interfaces by tunneling and/or thermionic emission can give a *FF* improving with temperature [21].

A drawback of Eq. (2.14) is that it doesn't consider shunt resistance losses that can be important in multicrystalline silicon solar cells [22] or in interdigitated back-contacted cells [23].

2.4 Temperature coefficient of the efficiency

The efficiency can be expressed as the product of the I_{sc}, the V_{oc} and the *FF*. When differentiating and dividing by the efficiency we obtain the following equation:

$$\beta_{\eta} = \beta_{I_{\mathrm{sc}}} + \beta_{V_{\mathrm{oc}}} + \beta_{FF_{\mathrm{s}}}. \tag{2.15}$$

The temperature sensitivity of a solar cell is the sum of the three previously presented temperature coefficients. Both $\beta_{V_{\mathrm{oc}}}$ and $\beta_{FF_{\mathrm{s}}}$ are negative and their absolute values are larger than $\beta_{I_{\mathrm{sc}}}$. For a multicrystalline PERC solar cell with a temperature sensitivity of $\beta_{\eta} = -0.38$ %·°C^{-1} the relative temperature coefficient of the V_{oc} accounts for around 75% of it. As an increased V_{oc} benefits both the relative temperature coefficient of the V_{oc} and of the *FF*, it is therefore the main parameter to optimize in order to reduce the temperature sensitivity. This relation between the V_{oc} and the temperature sensitivity was understood with the arrival of the first high performance cell structures [15, 19].

Chapter 3

Experimental setups

In this chapter, the experimental procedure for light-soaking is explained. Then a description of the sun simulator and the method to measure temperature coefficients are provided. The uncertainties of the temperature coefficient measurement is discussed in subsection 3.3. Finally the type of feedstocks used in this work are described.

3.1 Light-soaking bench

The solar cells which were exposed to light-soaking, were illuminated for 48 hours. An array of 6 halogen lamps, each with a power of 500 W, was used to provide an approximate light intensity of 1 sun (1000 $\pm$ 100 W·m^{-2}) as shown in Fig. 3.1. The temperature range reached by the cells on the array is 50°C $\pm$ 10°C. This way the solar cells received an initial light-induced degradation (LID) and are in an identical degraded state. When the effect of LID was under investigation then some cells were measured as-processed to be compared with light-soaked cells.

It has been shown that compensated silicon present different LID kinetics from non-compensated silicon which can lead to different degraded states [24, 25]. However no significant difference in efficiency after LID was measured between cells made of the studied UMG-Si and cells made of polysilicon [5, 26, 27]. Therefore we assume the degraded state after LID is the same for cells made of both feedstocks.

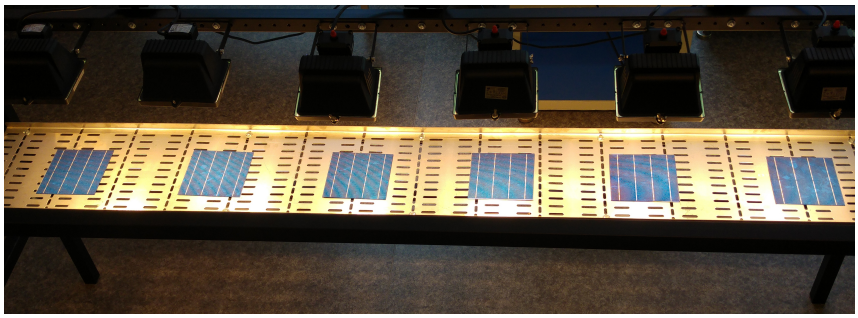

Figure 3.1: Light induced degradation setup consisting of six 500 W halogen lamps. One solar cell is placed under each lamp to receive about one sun illumination.

3.2 Sun simulator

To perform IV characterisation, a NeonSee® AAA sun simulator was used. The solar cells were placed on a copper sample holder for electrically contacting its rear surface. The busbars on front of the solar cell were contacted by metal pins with one contacting bar for each busbar as shown in Fig. 3.2 . The I-V sweeps were performed under illumination with AM1.5 global spectrum. The temperature of the solar cell was measured by a PT100 sensor, situated in the middle of the sample holder. Hot/cold water flowed through the sample holder to regulate any desired temperature.

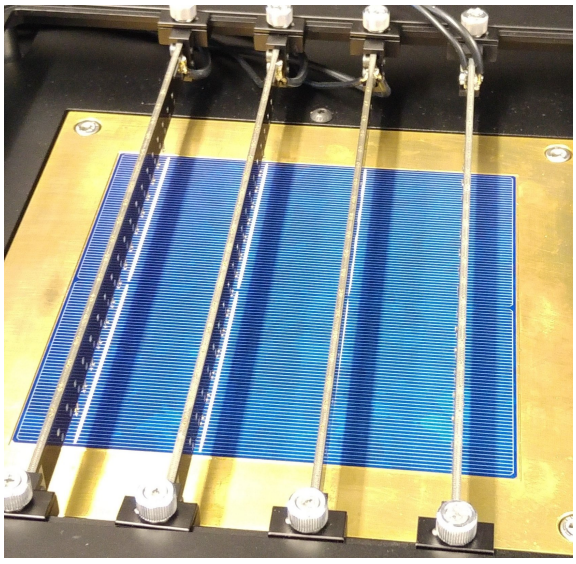

Figure 3.2: Solar cell placed on the sample holder in the sun simulator.

To measure temperature coefficients, the solar cells were illuminated at one sun

and I-V characteristics were measured from 25°C to 70°C with a 2- or 5-degree step. Then a linear fitting is performed to extract the slope as shown in Fig. 3.3.

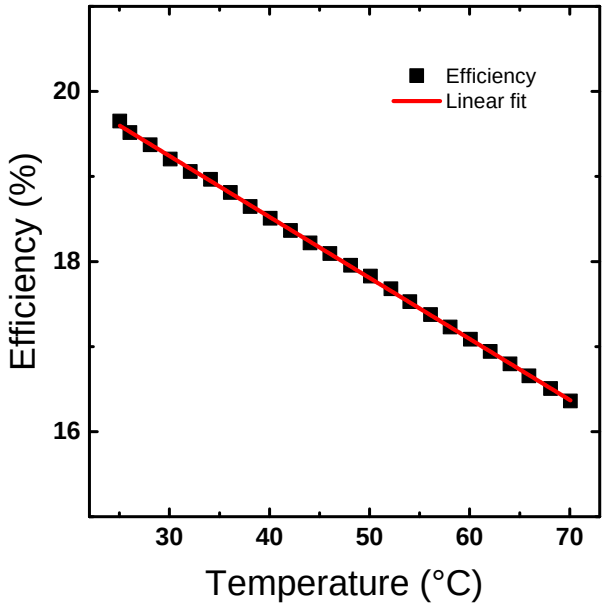

Figure 3.3: Example of fitting for the temperature coefficient of the efficiency.

3.3 Uncertainties of the temperature coefficient measurements

The nonuniformity of the temperature of the metal plate where the solar cell is placed is part of the systematic errors that occur. A temperature gradient between the front and the rear-side of a solar cell is created when the cell is illuminated from above. More errors were described by Emery et al. in Ref. [28].

The presence of intensity peaks in the lamp spectrum can also affect the temperature coefficient of the I_{sc}, this was pointed out in Ref. [16, 29]. Due to these systematic errors the experimental results presented in this thesis and in the appended articles are not aimed to be compared with results from other laboratories without further analysis.

The repeatability of the measurements is strongly related to the fluctuations in the calibration of the sun simulator. If not considering calibration differences,

the standard deviation of the temperature coefficient measurements is found to be approximately 0.002 %.°C^{-1} (typical values for the temperature coefficient of the I_{sc} are around 0.06 %.°C^{-1}). Yet when calibration variations are considered, this value rises to 0.004%.°C^{-1}.

All graphs presented in this dissertation and in the appended papers do not include error bars even though the standard deviation is relatively important. The author has purposely decided to not include error bars in the figures because the drawn conclusions are always statistically significant, and it preserves the clarity of the graphs.

3.4 Studied silicon feedstocks

The silicon produced by Elkem Solar® was used to study compensated silicon. This SoG-Si is called Elkem Solar Silicon (ESS®) It is a lightly compensated silicon[1] with typical concentrations of boron and phosphorus being respectively 0.18 ppmw, 0.60 ppmw. More dopants could be added to obtain a specific resistivity, or gallium could be added to do compensation engineering, which is explained in section 4.3. It is a material with larger impurity concentrations than a silicon intentionally compensated from the Siemens process as can be seen in Table 3.1 where the chemical composition of ESS® is summarized. However the effect on cell performance, considering only mc-Si solar cells, is not noticeable as shown in section 4.4.

Table 3.1: Chemical analysis

Element	Method of analysis	Content (in ppmw)	Typical metal content measured by GDMS (in ppmw)
B	ICP-MS	0.18	-
P	ICP-OES	0.60	-
Fe	ICP-OES	<2	<0.05
Ti	ICP-OES	<0.2	<0.005
K	ICP-OES	<5	<0.05

[1] In the following, when the author will refer to a lightly compensated material, it would mean that the dopant concentrations are in the same order of magnitude as the majority carrier concentration.

ICP-MS and ICP-OES stands for inductively coupled plasma - mass spectrometry, and optical emission spectrometry.

The detection limits of the apparatus are quite much higher than the real content in ESS® for the metals in general, so a glow discharge mass spectrometry (GDMS) analysis was carried out externally to confirm the low metal content.

REC Silicon uses a fluidized bed reactor (FBR) to produce silicon. The main advantage of this technique is the continuous production of silicon whereas in the Siemens process, the rods with deposited silicon have to be extracted at regular intervals. This allows a large cost reduction for this material. However the product in a FBR are grains. These grains mean that a dense filling for casting is not simple. Therefore the reference non-compensated silicon was a mix of polysilicon and silicon from REC.

Chapter 4

Solar grade silicon produced by metallurgical routes

Polysilicon is the raw material used both in the electronic, and in the photovoltaic industry. These two industries have different requirements regarding the purity. SoG-Si is from ∼99.9999% pure silicon whereas EG-Si is ∼99.999999999% pure. Among SoG-Si we can distinguish two types of silicon. Polysilicon is the dominant feedstock and it is produced by the Siemens process which is a chemical purification process. The conventional Siemens process produces EG-Si but a modified process, with slightly less energy demand, can produce the SoG-Si. The alternative silicon feedstock is SoG-Si produced by metallurgical routes, also called UMG-Si.

In 2008 when the price of one kilogramme of polysilicon peaked at $475 because of the exponentially growing cell production capacity causing a shortage of silicon suppliers, different routes of production of polysilicon emerged based on metallurgical routes. These new producers were making UMG-Si at a much lower cost than polysilicon from the Siemens process thanks to the lower energy needs of the purification steps [30, 31]. Yet when the prices fell down below $15/kg in 2013, their main selling argument, that is the low-cost silicon, disappeared with all suppliers aligning their prices. Therefore all the UMG-Si suppliers producing a material with a low purity ceased their activity. Among the remaining UMG-Si producers, the current largest one is Elkem Solar® but a few other producers can be mentioned such as Photosil, or Silicor Materials.

UMG-Si is often associated with compensated silicon due to the difficulty of

removing elements close to silicon in Mendeleiev's table, that is aluminium, calcium, boron, phosphorus, carbon, and nitrogen. The presence of both acceptors (Al and B) and donors (P) will reduce the net doping because of dopants "cancelling out" each other. This is called dopant compensation and all of the producers of UMG-Si, to the author's knowledge, are manufacturing compensated silicon. This material presents different electronic properties, especially a lower mobility than non-compensated silicon which in theory may cause a lower obtainable efficiency [32]. However efficiencies above 19% have been reported on n-type Cz UMG-Si [3, 33, 34], demonstrating the potential for high performance solar cells with this feedstock. In this work where only multicrystalline silicon (mc-Si) solar cells were studied, no significant difference in efficiency was observed. Crystallographic defects are the main performance limiting parameters, independently of the presence of doping compensation or not.

Despite this, solar cells made of compensated silicon with lower temperature sensitivities were reported, causing higher energy yield for this material than for polysilicon [35, 36].

In the following section an overview of the manufacturing route used by Elkem Solar® to produce UMG-Si is given together with its principal assets. Then in section 4.2 the electronic properties of compensated silicon will be described. It is followed by section 4.3 where compensation engineering is explained, with the advantages of adding gallium in the feedstock. Finally in section 4.4, the consequences of dopant compensation on the principal cell parameters are presented.

4.1 Fundamentals of upgraded metallurgical grade silicon

Currently, silicon is still the most used material to manufacture solar cells and it represents more than 90% of the total market share [37]. The rapid growth of the photovoltaic industry requires an increase of the silicon supply. One option is to use low-cost SoG-Si produced by metallurgical processes. Even though the cost of silicon represents a significant contribution, it is only one part of the total cost of a solar module it is therefore imperative that the solar cells do not suffer large efficiency losses [38]. To prevent performance reduction when using UMG-Si as a

feedstock, a certain purity is required [6]. Above a certain impurity concentration, specific for each element, the efficiency can be severely reduced as shown in Fig. 4.1.

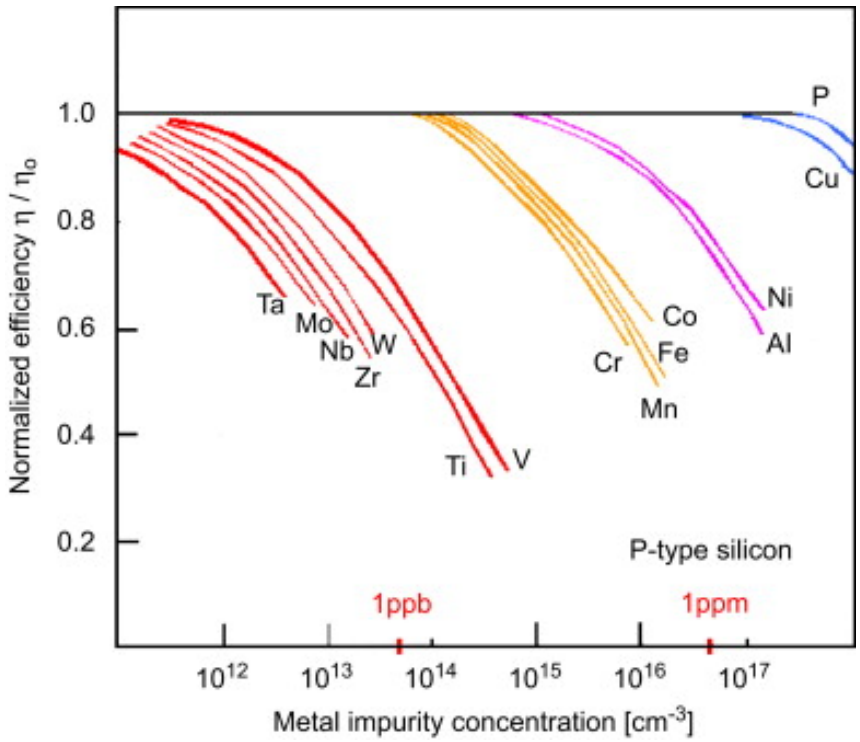

Figure 4.1: Effect of metallic impurity content (in at·cm^{-3}) in single crystal silicon on the normalized efficiency of solar cells. Reprinted from [6].

In the work presented here and in the appended papers, ESS® is used as the reference compensated material.

Elkem Solar® is the largest producer of UMG-Si and its route is based on pyrometallurgical refinement. It consists of five steps. The first one is the production of MG-Si in an electric arc furnace. A great attention is paid to raw material's purity to avoid as much transition metals and boron/phosphorus as possible. This is followed by a slag treatment where liquid silicon is mixed with slag to remove the impurities present in the material. Then a leaching is made followed by a directional solidification to segregate the impurities at the top of the ingot. Finally a post treatment cuts the sides, bottom and top parts and cleans the surfaces. ESS® is obtained at this point. Then it is sent to solar cell manufacturers, together with the boron and phosphorus concentration details so that the customer can add more dopants in their solidification step to match their resistivity target. Gallium can

also be added for reasons explained in subsection 4.3.2.

This route enables ESS® to have a carbon footprint three to four times lower than silicon from the Siemens process. This means that the production of polysilicon generates at least three times more greenhouse gases than the production of ESS®. Moreover the energy payback time for the energy invested in the production of ESS® is only one month [31]. The very low energy consumption of this process is what enables a low cost material.

4.2 Electronic properties

Mobility and lifetime are two fundamental parameters describing a semiconductor, and they are of very high importance in optoelectronic devices design. The first one indicates the quality of carrier transport, more precisely it characterizes how quickly a carrier can move through a metal or semiconductor. Whereas the lifetime is the average time before recombination that a carrier can spend in an excited state after electron-hole generation. Both parameters have been extensively studied lately in UMG-Si where the impact of compensation and the presence of more impurities is of critical interest. This section aims at defining the compensation level and briefly reviewing recent studies on both mobility and lifetime in compensated material.

4.2.1 Compensation level

Compensated silicon is a material where the acceptor and donor dopants are in relatively similar concentrations. The equilibrium carrier concentration is defined as:

$$n_{\mathrm{maj}} = \left| N_{\mathrm{A}}^{-} - N_{\mathrm{D}}^{+} \right| \tag{4.1}$$

where n_{maj} is the equilibrium majority carrier concentration, N_{A} is the acceptor concentration and thus N_{A}^{-} the ionized acceptor concentration. Similarly for N_{D} which is the donor concentration and N_{D}^{+} the ionized donor concentration. In p-type silicon, Eq. (4.1) becomes:

$$p_0 = N_A^- - N_D \approx N_A - N_D. \tag{4.2}$$

with p_0 the equilibrium hole concentration.

The ionized concentration of acceptor is equal to the total concentration of acceptor if all dopants are ionized. Incomplete ionization does not affect donor atoms in p-type compensated Si [32], which justifies using N_D in Eq. (4.2). Incomplete ionization occurs with dopant concentrations around 10^{17} - 10^{18} cm^{-3}, and a percentage of 25% non-ionized dopant can be reached for a boron concentration of 2×10^{18} cm^{-3}. In non-compensated silicon the typical doping range is 0.5-2$\times10^{16}$ cm^{-3} and thus incomplete ionization can be neglected. Whereas in compensated silicon, to obtain a similar equilibrium hole concentration, higher dopant concentrations must be achieved. The typical range of boron concentrations in ESS® to produce mc-Si solar cells is 2-4$\times10^{16}$ cm^{-3}. Hence the incomplete ionization was neglected for this material in the present work. Note that this assumption can be questionable and lead to small errors, but the results found on the temperature coefficients dependence with compensation level show that for lightly compensated material, no clear trend can be observed (as shown in paper A). Questioning the precision of the calculations becomes thus irrelevant.

Compensated materials can be characterized by their compensation levels. It is defined as:

$$C_l = \frac{N_A + N_D}{n_{maj}} \tag{4.3}$$

The ratio goes from 1 for non-compensated material (because $n_{maj} = N_A$ for p-type and $n_{maj} = N_D$ for n-type) to $+\infty$ for fully compensated, that is when $N_A = N_D$ (with full ionization).

4.2.2 Mobility

The scattering time of a carrier is the time frame a carrier is ballistically accelerated by the electric field until it scatters (collides) with something that modifies its direction and/or energy. Carrier mobility is directly proportional to the scattering time. Many scattering mechanisms can reduce the scattering time and therefore

the mobility. Ionized impurity scattering and phonon scattering are the two main ones. We can sum up the contributions of each scattering mechanism by using Matthiessen's rule:

$$\frac{1}{\mu} = \sum_{i=1}^{N} \frac{1}{\mu_i}. \tag{4.4}$$

where μ is the mobility and μ_i the mobility of the scattering mechanism i.

Carrier mobility in non-compensated semiconductors is normally well described, by Klassen's model [39, 40]. However experimental evidence [32, 41, 42] have shown that both the minority and majority carrier mobilities were overestimated in Klassen's model for compensated silicon.

Schindler et al. [43] has come up with an empirical model based on Klassen's work describing the majority and minority hole and electron mobilities in compensated p- and n-type silicon. In this model the reduction of mobility is attributed to reduced screening. However no experimental data of the temperature dependence of minority carrier mobilities in compensated silicon exist. Therefore the assumption of a temperature dependence of the minority carrier mobility similar to the dependence of the majority carrier mobility is made by Schindler et al.

Table 4.1: Ionized dopant concentrations and compensation level at 300 K for the samples shown in Fig. 4.2.

Sample	Type	N_A (cm^{-3})	N_D (cm^{-3})	C_l at RT
Cz6-012	n	9.20×10^{16}	1.00×10^{17}	24
Cz6-326	n	2.02×10^{17}	2.14×10^{17}	34
Cz1-200	p	9.83×10^{16}	8.60×10^{16}	15
Cz5-130	p	2.32×10^{17}	2.09×10^{17}	19
Cz5-298	p	2.80×10^{17}	2.62×10^{17}	30
Cz5-396	p	3.37×10^{17}	3.27×10^{17}	67
Cz5-478	p	4.34×10^{17}	4.28×10^{17}	146

The majority carrier mobility is plotted as a function of temperature for different compensation levels in Fig. 4.2. The respective dopant concentrations of the samples are summarized in Table 4.1. If we examine the effect of compensation at room temperature ($\sim$300 K), we see that a high compensation level tends to reduce

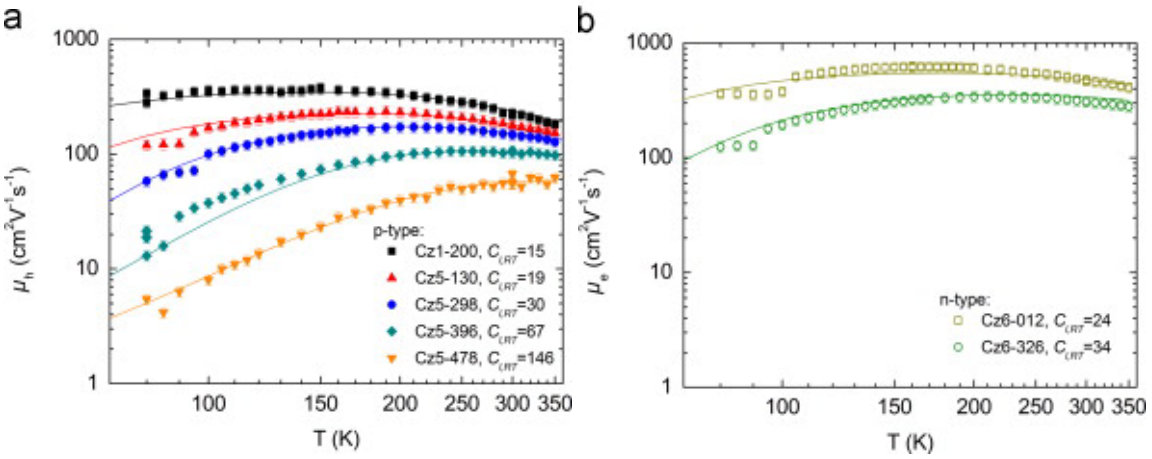

Figure 4.2: Experimental temperature-dependent majority carrier mobility of (a) five compensated p-type and (b) two compensated n-type samples with a wide range of compensation levels compared to the model derived by Schindler et al. (lines). Reprinted from [43].

the mobility for both n- and p-type silicon. It should be noted that dopant concentrations increased as well (up to five times for the donor dopant in the p-type silicon samples) which can influence also the mobility due to ionized impurity scattering. At low temperature, ionized impurity scattering is predominant for compensated silicon because incomplete ionization becomes less effective with high compensation level [41].

In summary, silicon with a high compensation level will see its mobility vary less with temperature (around room temperature) due to an already lowered mobility compared to non-compensated silicon where the mobility will be decreasing. The effect of phonon scattering will become predominant at higher temperatures for both, making their mobilities converge. This gives a seemingly advantageous temperature dependence of the mobility for compensated silicon. Yet the mobility will not exceed the one of non-compensated silicon for any given temperature. No available experimental data on the temperature dependence of the minority carrier mobilities was found, therefore it is suggested in Ref. [43] to use the same correction for the minority carrier in compensated silicon. Therefore we assume that the conclusions drawn on the majority carrier mobility can be applied to the minority carrier mobility.

4.2.3 Lifetime

Obtaining a high minority carrier lifetime is one of the principal objectives in the PV industry in order to achieve high performance solar cells. It has a direct impact on the efficiency as shown in Ref. [44]. Multicrystalline ingots will show lower lifetimes than mono-Si because of the crystallographic defects. UMG-Si which presents more contamination by impurities than EG-Si can show an even further reduced lifetime.

The recombination can be largely controlled by the majority carrier density n_{maj} as Ref. [45] has shown. Fig. 4.3a shows the intrinsic lifetime (that is with only radiative and Auger recombination) in compensated silicon with three distinct acceptor dopant concentration and a varying donor concentration. The best lifetimes are obtained at full compensation when $N_{\mathrm{A}} = N_{\mathrm{D}}$, these intrinsic points are shown by the vertical dashed lines. To the left of the intrinsic point, the material is p-type, and to the right, n-type. On the p-type side, the lifetime is limited by the doping in acceptor, causing the three different curves. On the n-type side, the lifetime is on the contrary limited by the doping in donor resulting in a convergence of all three curves.

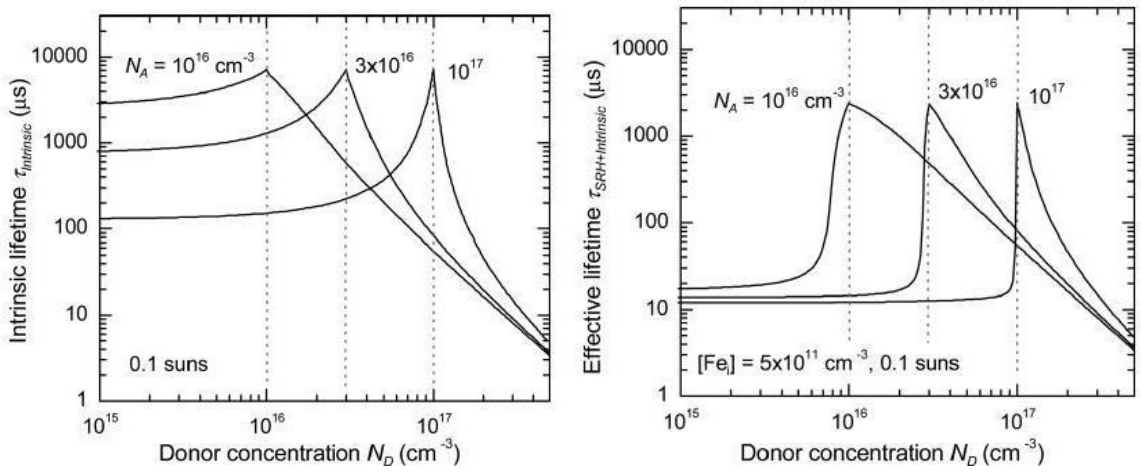

(a) (b)

Figure 4.3: (a) The intrinsic lifetime due to Auger and radiative recombination in silicon as a function of the concentration of compensating donor atoms added N_{D}, under an illumination intensity of 0.1 suns. Three different acceptor concentrations N_{A} are shown, with the vertical dashed lines representing the intrinsic points where $N_{\mathrm{A}} = N_{\mathrm{D}}$. (b) Effective lifetime due to an interstitial iron concentration of $5 \times 10^{11} cm^{-3}$ with the intrinsic recombination. Reprinted from [45].

When an impurity is introduced (here interstitial iron), Shockley-Read-Hall (SRH) recombination is added to the intrinsic recombination mechanisms and Fig. 4.3b is obtained. The effective lifetime can be expressed as:

$$\frac{1}{\tau_{\text{eff}}} = \frac{1}{\tau_{\text{intrinsic}}} + \frac{1}{\tau_{\text{SRH}}} \tag{4.5}$$

with τ_{eff} the effective lifetime, $\tau_{\text{intrinsic}}$, the intrinsic lifetime and τ_{SRH} the SRH lifetime.

Interstitial iron has a larger capture cross section for electrons than holes and has a deep level in the bandgap. Therefore it manifests a strong injection-dependent lifetime which is seen in the significant increase of several order of magnitude of the lifetime near the intrinsic points. On the n-type side the lifetime is very similar to the one of the intrinsic lifetime because of the quasi absence of injection dependence of the lifetime due to a much smaller capture cross section for holes than electrons for this defect.

It should be noted that a deep level with an opposite asymmetric capture cross section (larger for holes than electrons), would give a graph similar to Fig. 4.3b, but the donor and acceptor concentrations would be swapped.

Another phenomenon called ”Fermi-level effect” can take place for shallow level defects with an energy level near the Fermi level. However the most detrimental defects to the lifetime are deep levels, therefore this shallow level effect will not be explained here. Note that a comparable beneficial effect is observed with compensation for these shallow defects [45].

Compensation engineering, that is adjusting the concentrations in donor and acceptor dopants, can improve dramatically the lifetime by lowering the majority carrier concentration. This was observed experimentally in Ref. [46]. However recent studies showed that the performance of solar cells with activated boron-oxygen defects does not improve with the compensation level [47, 48].

4.2.4 Boron-Oxygen defect

The main lifetime limiting parameter in p-type Cz- and mc-Si is the boron-oxygen defect due to a high concentration of oxygen coming from the crucible [49]. N-type compensated silicon suffers as well from LID owing to the presence of boron.

This could cause a rejection of this material in favor of non-compensated silicon for n-type solar cells [50].

This defect is created under illumination or carrier injection. The formation of this defect is still debated but it appears to be the result of two distinct and independent recombination centers, a fast-forming center (referred to as FRC) and a slow-forming center (SRC). It was shown that the B-O defect density depends on the net doping rather than the boron concentration, resulting in a beneficial effect of compensation [24, 51]. However a more recent study has argued that the influence of oxygen was neglected in these studies, and it could have misled the interpretation of the results [47]. Fig. 4.4 shows the separate effects of boron concentration (for two different majority carrier concentrations) and majority carrier concentration (for two different boron concentrations). It is clear that the normalized effective B-O defect density depends on the total boron concentration whereas for the majority carrier density no trend is observed.

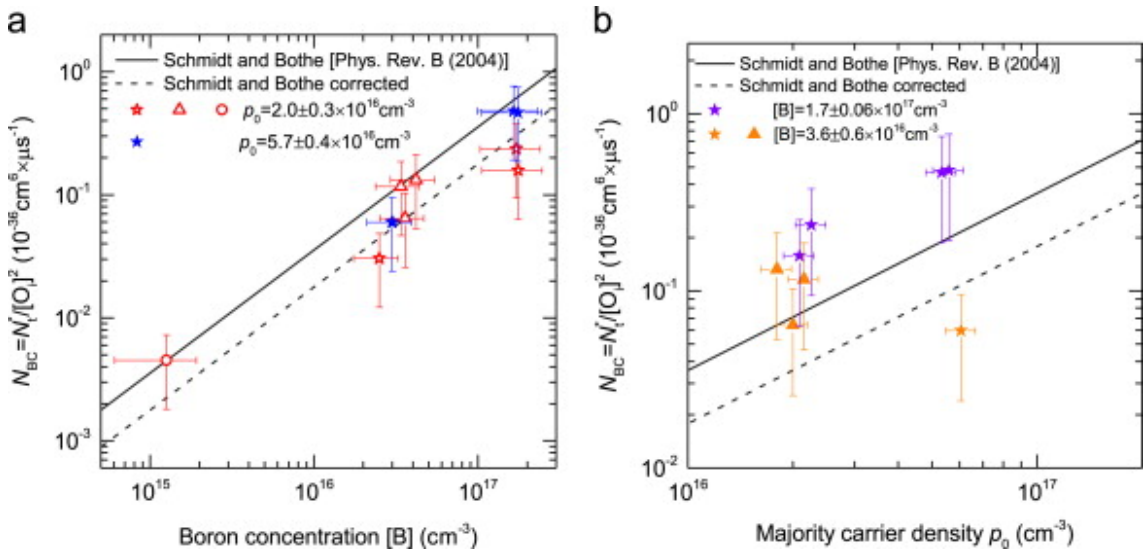

Figure 4.4: Normalized effective B-O defect density plotted as a function of the total boron concentration (a) or as a function of the majority carrier density (b). Solid line is a fit to experimental data on B-doped Si from Ref. [52]. Dashed line corresponds to the same fit divided by a correction factor of 2 to account for the BO defect density reduction expected in P-diffused Si (see Ref. [53]). Samples co-doped with B and P are represented by triangles, samples co-doped with B and Ga are represented by circles and samples co-doped with B, P and Ga are represented by stars. Reprinted from [47].

These results tend to show that a material presenting a high concentration of

boron, such as UMG-Si, will suffer more from this recombination center than silicon from the Siemens process. This is further confirmed by the fact that this deep-level defect has very symmetrical capture cross sections (meaning comparable capture cross sections for holes and electrons) [54] causing no significant injection-dependent lifetime, which prevents any compensation engineering to increase the lifetime.

The compensated silicon studied in this work, Elkem Solar Silicon®, has not exhibited a significant difference in efficiencies after LID compared to polysilicon [5, 26, 27, 55]. The boron concentration in ESS® is typically two times higher than in polysilicon , which is not a very large discrepancy. This could explain the similar efficiencies after LID. In addition, the formation of the B-P complex, reported in Ref. [56], preventing the formation of the B-O complex can be a second cause.

We can conclude that compensated silicon contain higher concentrations of dopants, which reduces the lifetime. However practically the lifetime would be limited by impurities, or crystallographic defects. In this case compensation can increase the lifetime by decreasing the majority carrier concentration for some recombination centers. But this doesn't apply to the B-O defect. Therefore in mc-Si and Cz-Si where a high concentration of oxygen is found, a low boron concentration is recommended if no regeneration step is applied. Note that the formation of the B-P complex can help compensated silicon to tolerate higher boron concentrations without any noticeable impact on the efficiency after degradation [56].

4.3 Compensation engineering

Compensation engineering is the control of the concentrations of both types of dopants to obtain the desired bulk resistivity. The effects of adjusting the resistivity will be explained in the next subsection. Then the benefits of adding gallium in the solidification step are presented.

4.3.1 Control of the majority carrier concentration

The removal of phosphorus and boron by alternative purification methods to the Siemens process can be challenging. If a high concentration of one of these elements remain in the final product, compensation engineering is a good method

to adjust the majority carrier concentration, and thus the recombination lifetime. Forster et al. has shown experimentally the enhancement of lifetime by compensation engineering in Ref. [47].

The ingots Cz♯U1 and Cz♯U2 from Ref. [47] were grown with the same crystallization process, in the same conditions and with the same silicon feedstock. They have identical impurity profiles apart from phosphorus and gallium which were added in Cz♯U2 to reduce the majority carrier concentration. Adding gallium allows a better control of the resistivity profile together with the removal of a possible p/n changeover along the ingot. This will be explained in further details in the next subsection. The lifetime along the ingot is diplayed in Fig. 4.5. The ingot Cz♯U2 shows a clearly higher lifetime compared to ingot Cz♯U1, proving the effect of compensation engineering on the lifetime.

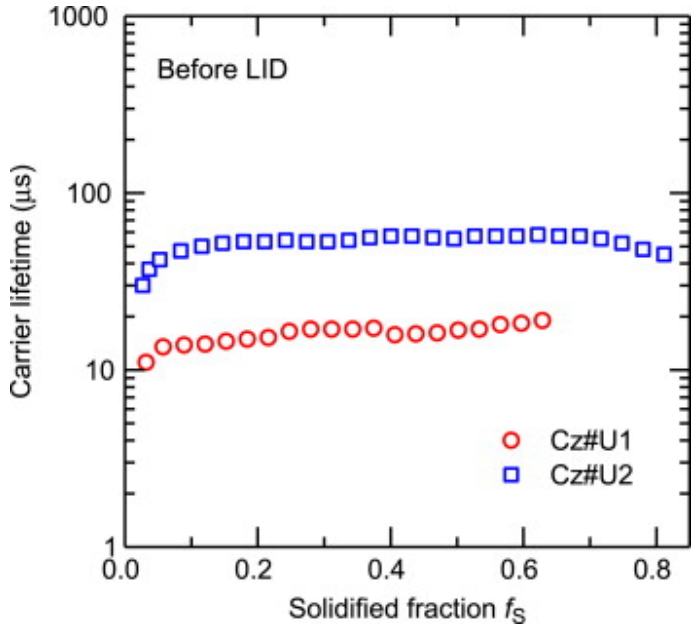

Figure 4.5: Carrier lifetime measured by μW-PCD along ingots Cz♯U1 and Cz♯U2. Reprinted from [47].

The drawback is that after LID the B-O defect is formed and becomes the main lifetime-limiting recombination center. This means that the lifetimes of the two ingots equal, and the lower mobility of the more compensated ingot (Cz♯U2) will give lower efficiencies. Therefore compensation engineering is a good solution for feedstock containing a high concentration of either boron or phosphorus, but as long as the lifetime is ruled by the B-O recombination center, having the lowest

possible concentration of boron (without reducing the global performances) can only be advantageous. The main asset of n-type silicon where boron is not present is the absence of LID. However n-type compensated silicon contains boron, and therefore suffers of performance losses after LID, making this material not very attractive for solar cells manufacturing.

4.3.2 Addition of gallium

P-type compensated silicon, when only containing boron and phosphorus (which is the case of UMG-Si), can have a low ingot yield due to a p/n changeover along the ingot. It is caused by different segregation coefficients: 0.8 for boron, and 0.35 for phosphorus. A segregation coefficient of 1 would give a uniform distribution of the element along the ingot, while a coefficient close to 0 would give a quasi absence of this element till the very top of the ingot where it would be found in extremely high concentration. This means phosphorus, with a segregation coefficient lower than boron, will be found in larger proportions in the top-part, causing the doping to change from p ([B]>[P]) to n ([P]>[B]). Even though the industry proceeds to a top-cut to remove impurities, for standard resistivities the p/n changeover occurs at $\sim 80\%$ of the solidified fraction. This reduces greatly the ingot yield.

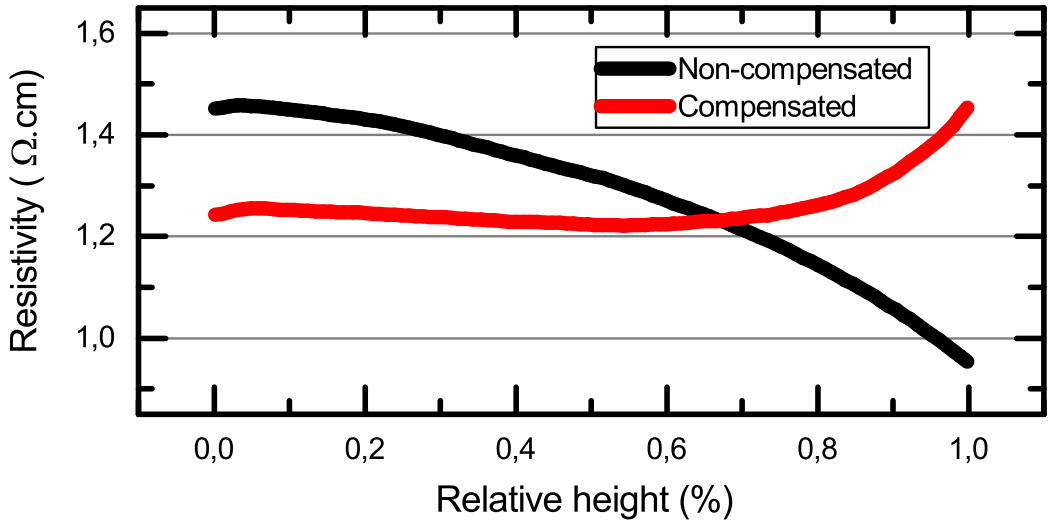

Figure 4.6: Resistivity measured by Semilab Eddy current along a compensated ingot and a non-compensated ingot for a targeted resistivity of 1.3Ω.cm.

To cope for this loss, a solution was proposed in Ref. [57] by the introduction

of gallium in the melt. This element has a segregation coefficient of 0.008. If the amount of boron, phosphorus and gallium are correctly adjusted then no p/n changeover is observed along the ingot. The addition of gallium can even give a quasi-constant resistivity profile [32, 58]. The resistivity profiles of a compensated ingot containing gallium and a non-compensated ingot are shown in Fig. 4.6. The targeted resistivity was 1.3 Ω·cm for both ingots. The non-compensated ingot shows the typical decrease due to the increase of the boron concentration, and the difference in resistivity from top to bottom is 0.5 Ω·cm. For non-compensated ingot, the resistivity is constant up to 80% of the ingot and then it starts to rise due to the concentration in phosphorus which increases faster than the boron concentration. Gallium should invert the curve at the top part and the resistivity should drop, but the top-cut (not shown in the figure) removed this part. Moreover the resistivity difference between the top and the bottom is only 0.2 Ω·cm. This shows the clear advantage of using gallium to control the resistivity profile and get a more constant resistivity.

4.4 Impact of dopant compensation on the performances of solar cells

As mentioned earlier, compensation has an impact on both lifetime and mobility. Compensation engineering enables the control of the majority carrier concentration through which high lifetime can be obtained. However UMG-Si present more impurities than EG-Si, resulting in a reduced minority carrier lifetime [3]. This drawback can become even worse after LID due to the higher concentration of boron in compensated material [24, 27, 47, 51]. However the formation of the B-P complex can prevent the formation of the B-O complex [56]. This can explain why no significant difference in efficiencies after LID is observed between ESS® and polysilicon [5, 26, 27, 55].

Both majority and minority mobilities are also reduced in compensated silicon, and the effect is stronger for dopant concentrations where incomplete ionization happens [41, 42, 43, 59].

I_{sc} increases as a function of the minority carrier diffusion length (L_{min}), which can be written as:

$$L_{\text{min}} = \sqrt{\tau_{\text{eff}} \times \mu_{\text{min}} \times \frac{kT}{q}}. \tag{4.6}$$

We see that both the effective lifetime and the carrier mobility (μ_{min}) of the minority carrier have to be maximized to get the best current.

The maximum V_{oc} is obtained when a trade-off between the excess carrier and the majority carrier concentrations is found. This is shown in the next equation:

$$V_{\text{oc}} \approx kT \times \ln\left(\frac{\left(n_{\text{maj}} + \Delta n\right) \times \Delta n}{n_{\text{i}}^2}\right) \tag{4.7}$$

where Δn is the excess carrier concentration.

As explained in the section 4.3, a low majority carrier concentration will raise the lifetime, improving at the same time the excess carrier concentration. So these two parameters are negatively correlated, hence the need for a maximization investigation.

If we sum up, V_{oc} needs a high majority carrier concentration, which will reduce both the lifetime and the mobility. This goes against a high I_{sc}. This shows the challenge of achieving the highest efficiencies. On top of that comes compensation engineering for material containing both types of dopants. A thorough analysis of the impact of compensation on cell parameters can be found in Ref. [60]. In summary, a solar cell made of compensated silicon should theoretically show reduced lifetime and mobility because of the higher dopant concentrations, and thus a lower efficiency. However in mc-Si solar cells and for lightly compensated material, no significant difference is observed [5, 26, 27, 55]. Crystallographic defects and the B-O complex are the main causes of performance losses.

Chapter 5

Temperature coefficients of compensated silicon solar cells

In this chapter a review of the different studies on temperature coefficients of UMG-Si will be given in the first section. Then the impact of the compensation level on the temperature sensitivity will be presented. Finally a method to improve the temperature sensitivity of a solar cell will be described in section 5.3.

5.1 Review

A reduced degradation with temperature of the conversion efficiency of solar cells made of compensated silicon was first observed on the cell level by Tanay et al. in Ref. [7] where the temperature coefficient of the I_{sc} was larger for compensated material. This difference was explained to originate from two different mechanisms. These are:

- the mobility of compensated silicon that is quasi-constant with temperature for high concentrations of dopants because of the ionized impurity scattering dominating at low temperature as explained in subsection 4.2.2.

- decorated crystallographic defects or impurities limiting the diffusion length which are temperature dependent. This can be explained by a capture cross section which decreases with temperature (such as molybdenum, manganese, or interstitial iron [61, 62]).

The same year Petter et al. found that modules made of compensated silicon were having better energy output in the summer than those made of polysilicon from the Siemens process [35]. This gives indications of a favorable behavior of compensated silicon at higher operating temperature.

Several other studies comparing the temperature sensitivity or the energy yield of compensated silicon solar cells or modules with non-compensated silicon found similar results [8, 9, 10, 12, 36]. The reason was always a favorable temperature coefficient of the I_{sc} for compensated silicon.

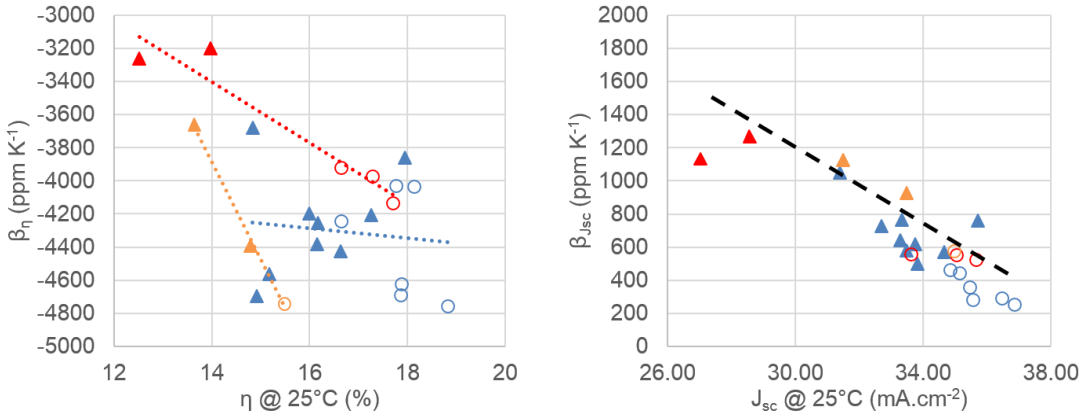

(a) (b)

Figure 5.1: Temperature coefficients of solar cells made from standard EG-Si (open circles) and compensated Si (filled triangles). The data in red, blue and orange are from Ref. [7, 12, 10] respectively. Note that the values plotted in red were estimated from the data in Ref. [7]. a) Temperature coefficient of the efficiency density plotted against efficiency at 25°C. The dotted lines are linear fits that are not based on any physical model but are simply plotted here to show the trends in the data. The linear fit on the data from [12] is really poor. This may be caused by the fact that difference fabrication processes were used for the cells in this study. b) Temperature coefficient of the short-circuit current density plotted against short-circuit current density at 25°C. Reprinted from [63].

Dupré in Ref. [63] gathered the data from Ref. [7, 10, 12] into Fig. 5.1. We see that the lowest efficiency cells possess the best temperature coefficients (Fig. 5.1a). This is somewhat surprising because the temperature coefficient of V_{oc} normally accounts for most of the temperature coefficient of the efficiency. And a larger V_{oc} improves both the efficiency and the temperature coefficient of V_{oc} (and therefore of the efficiency) as shown in Eq. 2.7 and 2.15. This inverse correlation is explained in Fig. 5.1b where the temperature coefficient of J_{sc} is

plotted as a function of J_{sc}. The compensated silicon solar cells show the lowest currents, explaining partially the lower efficiencies. The reason is a combination of a lower mobility and lifetime in this material, as explained in section 4.2. However they have the best temperature coefficients of J_{sc}. An almost linear trend is found between the temperature coefficients of J_{sc} and J_{sc}.

This lower J_{sc} for compensated silicon solar cells is partly due to a lower mobility, because of more ionized impurity scattering. This weakens the temperature dependence of the mobility at room temperature for both the majority and the minority carriers (see subsection 4.2.2). This may explain at least partially the better temperature coefficient of J_{sc} [7].

The second part is a lower lifetime, causing a lower diffusion length (see subsection 4.2.3). Many recombination centers have a capture cross section decreasing with temperature [61, 62]. Thus the lifetime of compensated silicon, more limited by these defects would come closer to the lifetime of non-compensated silicon samples at high temperature. This results in a larger temperature coefficient of J_{sc} [7].

These results seem to indicate that the closer the efficiency of compensated silicon solar cells will get to the efficiency of non-compensated silicon solar cells, the smaller will be the beneficial temperature dependence of the compensated silicon solar cells, as pointed out by Dupré in Ref. [63].

5.2 Results

In this section, we are presenting part of the work in the papers A and E where mc-Si solar cells with different compensation levels were investigated. The solar cells are processed from wafers from the centre brick of four different ingots with the same targeted resistivity. These ingots were made of a blend-in of compensated silicon (ESS®) and non-compensated silicon (from a FBR). The wafers were then manufactured into Al-BSF cells in a laboratory production line. The description of the solar cells is given in Table 5.1.

The four different blend-in-ratios will vary the compensation level at the bottom of the ingots, from 1.4 for the lowest blend-in-ratio to 2.2 for the highest. Then this compensation level will naturally increase according to the different segregation coefficients of boron and phosphorus. The relative temperature coefficient of

Table 5.1: Description of the ingots.

Ingot name	Mean resistivity (Ω.cm)	Dopants	Blend-in ratio (% ESS®)
CL1	1.22	B-P	25
CL2	1.25	B/Ga-P	40
CL3	1.25	B/Ga-P	56
CL4	1.27	B/Ga-P	73

the efficiency is plotted as a function of the compensation for the four different ingots in Fig. 5.2. All four ingots have the same trend, an increasing temperature coefficient with an almost constant compensation level at the bottom, then the compensation level starts increasing while the temperature coefficient keeps increasing steadily. This is an artefact of the effect of the relative height of the as cast ingots on the temperature coefficients as explained in Ref. [64]. The improvement of the temperature coefficient is only due to an increase of the relative height, which is correlated to the compensation level (especially at the end). This is further confirmed by the fact that all four ingots present the same trend only shifted along the compensation level axis.

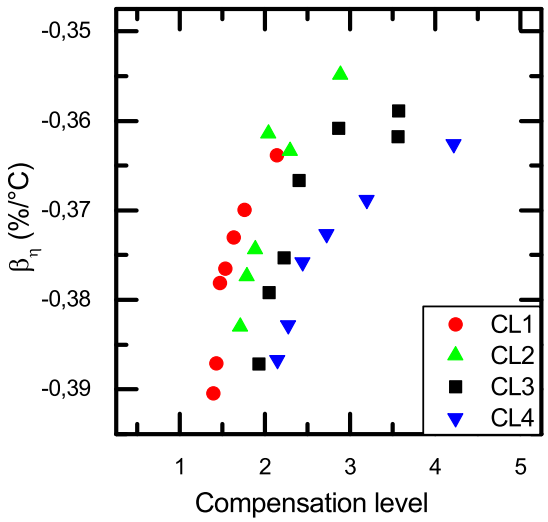

Figure 5.2: Relative temperature coefficient of the efficiency as a function of the compensation for the four different ingots described in Table 5.1

To check the absence of correlation we plotted the mean values of the relative temperature coefficient of the efficiency shown in Fig. 5.2 with error bars

which represent two times the standard deviation for the four ingots. We observe that there is no statistically significant difference between the ingots with different blend-in-ratios.

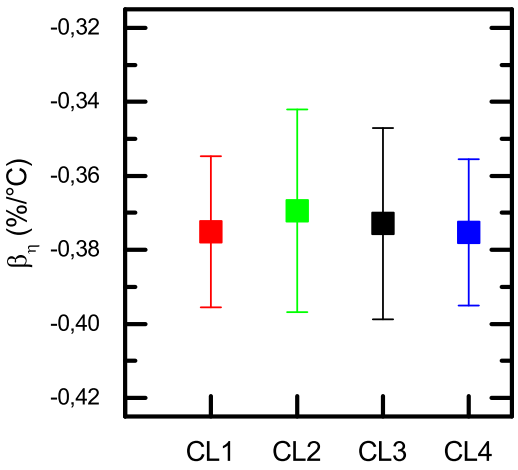

Figure 5.3: Mean relative temperature coefficient of the efficiency shown in Fig 5.2. The error bars represent two times the standard deviation.

In conclusion, on this small compensation level range (ESS® being a lightly compensated silicon as discussed in subsection 3.4), no effect of the compensation is observed. Moreover increasing the blend-in-ratio of ESS® can raise the impurity concentrations. Moreover certain impurities show a positive temperature dependence of the lifetime (such as the B-O defect), which can explain an improved temperature coefficient [7]. This is not observed in this study neither.

5.3 Reducing the temperature sensitivity by compensation engineering

The temperature coefficient is rarely considered as a design parameter. The main contribution of the temperature coefficient of the efficiency is the temperature coefficient of V_{oc}, which improves with V_{oc}. This means that the solar cells with the best efficiencies will normally present the lowest temperature sensitivities. Therefore a good efficiency should also give a small temperature sensitivity.

Furthermore silicon heterojunction solar cells, which have the record V_{oc} for silicon solar cells [65], and thus very high temperature coefficients of V_{oc} [66], benefit as well from a reduced temperature coefficient of their FF due to a positive dependence with temperature of their transport mechanisms (thermionic emission and tunneling) [21, 67]. This reduces even more their temperature sensitivity.

In 1994, Landis et al. in Ref. [16] envisaged to have the temperature coefficients as a design parameter, and that "increasing open-circuit voltage, even at the expense of decreases in other cell parameters (for example, by increasing base doping of the cell) may result in higher power under actual space operating conditions". It was shown in Ref. [11] that decreasing the bulk resistivity improves all temperature coefficients (V_{oc}, I_{sc}, FF and conversion efficiency). Ponce-Alcántara et al. in Ref. [12] showed that the resistivity has a very strong influence on the temperature coefficients. Similar results were obtained in Ref. [68].

Compensation engineering, with the addition of gallium during the solidification step, enables relatively constant resistivity. This means that low bulk resistivities are possible for compensated silicon. Whereas for non-compensated silicon, the continuously decreasing resistivity along the ingot would greatly diminish the efficiencies at the top part of the ingot if too low resistivities were achieved. It can therefore be suggested that compensated silicon is the best choice for reducing the temperature sensitivity by increasing the base doping.

When the temperature coefficients of UMG-Si were compared to those of silicon from the Siemens process, the bulk resistivity was rarely taken into account [7, 8, 9, 10, 35, 36]. Lower bulk resistivities, compared to non-compensated silicon, were used to maximize the ingot yield in presence of a p/n changeover, when no gallium was added. This might have contributed to the better results reported for the temperature sensitivity of UMG-Si.

Chapter 6

Summary of papers

Paper A: Temperature coefficients of compensated silicon solar cells – influence of ingot position and blend-in-ratio

In this article, a preliminary study is made on the influence of the blend-in-ratio between compensated and non-compensated silicon on the temperature coefficients. Two ingots with different blend-in-ratios, and thus compensation levels, were investigated. Solar cells covering the whole ingots height were measured. No statistically significant difference was noticed between the temperature coefficients of the cells from the two ingots. This indicates that the compensation level does not have a strong influence, if any, on the temperature coefficients. However a clear trend along the ingot height was observed. And the cells with the smallest temperature sensitivities are found at the top of the ingot.

Paper B: Temperature dependent quantum efficiencies in multicrystalline silicon solar cells

This article was made in parallel with the previous one. EQE measurements were made at two different temperatures. The equivalent short-circuit currents were calculated from these measurements, as well as the temperature coefficients of the short-circuit current. It confirms the previous result that the best temperature coefficients of the short-circuit current are measured at the top of the ingot. The dif-

ference between compensated and non-compensated silicon was also investigated. The temperature coefficient of the short-circuit current of compensated silicon solar cells is larger than the one of non-compensated silicon solar cells. The study has only considered two cells of each type, which does not allow any affirmation. However this result is in agreement with previous studies. This difference comes from a slightly larger improvement with temperature in the 800 nm to 1100 nm wavelength range for the compensated silicon solar cells.

Paper C: Reduced temperature sensitivity of multicrystalline silicon solar cells with low ingot resistivity

In this article the temperature coefficients of three ingots with different resistivities were studied. A reference ingot made only of non-compensated silicon was also present. Raising the net doping increases the open-circuit voltage which gives better temperature coefficients of both the open-circuit voltage and the fill factor. However the short-circuit current was reduced, which decreases the efficiencies of the cells from the lowest resistivity ingot. But this reduction in short-circuit current has a positive impact on its temperature coefficient. The role of the net doping on the temperature coefficients was already known. So this study confirmed it on the material used in this experiment, and showed the efficiency decrease that can be caused by an increase of the net doping.

Paper D: Reduction of temperature coefficients in multicrystalline silicon solar cells after light-induced degradation

Studies reporting temperature coefficients do not always specify if the measurements were made before or after light-induced degradation. This paper shows that the temperature coefficient of the efficiency can be greatly reduced after light-soaking. This worsening comes from the diminution of all three temperature coefficients (short-circuit current, open-circuit voltage and fill factor). And the degradation of the temperature coefficients is more pronounced at the top of the ingot.

Paper E: Temperature sensitivity of multicrystalline silicon solar cells

This paper presents measured temperature coefficients of multicrystalline solar cells. An overview of the impact of different bulk resistivities, compensation levels, cell structures and relative heights along a brick is given. The influence of increasing the base net doping on the temperature sensitivity is explained in more details. It is shown that the parameter gamma (in the temperature coefficient of the open-circuit voltage) varies with the relative height. The temperature coefficient profile along the ingot depends on this parameter, and the variations of the cell parameters with the relative height. Therefore the best temperature coefficients are situated at different heights of the ingot depending on the cell structure. Light-induced degradation has a negative effect on the cell performances as well as on the temperature coefficients. It is observed that solar cells which are lightly compensated (with a majority carrier concentration in the same order of magnitude as the dopants concentrations) dont show an advantageous temperature coefficient compared to solar cells made of non-compensated silicon.

Paper F: On the variability of the temperature coefficients of mc-Si solar cells with irradiance

The objective of this article was to investigate the irradiance dependence of the temperature coefficients. As cell parameters are varying with irradiance, the temperature coefficients should be influenced as well. In the models found in the literature, a constant temperature coefficient with irradiance is always assumed, which can lead to some errors. It was shown that the temperature sensitivity is greatly increased at low irradiance, because of the decrease of the open-circuit voltage. However as it is at low irradiance, when temperatures are the lowest, the expected impact on device modelling is not significant.

Chapter 7

Conclusions and Outlook

This Ph.D. dissertation has presented experimental results on the temperature coefficients of multicrystalline silicon solar cells. A special interest was given on the choice of the feedstock to attain the best temperature coefficients. The different factors influencing the temperature coefficients in a complete ingot were discussed. This thesis can help solar cell manufacturers to have more insights on how they can control and improve their temperature coefficients.

7.1 Conclusions on the temperature coefficients in mc-Si

In this thesis it is shown that the temperature sensitivities of solar cells made from an ingot are influenced by many parameters. Reducing the ingot resistivity is a promising way to reach good temperature coefficients, and compensated silicon is a promising material to achieve that thanks to the resistivity control that can be obtained by the addition of gallium. However increasing the net doping leads to a lower efficiency and a compromise should be found. Moreover a higher net doping conduces to a lower breakdown voltage which can be harmful to the solar cells.

The temperature coefficients are varying along the ingot. While the Al-BSF cells have the lowest temperature coefficients in magnitude at the top of the ingot, PERC cells have them in the middle. This is explained by a combination of the cell parameters variation along the ingot and the changes of recombination mechanisms.

Light-induced degradation has a negative effect on the temperature coefficients.

This is only due to the cell parameters decrease. A possible effect on the gamma parameter of the temperature coefficient of the open-circuit voltage was not observed. Therefore when reporting temperature coefficients, we suggest to specify if it was measured before or after light-induced degradation.

The impact of irradiance on the temperature coefficients is rather small. The temperature sensitivity of a silicon solar cell is the strongest at low irradiance, which is when the temperature is the lowest. An example of where this model would bring more accuracy is in polar conditions. It is in low irradiance conditions in summer for a very long period (up to 24 hours above the Arctic circle or below the Antarctic circle) with temperatures often below 25°C. In this case a solar module would perform better than what the model would predict.

7.2 Future Work / Outlook

It was shown that reducing the ingot resistivity would give better temperature coefficients. However the efficiency and the breakdown voltage can be reduced. A further analysis would be needed to assess if a small efficiency loss with a better temperature coefficient can result in a higher energy yield in field operation. If it is the case, the study of how far can the energy yield be increased while still complying with breakdown voltages standards should be done.

Depending on the solar cell design and thus if a gap large enough between the cells with the highest temperature coefficients and the cells with the lowest temperature coefficients is observed, splitting these cells to produce different solar panels might be an interesting idea. Previously the solar cells were selected according to their efficiencies. Yet with the high performance crystallisation techniques the variation of the efficiency along the ingot was greatly reduced. Therefore manufacturing solar panels with comparable efficiencies, but different temperature coefficients is something to investigate.

We have observed a variation of the gamma parameter in the temperature coefficient of the open-circuit voltage along the ingot height. This is coming from a variation of the recombination mechanisms along the ingot. This parameter could be a new way to give information about recombination mechanisms.

References

[1] M. A. Green, K. Emery, Y. Hishikawa, W. Warta, and E. D. Dunlop, "Solar cell efficiency tables (version 45)," *Progress in photovoltaics: research and applications*, vol. 23, no. 1, pp. 1–9, 2015.

[2] "Technology roadmap – solar photovoltaic energy," International Energy Agency, Tech. Rep., 2014.

[3] F. Rougieux, C. Samundsett, K. C. Fong, A. Fell, P. Zheng, D. Macdonald, J. Degoulange, R. Einhaus, and M. Forster, "High efficiency umg silicon solar cells: impact of compensation on cell parameters," *Progress in Photovoltaics: Research and Applications*, vol. 24, no. 5, pp. 725–734, 2016.

[4] P. Engelhart, J. Wendt, A. Schulze, C. Klenke, A. Mohr, K. Petter, F. Stenzel, S. Hörnlein, M. Kauert, M. Junghänel *et al.*, "R&d pilot line production of multi-crystalline si solar cells exceeding cell efficiencies of 18%," *Energy Procedia*, vol. 8, pp. 313–317, 2011.

[5] S. Zhang, E. J. Øvrelid, M. Di Sabtino, M. Juel, and G. Tranell, "Cz-silicon produced from solar-grade and recycled materials. part ii: Investigating performances of solar cell produced from solar-grade cz-silicon," *Metallurgical and Materials Transactions E*, vol. 2, no. 1, pp. 20–26, 2015.

[6] S. Pizzini, "Towards solar grade silicon: Challenges and benefits for low cost photovoltaics," *Solar Energy Materials and Solar Cells*, vol. 94, no. 9, pp. 1528–1533, 2010.

[7] F. Tanay, S. Dubois, N. Enjalbert, and J. Veirman, "Low temperature-coefficient for solar cells processed from solar-grade silicon purified by metallurgical route," *Progress in Photovoltaics: Research and Applications*, vol. 19, no. 8, pp. 966–972, 2011.

[8] L. Cai, X. Ren, B. Fan, J. Zheng, and C. Chen, "Effect of temperature on crystalline silicon solar cells processed from chemical and metallurgical route," *Optik - International Journal for Light and Electron Optics*, vol. 125, no. 15, pp. 3918–3921, 2014.

[9] M. Tayyib, J. O. Odden, and T. O. Saetre, "Effect of temperature and sun intensity on multicrystalline silicon solar cells," in *European Photovoltaic Energy Solar Conference (EU PVSEC)*, 2013, Conference Proceedings.

[10] C. Xiao, X. Yu, D. Yang, and D. Que, "Impact of solar irradiance intensity and temperature on the performance of compensated crystalline silicon solar cells," *Solar Energy Materials and Solar Cells*, vol. 128, pp. 427–434, 2014.

[11] M. Mueller, A. Schulze, J. Isemberg, B. Hund, and H. G. Beyer, "Influence of the wafer resistivity on the temperature coefficients of industrial silicon solar cells and on the expected performance behaviour," in *Prceeding of 25th EU PVSEC/WCPEC-5 conference*, 2010, pp. 2600–2603.

[12] S. Ponce-Alcántara, J. P. Connolly, G. Snchez, J. M. Mguez, V. Hoffmann, and R. Ords, "A statistical analysis of the temperature coefficients of industrial silicon solar cells," *Energy Procedia*, vol. 55, pp. 578–588, 2014.

[13] M. A. Green, "General temperature dependence of solar cell performance and implications for device modelling," *Progress in Photovoltaics: Research and Applications*, vol. 11, no. 5, pp. 333–340, 2003.

[14] O. Dupr, R. Vaillon, and M. A. Green, "Physics of the temperature coefficients of solar cells," *Solar Energy Materials and Solar Cells*, vol. 140, pp. 92–100, 2015.

[15] J. Zhao, A. Wang, S. Robinson, and M. Green, "Reduced temperature coefficients for recent highperformance silicon solar cells," *Progress in Photovoltaics: Research and Applications*, vol. 2, no. 3, pp. 221–225, 1994.

[16] G. A. Landis, "Review of solar cell temperature coefficients for space," in *XIII Space Photovoltaic Research and Technology Conference (SPRAT XIII)*, vol. 3278, 1994, Conference Proceedings, p. 385.

[17] M. A. Green, "Radiative efficiency of state-of-the-art photovoltaic cells," *Progress in Photovoltaics: Research and Applications*, vol. 20, no. 4, pp. 472–476, 2012.

[18] Y. Lee, C. Park, N. Balaji, Y. Lee, and V. A. Dao, "Highefficiency silicon solar cells: A review," *Israel Journal of Chemistry*, vol. 55, no. 10, pp. 1050–1063, 2015.

[19] M. Green, K. Emery, and A. Blakers, "Silicon solar cells with reduced temperature sensitivity," *Electronics Letters*, vol. 18, no. 2, pp. 97–98, 1982.

[20] M. A. Green, "Solar cell fill factors: General graph and empirical expressions," *Solid-State Electronics*, vol. 24, pp. 788 – 789, 1981, ¡br /¿.

[21] J. P. Seif, A. Descoeudres, M. Filipi, F. Smole, M. Topi, Z. C. Holman, S. De Wolf, and C. Ballif, "Amorphous silicon oxide window layers for high-efficiency silicon heterojunction solar cells," *Journal of Applied Physics*, vol. 115, no. 2, p. 024502, 2014.

[22] M. Langenkamp and O. Breitenstein, "Classification of shunting mechanisms in crystalline silicon solar cells," *Solar energy materials and solar cells*, vol. 72, no. 1, pp. 433–440, 2002.

[23] J.-H. Guo, P. J. Cousins, and J. E. Cotter, "Investigations of parasitic shunt resistance in n-type buried contact solar cells," *Progress in Photovoltaics: Research and Applications*, vol. 14, no. 2, pp. 95–105, 2006.

[24] J. Geilker, W. Kwapil, and S. Rein, "Light-induced degradation in compensated p- and n-type czochralski silicon wafers," *Journal of Applied Physics*, vol. 109, no. 5, p. 053718, 2011.

[25] S. Dubois, N. Enjalbert, and J. P. Garandet, "Slow down of the light-induced-degradation in compensated solar-grade multicrystalline silicon," *Applied Physics Letters*, vol. 93, no. 10, p. 103510, 2008.

[26] J. Odden, T. Lommasson, M. Tayyib, J. Vedde, T. Buseth, K. Friestad, H. Date, and R. Tronstad, "Results on performance and ageing of solar modules based on elkem solar silicon (ess) from installations at various locations," *Solar Energy Materials and Solar Cells*, vol. 130, pp. 673–678, 2014.

[27] M. Tayyib, Y. H. Rao, M. Ramanjaneyulu, T. Surendra, J. O. Odden, and T. O. Saetre, "Initial light-induced degradation study of multicrystalline modules made from silicon material processed through different manufacturing

routes," in *Photovoltaic Specialists Conference (PVSC), 2012 38th IEEE*. IEEE, 2012, pp. 002 395–002 399.

[28] K. Emery, J. Burdick, Y. Caiyem, D. Dunlavy, H. Field, B. Kroposki, T. Moriarty, L. Ottoson, S. Rummel, and T. Strand, "Temperature dependence of photovoltaic cells, modules and systems," in *Photovoltaic Specialists Conference, 1996., Conference Record of the Twenty Fifth IEEE*. IEEE, 1996, Conference Proceedings, pp. 1275–1278.

[29] O. Dupre, R. Vaillon, and M. A. Green, "Experimental assessment of temperature coefficient theories for silicon solar cells," *Photovoltaics, IEEE Journal of*, vol. 6, no. 1, pp. 56–60, 2016.

[30] J. Safarian, G. Tranell, and M. Tangstad, "Processes for upgrading metallurgical grade silicon to solar grade silicon," *Energy Procedia*, vol. 20, pp. 88–97, 2012.

[31] R. Glöckner and M. de Wild-Scholten, "Energy payback time and carbon footprint of elkem solar silicon®," *Proceedings of the 27 th EUPVSEC, Frankfurt, Germany*, 2012.

[32] A. Cuevas, M. Forster, F. Rougieux, and D. Macdonald, "Compensation engineering for silicon solar cells," *Energy Procedia*, vol. 15, pp. 67–77, 2012.

[33] J. Degoulange, R. Einhaus, J. Kraiem, F. Cocco, D. Grosset, Y. Andrault, and P. Pappet, "High efficiency heterojunction solar cells on highly purified n-type umg cz wafers," *Energy Procedia*, 2012.

[34] P. Preis, F. Buchholz, P. Diaz-Perez, J. Glatz-Reichenbach, C. Peter, S. Schmitt, J. Theobald, K. Peter, and A.-K. Søiland, "Towards 20% solar cell efficiency using silicon from metallurgical process route," *Energy Procedia*, vol. 55, pp. 589–595, 2014.

[35] K. Petter, M. Strobel, D. Buss, M. Mette, Y. Ludwig, S. Malik, S. Rupp, and P. Wawer, "Long term stability of solar modules made from compensated sog-si or umg-si solar cells," *Energy Procedia*, vol. 8, pp. 365–370, 2011.

[36] M. Tayyib, J. O. Odden, and T. O. Saetre, "Irradiance dependent temperature coefficients for mc solar cells from elkem solar grade silicon in comparison with reference polysilicon," *Energy Procedia*, vol. 55, pp. 602–607, 2014.

[37] "Photovoltaics report," Fraunhofer Institute for Solar Energy Systems, ISE, Tech. Rep., 06 2016.

[38] G. del Coso, C. del Caizo, and W. C. Sinke, "The impact of silicon feedstock on the pv module cost," *Solar Energy Materials and Solar Cells*, vol. 94, no. 2, pp. 345–349, 2010.

[39] D. Klaassen, "A unified mobility model for device simulation–I. Model equations and concentration dependence," *Solid-State Electronics*, vol. 35, no. 7, pp. 953–959, 1992.

[40] D. Klaassen, "A unified mobility model for device simulatio–II. Temperature dependence of carrier mobility and lifetime," *Solid-State Electronics*, vol. 35, no. 7, pp. 961–967, 1992.

[41] M. Forster, A. Cuevas, E. Fourmond, F. E. Rougieux, and M. Lemiti, "Impact of incomplete ionization of dopants on the electrical properties of compensated p-type silicon," *Journal of Applied Physics*, vol. 111, no. 4, p. 043701, 2012.

[42] F. E. Rougieux, D. Macdonald, A. Cuevas, S. Ruffell, J. Schmidt, B. Lim, and A. P. Knights, "Electron and hole mobility reduction and hall factor in phosphorus-compensated p-type silicon," *Journal of Applied Physics*, vol. 108, no. 1, p. 013706, 2010.

[43] F. Schindler, M. Forster, J. Broisch, J. Schn, J. Giesecke, S. Rein, W. Warta, and M. C. Schubert, "Towards a unified low-field model for carrier mobilities in crystalline silicon," *Solar Energy Materials and Solar Cells*, vol. 131, pp. 92–99, 2014.

[44] H. Wagner, J. Hofstetter, B. Mitchell, P. P. Altermatt, and T. Buonassisi, "Device architecture and lifetime requirements for high efficiency multicrystalline silicon solar cells," *Energy Procedia*, vol. 77, pp. 225–230, 2015.

[45] D. Macdonald and A. Cuevas, "Recombination in compensated crystalline silicon for solar cells," *Journal of Applied Physics*, vol. 109, no. 4, pp. 043 704–043 704–8, 2011.

[46] S. Dubois, N. Enjalbert, and J. P. Garandet, "Effects of the compensation level on the carrier lifetime of crystalline silicon," *Applied Physics Letters*, vol. 93, no. 3, p. 032114, 2008.

[47] M. Forster, P. Wagner, J. Degoulange, R. Einhaus, G. Galbiati, F. E. Rougieux, A. Cuevas, and E. Fourmond, "Impact of compensation on the boron and oxygen-related degradation of upgraded metallurgical-grade silicon solar cells," *Solar Energy Materials and Solar Cells*, vol. 120, pp. 390–395, 2014.

[48] S. Bernardini, D. Saynova, S. Binetti, and G. Coletti, "Light-induced degradation in compensated mc-si p-type solar cells," in *Photovoltaic Specialist Conference (PVSC), 2012 IEEE 38th*. IEEE, 2012.

[49] J. Schmidt, B. Lim, D. Walter, K. Bothe, S. Gatz, T. Dullweber, and P. P. Altermatt, "Impurity-related limitations of next-generation industrial silicon solar cells," *IEEE JOURNAL OF PHOTOVOLTAICS*, vol. 3, no. 1, pp. 114–118, 2013.

[50] T. Niewelt, J. Schön, J. Broisch, S. Rein, J. Haunschild, W. Warta, and M. C. Schubert, "Experimental proof of the slow light-induced degradation component in compensated n-type silicon," in *Solid State Phenomena*, vol. 242. Trans Tech Publ, 2016, pp. 102–108.

[51] B. Lim, F. Rougieux, D. Macdonald, K. Bothe, and J. Schmidt, "Generation and annihilation of boron?oxygen-related recombination centers in compensated p- and n-type silicon," *Journal of Applied Physics*, vol. 108, pp. 103 722–9, 11 2010.

[52] J. Schmidt and K. Bothe, "Structure and transformation of the metastable boron-and oxygen-related defect center in crystalline silicon," *Physical review B*, vol. 69, no. 2, p. 024107, 2004.

[53] K. Bothe, R. Sinton, and J. Schmidt, "Fundamental boron–oxygen-related carrier lifetime limit in mono-and multicrystalline silicon," *Progress in Photovoltaics: Research and Applications*, vol. 13, no. 4, pp. 287–296, 2005.

[54] S. Rein and S. Glunz, "Electronic properties of the metastable defect in boron-doped czochralski silicon: Unambiguous determination by advanced lifetime spectroscopy," *Applied Physics Letters*, vol. 82, no. 7, pp. 1054–1056, 2003.

[55] R. Søndenå, A.-K. Søiland, H. Angelskår, and A. Holt, "Light induced degradation in mc-si based on compensated silicon," *Energy Procedia*, vol. 27, pp. 70–75, 2012.

[56] K. Peter, R. Kopecek, M. Wilson, J. Lagowski, E. Enebakk, A. Soiland, and S. Grandum, "Multicrystalline solar grade silicon solar cells," in *Photovoltaic Specialists Conference (PVSC), 2010 35th IEEE*. IEEE, 2010, pp. 000 799–000 805.

[57] J. Kraiem, R. Einhaus, and H. Lauvray, "Doping engineering as a method to increase the performance of purified mg silicon during ingot crystallisation," in *Photovoltaic Specialists Conference (PVSC), 2009 34th IEEE*. IEEE, 2009, pp. 001 327–001 330.

[58] M. Forster, E. Fourmond, R. Einhaus, H. Lauvray, J. Kraiem, and M. Lemiti, "Ga co-doping in cz-grown silicon ingots to overcome limitations of b and p compensated silicon feedstock for pv applications," *physica status solidi (c)*, vol. 8, no. 3, pp. 678–681, 2011.

[59] J. Veirman, S. Dubois, N. Enjalbert, J. P. Garandet, and M. Lemiti, "Electronic properties of highly-doped and compensated solar-grade silicon wafers and solar cells," *Journal of Applied Physics*, vol. 109, no. 10, p. 103711, 2011.

[60] M. Forster, "Compensation engineering for silicon solar cells," Ph.D. dissertation, INSA de Lyon, 2012.

[61] B. Paudyal, K. McIntosh, D. Macdonald *et al.*, "Temperature dependent electron and hole capture cross sections of iron-contaminated borondoped silicon," in *34th IEEE Photovoltaic Specialist Conference*, 2009, pp. 1588–1593.

[62] B. B. Paudyal, K. R. McIntosh, D. H. Macdonald, and G. Coletti, "Temperature dependent carrier lifetime studies of mo in crystalline silicon," *Journal of Applied Physics*, vol. 107, no. 5, 2010.

[63] O. Dupré, "Physics of the thermal behavior of photovoltaic devices," monograph, INSA de Lyon, 2015.

[64] C. Berthod, R. Strandberg, and J. O. Odden, "Temperature coefficients of compensated silicon solar cellsinfluence of ingot position and blend-in-ratio," *Energy Procedia*, vol. 77, pp. 15–20, 2015.

[65] K. Masuko, M. Shigematsu, T. Hashiguchi, D. Fujishima, M. Kai, N. Yoshimura, T. Yamaguchi, Y. Ichihashi, T. Mishima, N. Matsubara *et al.*, "Achievement of more than 25% conversion efficiency with crystalline silicon heterojunction solar cell," *IEEE Journal of Photovoltaics*, vol. 4, no. 6, pp. 1433–1435, 2014.

[66] T. Mishima, M. Taguchi, H. Sakata, and E. Maruyama, "Development status of high-efficiency hit solar cells," *Solar Energy Materials and Solar Cells*, vol. 95, no. 1, pp. 18–21, 2011.

[67] J. P. Seif, G. Krishnamani, B. Demaurex, C. Ballif, and S. D. Wolf, "Amorphous/crystalline silicon interface passivation: Ambient-temperature dependence and implications for solar cell performance," *Photovoltaics, IEEE Journal of*, vol. 5, no. 3, pp. 718–724, 2015. [Online]. Available: http://ieeexplore.ieee.org/ielx7/5503869/7088664/07052350.pdf?tp=&arnumber=7052350&isnumber=7088664

[68] C. Berthod, R. Strandberg, J. O. Odden, and T. O. Stre, "Reduced temperature sensitivity of multicrystalline silicon solar cells with low ingot resistivity," in *Photovoltaic Specialist Conference (PVSC), 2016 IEEE 43rd*. IEEE, Conference Proceedings.

Paper A

Temperature coefficients of compensated silicon solar cells – influence of ingot position and blend-in-ratio

Charly Berthod, Rune Strandberg, Jan Ove Odden

This paper has been published as:

Berthod, C., Strandberg, R. and Odden, J.O. *5th International Conference on Silicon Photovoltaics, SiliconPV 2015* Konstanz, Germany.

Available online at www.sciencedirect.com

ScienceDirect

Energy Procedia 77 (2015) 15 – 20

Energy Procedia

5th International Conference on Silicon Photovoltaics, SiliconPV 2015

Temperature coefficients of compensated silicon solar cells – influence of ingot position and blend-in-ratio

Charly Berthod[a]*, Rune Strandberg[a], Jan Ove Odden[b]

[a]*Department of Engineering Sciences, University of Agder, Jon Lilletuns vei 9, 4879 Grimstad, Norway*
[b]*Elkem Solar AS, Fiskaaveien 100, 4621 Kristiansand S, Norway*

Abstract

Solar-grade silicon made from a metallurgical route presents boron and phosphorus compensation. Earlier work has shown that cells made from such material produce more energy than reference polysilicon modules when the temperature and irradiance is high. In the present study, solar cells from two different ingots with different blend-in-ratios were made from wafers at varying ingot heights in order to investigate how the temperature coefficients vary with compensation level and ingot height. The results suggest that solar modules made with solar cells from different ingot heights will perform differently at high temperature. It was also observed that the compensation level seems to have a smaller impact on the temperature coefficients than the ingot height.

Peer review by the scientific conference committee of SiliconPV 2015 under responsibility of PSE AG

Keywords: Compensated silicon; solar-grade silicon; temperature coefficient; ingot height; multicrystalline solar cells

1. Introduction

The ever present need for cost reductions in silicon production suggests replacing the well-established Siemens process [1] by metallurgical refining methods or even chemical routes. These processes offer not only well-known advantages, thanks to a reduction in the energy consumption and a lower carbon footprint of the solar cells [2], but also indications of a better temperature coefficient (TC) and larger specific electricity production in hot and sunny climate [3-6]. Elkem Solar Silicon® (ESS®) is produced by a metallurgical route that gives a low impurity

* Corresponding author. Tel.: +47 908 99 243.
E-mail address: charly.berthod@uia.no

Peer review by the scientific conference committee of SiliconPV 2015 under responsibility of PSE AG
doi:10.1016/j.egypro.2015.07.004

concentration [1]. It is a compensated material with both phosphorus and boron present because of the difficulty of removing these elements in metallurgical processes. Gallium can be added to increase the stability of the resistivity along the ingot and to secure an ingot yield not limited by resistivity or p/n changeover. The compensation leads to silicon with slightly different electronic properties, giving rise to differences in cell performance such as a lower short-circuit current (J_{sc}) and a higher open-circuit voltage (V_{oc}) [7].

The recent trend of replacing the Siemens process by cheaper methods in silicon production has led to an increase in the research on compensated silicon in order to determine the electronic properties of the solar cells made by such materials. In particular, the TC is of interest owing to the performance enhancements mentioned above [3-5]. These results on modules have been confirmed on cells, where the TCs of J_{sc}, V_{oc}, FF and efficiency of ESS®-cells were all found to be better compared to poly-silicon reference cells [8].

Understanding the variation of the efficiency of solar cells with temperature is important, and until now no comprehensive and general model has been developed that describes the TCs according to cell characteristics such as bulk resistivity, impurity content, dopants concentrations or compensation level. Since variations in the TCs are observed between different cells, it seems logical that a modification or an improvement of these coefficients is possible if the right measures are taken.

In the present study, the TCs were measured on solar cells made from wafers taken from different ingot heights of ingots consisting of compensated material mixed with poly-Si in two different blends. The results reveal information on how the compensation level and ingot height affects the temperature dependency of the solar cell characteristics.

2. Experimental procedure

Solar cells were selected from eight different heights along the ingot from the bottom to the top. The ingots came from the centre of a G5 furnace, and the solar cells were manufactured by the same producer, which is a research institute. This enables position tracking but gives lower efficiencies than compared to the industrial processing of the same wafers. The cells are multicrystalline silicon solar cells (15.6x15.6 cm^2) with a conventional aluminium back surface field (Al-BSF). The IV-characteristics were measured under a standard AM1.5G spectrum with a NeonSee™ AAA sun simulator at STC. The TCs were obtained by measuring the IV characteristics of a cell from 25°C to 50°C with one degree steps, and then performing a linear fitting of each parameter to get the temperature coefficients (as shown by Martin Green [9], over a limited temperature range the four IV parameters are linear with temperature.)

The blend-in ratios, resistivities and dopants of the two blended ingots (BIR-M and BIR-H), both having an ESS® blend-in ratio of >50%, are shown in Table 1.

Table 1. Ingots description.

Ingot name	Blend-in-ratio	Resistivity target (Ω cm)	Mean resistivity (Ω cm)	Dopants
BIR-M	medium	1.25	1.25	B/Ga-P
BIR-H	high	1.25	1.27	B/Ga-P

3. Results

The principal characteristics of the solar cells (J_{sc}, V_{oc} and the efficiency) are presented in Fig. 1. The trends along the ingot can be seen with the highest magnitude of the J_{sc}, V_{oc} and the efficiency near the bottom of the ingot where the lowest defect concentration is expected. Despite the different blend-in-ratios, no significant differences are seen on these cells, making them suited for a TC comparison without considering differences in the principal characteristics.

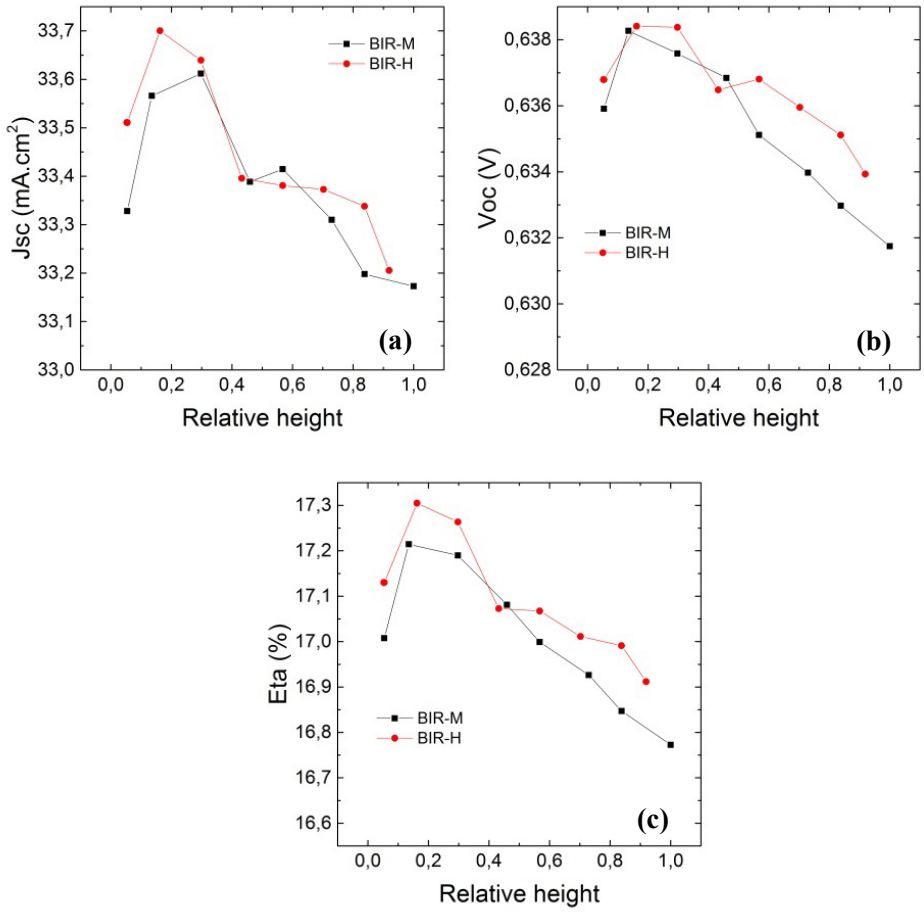

Fig. 1. (a) The short-circuit current density, (b) the open-circuit voltage and (c) the efficiency of the two different ingots taken on eight different locations along the ingots.

The relative TCs of the I_{sc}, V_{oc}, FF and the efficiency of the solar cells from both ingots are found to improve towards the top of the ingots, as shown in Fig. 2. The variation of these coefficients along the ingot is significant because earlier research has reported differences in the relative TC of the efficiency between compensated material and standard polysilicon in the range of 0.03%/°C ± 0.01 [5,8,10]. This work shows a difference of similar magnitude between a top and a bottom cell for both ingots (see Fig. 2d). The main contributing factor of the height-dependent variation of the TC for the efficiency is the variation of the TC of the I_{sc}, which increases at least 0.015%$_{abs}$/°C from bottom to top (see Fig. 2a).

Another observation to be made from Fig. 2 is that no particular discrepancy (or improvement) can be seen between ingots with different blend-in-ratios (i.e. different compensation levels). The variation along the ingot predominates over the difference between the two blend-in-ratios studied here. Reasons for this TC augmentation together with its implications will be discussed in the next part.

4. Discussion

It was noted above that the relative TC of the I_{sc} is the main contributor to the increase of the relative TC of the efficiency. This is the case although the relative TC of the I_{sc} is smaller in magnitude than the TCs of both the V_{oc} and the *FF* (Fig. 2). The I_{sc} increases slightly with temperature since the bandgap decreases with temperature and more photons are absorbed. Therefore, a rise in the TC of the I_{sc} along the ingot might be explained by an even stronger narrowing of the bandgap due to compensation. However, no difference between the ingots is visible, which discredits this hypothesis.

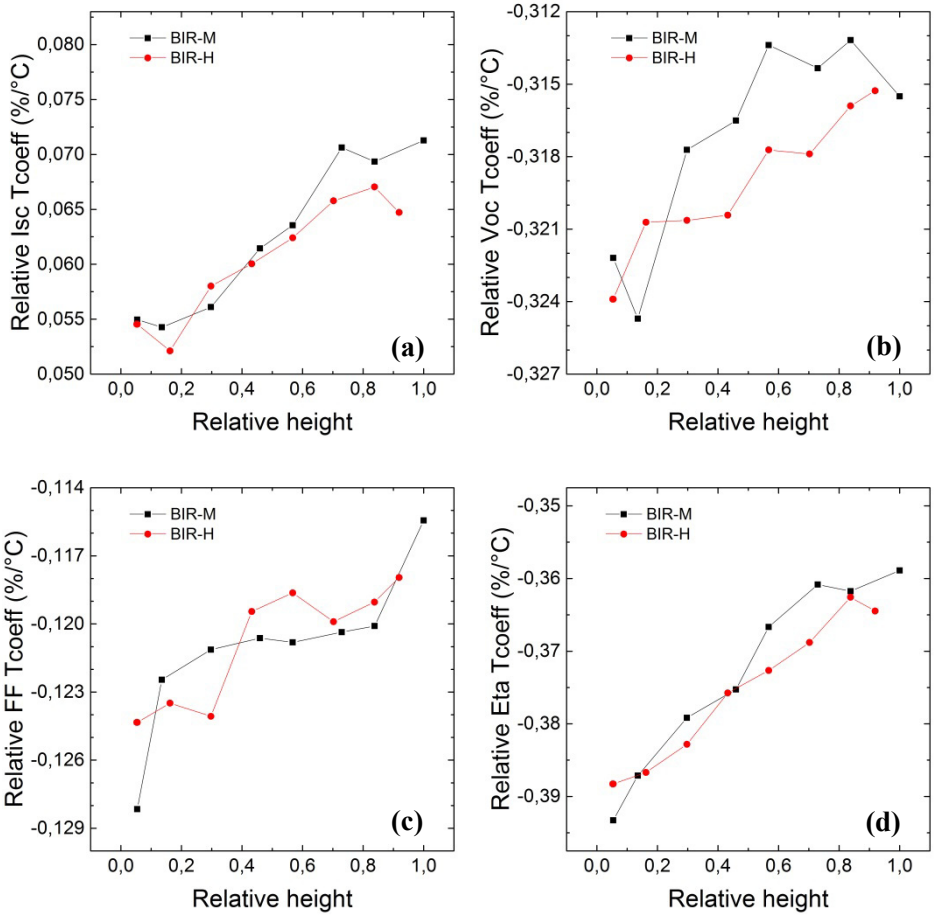

Fig. 2. The relative TCs of: (a) the short-circuit current, (b) the open-circuit voltage and (c) the fill factor and (d) the efficiency of the two different ingots taken on eight different locations along the ingots.

The relative TC of the V_{oc} is also increasing toward the top of the ingot (Fig. 2b), despite the fact that the V_{oc} decreases (Fig. 1b) mainly due to the increase in dislocation concentration towards the top. According to Ref. [9], the relative TC of the V_{oc} can be expressed as

$$\frac{1}{V_{OC}}\frac{dV_{OC}}{dT}=\frac{1}{T}-\frac{\frac{E_{g0}}{T}+k\gamma}{qV_{OC}} \quad (1)$$

where E_{g0} is the bandgap extrapolated linearly from the temperature of interest to 0 K, k is the Boltzmann's constant, γ is a constant equal to 3 and q is the elementary charge.

According to Equation (1), a decrease in the V_{oc} should actually decrease the relative TC of the V_{oc}. Thus the increase in the relative TC of V_{oc} is due to another mechanism. Our main assumption is that the increases of the relative TCs of the I_{sc} and V_{oc} are due to a recombination process that happens at larger rates in cells made from top wafers, due to impurity segregation, and that becomes less active with increasing temperature. If so, the lifetime and diffusion length would be longer at high temperature, improving the relative TC of the I_{sc} and V_{oc}. Since the impurity concentrations rises along the ingot, and the capture cross-sections of certain impurities decrease with temperature [11,12], this assumption seems plausible.

The relative TC of the *FF* is also rising with the ingot height (see Fig. 2c). This is caused by the increase of the relative TC of the V_{oc} which can be seen in the following equation from Ref. [9].

$$\frac{1}{FF}\frac{dFF}{dT}=\left(1-1,02FF_0\right)\left(\frac{1}{V_{OC}}\frac{dV_{OC}}{dT}-\frac{1}{T}\right) \quad (2)$$

Finally, the relative TC of the efficiency, which is the sum of all three factors, is also increasing with the ingot height (see Fig. 2d). Solar cells made from the top part of the investigated ingots will thus perform better under high temperature conditions compared to cells made from bottom material.

We conclude that the ingot position must be taken into account when comparing the TCs of cells made by different production routes or from different feedstock.

5. Summary

The temperature coefficients of solar cells made of different blends of compensated silicon and poly-Si show rather large variations within an ingot. The ingots included in this study have almost identical resistivities, despite the different blend-in ratios, as well as comparable performances which allow us to rule out differences in the resistivity and material quality as reasons for the observed differences between them. All four temperature coefficients (i.e. I_{sc}, V_{oc}, *FF* and efficiency) improve towards the top of the ingot. The reason for this is not yet determined, but a probable mechanism seems to be an impurity-related recombination process that has a capture cross-section diminishing with temperature (such as B-O complexes, or Fe and FeB for electrons).

References

[1] Søiland AK, Odden JO, Sandberg B, Friestad K, Håkedal J, Enebakk E, Braathen S. Solar silicon from a metallurgical route by Elkem Solar-viable alternative to virgin polysilicon. in: CSSC 6, Aix-les-bains, France, 2012.

[2] Gløckner R, De Wild-Scholten M. Energy payback time and carbon footprint of Elkem Solar Silicon®. 27th EUPVSEC, Frankfurt, Germany, 2012.

[3] Tayyib M, Odden JO, Ramchander N, Prakash MB, Surendra TS, Muneeshwar R,... & Saetre TO. Two years performance comparison of Elkem Solar multicrystalline silicon with polysilicon in a PV grid-connected system. 40th IEEE Photovoltaic Specialist Conference, Denver, Colorado, USA, 2014, pp. 3230-3233.

[4] Tayyib M, Odden JO, Ramchander N, Prakash MB, Surendra TS, Muneeshwar R, ... & Sætre TO. Performance assessment of a grid-connected mc-Si PV system made up of silicon material from different manufacturing routes. 39th IEEE Photovoltaic Specialist Conference, Tampa Bay, Florida, 2013, pp. 0109-0114.

[5] Tanay F, Dubois S, Enjabert N, Veirman J. Low temperature-coefficient for solar cells processed from solar-grade silicon purified by metallurgical route. Progr Photovolt: Res Appl 2011;19(8):966-72.

[6] Ponce-Alcántara S, Connolly JP, Sánchez G, Míguez JM, Hoffmann V, Ordás R. A statistical analysis of the temperature coefficients of industrial silicon solar cells. Energy Procedia 55 (2014), pp. 578-588.
[7] Cuevas A. The paradox of compensated silicon. Optoelectronic and Microelectronic Materials and Devices, 2008. COMMAD 2008. Conference on. IEEE, 2008, pp. 238-241.
[8] Tayyib M, Odden JO, Sætre TO. Effect of temperature and sun intensity on multicrystalline silicon solar cells. 28th EUPVSEC, Paris, France, 2013, pp. 1595-1598.
[9] Green MA. General temperature dependence of solar cell performance and implications for device modelling. Progress in Photovoltaics: Research and Applications 2003;11(5), pp. 333-340.
[10] Cai L, Ren X, Fan B, Zheng J, & Chen C. Effect of temperature on crystalline silicon solar cells processed from chemical and metallurgical route. Optik-International Journal for Light and Electron Optics (2014).
[11] Xiao C, Xuegong Y, Deren Y, & Duanlin Q. Impact of solar irradiance intensity and temperature on the performance of compensated crystalline silicon solar cells. Solar Energy Materials and Solar Cells 128 (2014), pp. 427-434.
[12] Paudyal BB, McIntosh KR, & Macdonald DH. Temperature dependent electron and hole capture cross sections of iron-contaminated boron-doped silicon. 34th IEEE Photovoltaic Specialist Conference (2009): pp. 1588-1593

Paper B

Temperature dependent quantum efficiencies in multicrystalline silicon solar cells

Rune Søndenå, Charly Berthod, Jan Ove Odden, Anne-Karin Søiland, Marie Syre Wiig, Erik Stensrud Marstein

This paper has been published as:

Søndenå, R., Berthod, C., Odden, J.O., Søiland, A.K., Wiig, M.S. and Marstein, E.S. *5th International Conference on Silicon Photovoltaics, SiliconPV 2015* Konstanz, Germany.

Available online at www.sciencedirect.com

ScienceDirect

Energy Procedia 77 (2015) 639 – 645

Energy Procedia

5th International Conference on Silicon Photovoltaics, SiliconPV 2015

Temperature dependent quantum efficiencies in multicrystalline silicon solar cells

Rune Søndenå[a]*, Charly Berthod[b], Jan Ove Odden[c], Anne-Karin Søiland[c], Marie Syre Wiig[a], Erik Stensrud Marstein[a]

[a]*Institute for Energy Technology, Instituttveien 18, 2007 Kjeller, Norway*
[b]*University of Agder, Gimlemoen 25A, 4630 Kristiansand S, Norway*
[c]*Elkem Solar AS, Fiskaaveien 100, 4621 Kristiansand S, Norway*

Abstract

Several field studies comparing modules based on Elkem Solar Silicon® (ESS®) cells with reference modules based on non-compensated virgin polysilicon show that the compensated ESS® modules outperform the reference modules with comparable installed capacity under certain operating conditions. At high temperatures and high irradiation conditions the modules based on compensated silicon produce more energy than the reference modules. In order to increase the understanding of the observed effect cells are studied at different temperatures by the means of IV-characteristics as well as quantum efficiencies. Quantum efficiency measurements show that the main difference between ESS® cells and polysilicon cells when increasing the temperature occurs in the 800 nm to 1100 nm wavelength range. Changes in this wavelength region are typically attributed the bulk properties of the material, i.e. the minority carrier lifetime and the carrier mobility.

Peer review by the scientific conference committee of SiliconPV 2015 under responsibility of PSE AG

Keywords: Compensated silicon; internal quantum efficiency; temperature coefficients

* Corresponding author. Tel.: (+47) 920 29 610.
E-mail address: rune.sondena@ife.no

Peer review by the scientific conference committee of SiliconPV 2015 under responsibility of PSE AG
doi:10.1016/j.egypro.2015.07.093

1. Introduction

PV energy production is growing and an increase in the demand for silicon for solar cell production can be expected in the future. By minimizing the energy consumption in the silicon feedstock production the energy pay-back time of installed solar modules can be reduced. Solar grade silicon (SoG_M-Si) produced through the metallurgical route is one of the most energy effective production methods for PV [1, 2]. A reduction in the greenhouse emissions follows the reduced energy consumption [3]. Elkem Solar Silicon® produced through the proprietary metallurgical process contains slightly higher concentrations of doping elements, both boron and phosphorus, compared to conventional polysilicon. Typical levels for [B] and [P] are 0.20 ppma and 0.60 ppma, respectively. In order to keep the resistivity in ingots in a range suitable for solar cell production phosphorus and gallium are added in order to compensate for the phosphorus present. Despite the additional doping elements the performance of cells based on such compensated silicon or blends containing both virgin polysilicon and compensated silicon rival those made from virgin polysilicon only [2, 4]. It has been reported that the increased total dopant concentration leads to a reduction of the carrier mobility in compensated silicon [5-8]. However, reduced recombination activity of defects in compensated silicon may counterbalance the reduced mobility by an increase in the minority carrier lifetime [9]. Typically lower short-circuit currents (and slightly higher open-circuit voltages) is observed in solar cells based on compensated silicon [5].

Field studies where modules consisting of Elkem Solar Silicon® are compared to reference modules with comparable specifications at standard test conditions show that the modules based on 100% ESS® solar cells outperform the reference modules under high temperature and high irradiation operating conditions [2]. Similar results where modules based on upgraded metallurgical silicon perform better than the references at summertime has also been reporter for other feedstock suppliers [10]. A test system at BVRIT in Hyderabad, India, containing 14 ESS® modules and 14 polysilicon reference modules, demonstrate that the modules based on Elkem Solar Silicon® produce more energy than the reference modules at elevated temperatures and irradiance [11, 12]. During the first year the ESS® modules produce more energy than the reference modules in most months of the year, despite a slightly lower installed capacity. This beneficial effect of temperature and/or irradiation intensity favoring ESS® cells has also been demonstrated on cells in more controlled laboratory experiments [13, 14]. Temperature dependent illuminated IV-measurements in a solar simulator show favorable temperature coefficients in ESS® cells for the short-circuit current (J_{SC}), open-circuit voltage (V_{OC}), fill-factor (FF) and efficiency (η) [13]. A higher operating temperature as well as high irradiance will benefit the modules based on Elkem Solar Silicon® [14].

In the present study the quantum efficiencies in cells containing ESS® as well as the reference cells based on conventional polysilicon will be studied in order to gain more insight into the observed effect favoring ESS® based cells. Quantum efficiencies will be evaluated at 25°C and 50°C.

2. Experimental details

Solar cells are chosen from the same batches as used in the field studies in Hyderabad. The wafers and cells are produced in 2011 under as identical conditions as possible; by the same producer in identical furnaces and in the same cell production line. Cells produced from the top 200 wafers of each block yield average efficiencies of 16.86% (range 16.43-17.33%) for ESS® and 16.96% (range 16.34-17.34) for the poly references. Cells from the bottom 200 wafers yield average efficiencies of 17.18% (range 16.20-17.56%) for ESS® and 17.27% (range 16.34-17.50%) for the references. Although differences in material quality between blocks and even within the same block may arise in multicrystalline wafers, the main differences in the cells are attributed the different silicon feedstock. Prior to measurements all cells were subject to annealing at 200°C for 20 minutes followed by a light soaking in order to stabilize the degradation caused by BO-related defects. The IV characteristics are measured using a commercially available AAA sun simulator. The temperature dependence of the IV data is found by taking measurements at even temperature intervals between 25°C and 70°C. Internal and external quantum efficiencies (IQE and EQE) are measured at 25°C and 50°C using a setup from PV-tools/LOANA.

Minimal temperature changes in reflection with the temperature increase are assumed and contacting properties are assumed to be identical for ESS® and poly cells. An estimate for the J_{SC} can be obtained by integrating Eq. 1 from 300 nm to 1200 nm.

$$J_{SC} = \frac{1}{A}\int_{\lambda} \frac{IQE(\lambda)\cdot f(\lambda)}{1-R(\lambda)-T(\lambda)}\cdot d\lambda = \frac{1}{A}\int_{\lambda} EQE(\lambda)\cdot f(\lambda)\cdot d\lambda \quad (1)$$

$R(\lambda)$ and $T(\lambda)$ are the reflectance and transmittance of light at the wavelength, λ, in a cell of area A, respectively. The AM1.5G spectrum is used as the incident photon flux, $f(\lambda)$. A complete conversion of photons absorbed in the material into charge carriers is assumed.

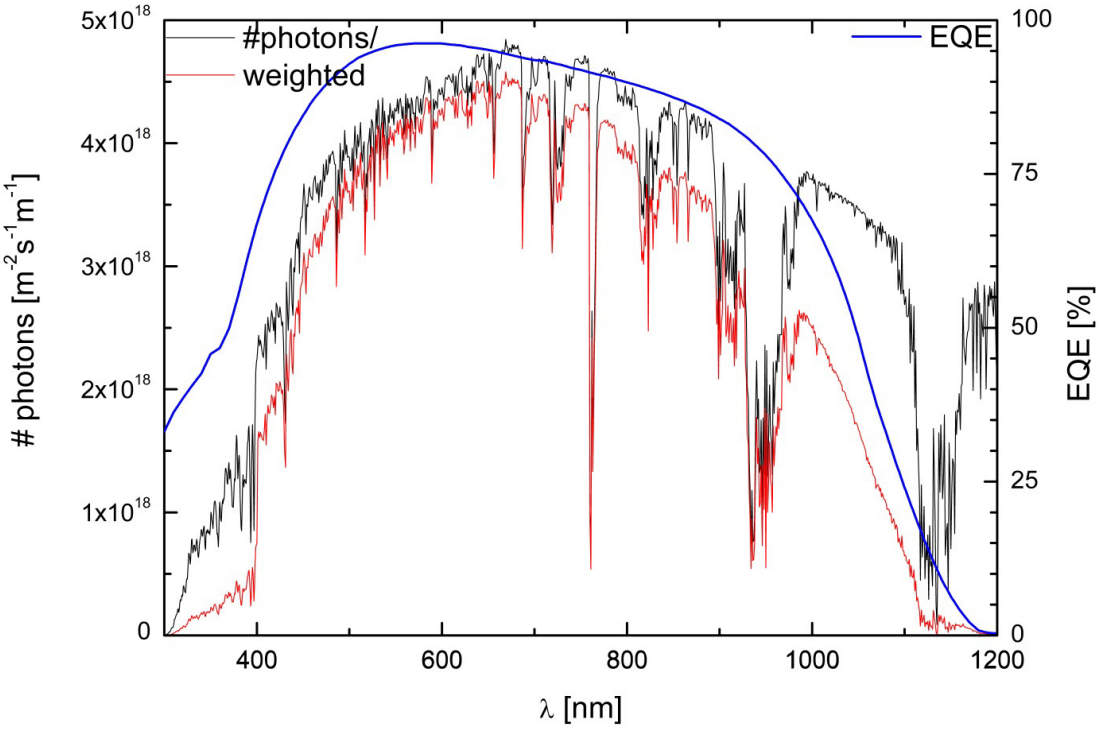

Fig. 1. The AM1.5G solar spectrum is shown in black, EQE for a cell in blue and the EQE weighted by the AM1.5G spectrum in red. By integrating the weighted EQE an estimate for the J_{SC} can be obtained.

3. Results

The batch of compensated cells have an overall average efficiency of 17.0% while the non-compensated references show a slightly higher performance of 17.1% in average (for positional details, see above). A general trend is that cells based on compensated silicon have lower J_{SC} and higher V_{OC} than corresponding polysilicon wafers [5]. IV-characteristics for the cells after light soaking are presented in Table I.

Table 1. IV-measurements at standard testing conditions (STC: 1 Sun illumination, AM1.5G spectrum and 25°C) for selected cells.

Cell	η [%]	J_{SC} [mA/cm^2]	V_{OC} [mV]	FF
ESS® top	17.2	34.4	631.2	79.1
ESS® bottom	16.7	34.2	630.9	77.6
Poly top	17.5	35.0	632.8	79.0
Poly bottom	17.4	35.1	631.7	78.7

Typical IQE curves for both 25°C and 50°C are shown in Figure 2. At low wavelengths the quantum efficiencies are slightly reduced for both compensated and non-compensated silicon solar cells when the temperature is increased, while quantum efficiencies are increased at higher wavelengths. The relative difference, $(IQE_{50} - IQE_{25})/IQE_{25}$, shows that in the 800 nm to 1100 nm range the compensated cell improves more than the non-compensated reference.

The J_{SC} and dJ_{SC}/dT calculated from the weighted EQE at 25°C and 50°C are shown in Table II. Temperature coefficients from IV-measurements are also included. An increase in the temperature coefficient of the J_{SC} benefiting ESS® based cells is found. This corresponds well with both field studies as well as previous measurements on cells. Testing of cells for module production is most likely performed under standard testing conditions. An elevated operating temperature may therefore explain why modules based on compensated silicon out-perform non-compensated reference modules of comparable installed capacity in tempered climates. Underlying mechanisms that may cause this effect are discussed below.

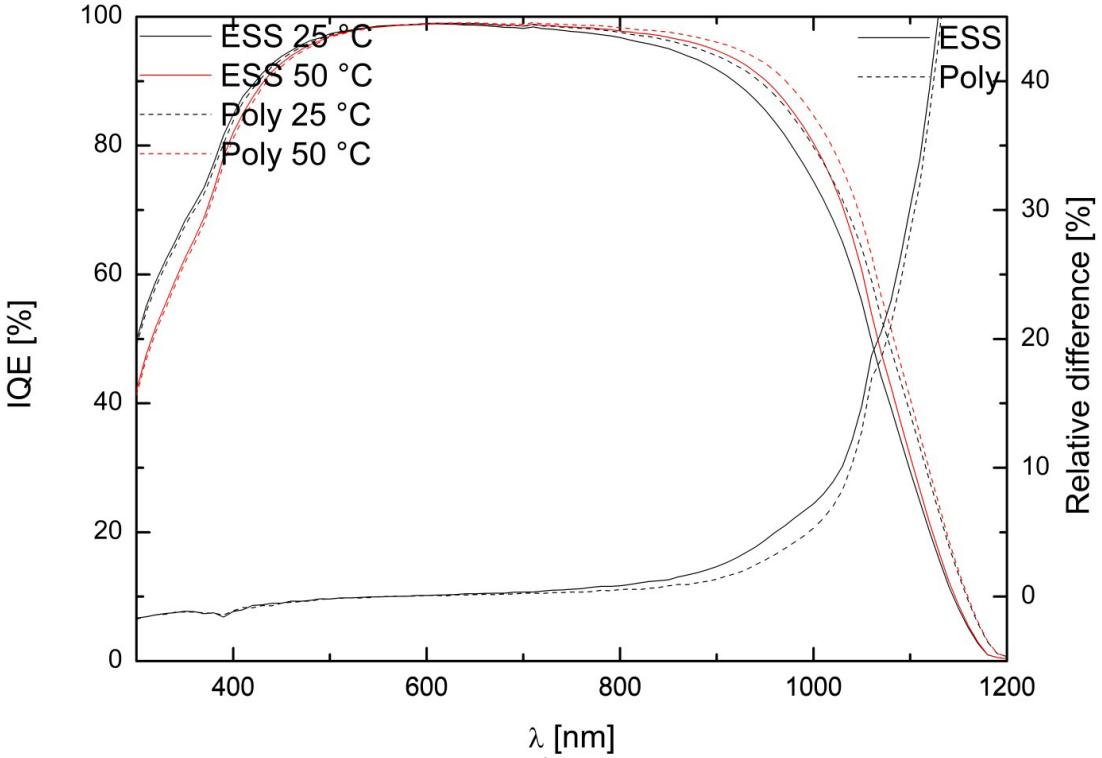

Fig. 2. IQE curves for cells at 25°C (black) and 50°C (red). Both ESS® (solid lines) and poly (dashed lines) cells show an increase in the red-response with increasing temperature. The relative difference show that ESS® increases more than the poly cell in the region from 800 nm to 1000 nm.

Table 2. Average temperature coefficient based on a J_{SC} estimated using a weighted EQE is compared to values from IV-measurements.

Cell	J_{SC-EQE} 25°C [mA/cm^2]	J_{SC-EQE} 50°C [mA/cm^2]	dJ_{SC}/dT_{EQE} [%/K]	dJ_{SC}/dT_{IV} [%/K]
ESS® top	37.16	36.9	6.6E-2	6.75E-2
ESS® bottom	35.1	36.4	6.2E-2	6.38E-2
Poly top	36.6	37.2	5.6E-2	5.24E-2
Poly bottom	36.7	37.2	5.6E-2	5.07E-2

4. Discussion

The metallurgical cleaning procedure is fundamentally different from the Siemens process. As less energy is used in the purification process of ESS® than conventional polysilicon impurity elements may be present in different amounts. Elemental analysis show that the differences in metallic impurities are minimal [1, 15]. Thus, the main difference between conventional polysilicon and compensated silicon is the additional dopant elements present in the latter. Boron-oxygen complexes are introduced as a possible explanation in by Tanay et al [16]. The hole capture cross section of boron-oxygen related defects is expected to diminish with increasing temperature [17], contributing to increased carrier lifetimes and diffusion lengths in the material. As manufacturers of SoG_M-Si use their own, often unique, technologies for feedstock purification, silicon from different suppliers can differ considerably in contaminants and concentrations thereof. The oxygen content in ESS® is found to be comparable to non-compensated polysilicon [1, 18] and the amount of BO-complexes in compensated silicon is determined by the net doping, p_0, and not the total boron concentration [19-21]. Comparable amounts of boron-oxygen complexes are therefore expected in both the ESS® cells and the non-compensated cells in this study. Comparable LID in the both the ESS® cells and the reference cells used in this study has previously been reported [22]. Peter et al. have, however, reported slightly elevated LID in ESS® cells previously [23].

Figure 2 shows that the effect favouring ESS® cells over the references occurs in the 800 nm to 1100 nm region. Differences in this wavelength range are generally attributed the bulk quality of the material. Thus, the beneficial effect of compensation on the performance of modules at high temperatures and irradiation is most likely related to the minority carrier lifetime and the carrier mobilities. It is known that compensation may lead to increased lifetimes in the material due to a shift in the Fermi level [9, 24]. This increase is countered by a reduction in mobility [6-8]. The effect on the mobility is related to scattering events. More dopants will act as scattering sites reducing the mobility in compensated silicon. However, the scattering is strongly linked to the temperature. With increasing temperatures the difference between compensated and non-compensated silicon will decrease. Thus, elevated temperatures are beneficial for compensated silicon as the effect of reduced in mobility will be evened out, while the beneficial lifetime effects largely will remain. As a result a relative improvement in diffusion length is expected in ESS® cells with increasing temperature.

The main focus of the discussion has been on the increased temperature, but also the increased irradiation may contribute to the improved performance of compensated silicon cells. As mentioned above a small increase in the lifetime in compensated silicon is expected due to a Fermi level shift [6-8] and the hole capture cross section of the BO-complex will decrease with increasing temperature [17]. With an increased solar irradiance the injection level during operation of the modules might be higher than at standard testing conditions. Depending on the nature of the dominating impurities in the silicon this may result in a further improvement of the carrier lifetime. Common impurities such as BO-complexes and interstitial iron both show increasing SRH-lifetimes with increasing injection levels [25, 26].

Improvements in the efficiency of solar cell in compensated silicon through the impurity photovoltaic (IPV) effect has previously been modelled [27]. Using IPV energy levels are introduced in the bandgap, for instance from added In or the CrB defect, enabling absorption of sub-bandgap photons. A beneficial effect from IPV will, however, only be visible in thin wafers (<50 μm). Band gap narrowing is known to occur with increasing doping levels. Using a recent model an additional band gap narrowing of 2-4 meV can be expected in compensated silicon [28]. However, Figure 2 shows that for a given temperature the IQE curves both compensated and non-compensated cells converge for high wavelengths. Thus, any beneficial effects of sub-bandgap absorption favouring compensated silicon are therefore unlikely.

5. Summary

The quantum efficiencies of the cells show a general decrease in the blue-response and an increase in the red-response for both ESS® and poly cells. When estimating the J_{SC} from the quantum efficiency an improvement corresponding roughly to the effect measured in the IV-characteristics is obtained. The main difference in the quantum efficiencies is found to be a slightly larger improvement with temperature in the 800 nm to 1100 nm

wavelength range for the ESS® cells. Towards 1200 nm the quantum efficiencies of both the ESS® cells and the reference cells at the same temperature converge.

Effects in the quantum efficiency in the wavelength region from 800 nm to 1100 nm are typically attributed bulk material properties, i.e. the carrier mobility and lifetime. The carrier mobility decreases less with increasing temperature in compensated silicon than in non-compensated silicon. An additional temperature effect on the boron-oxygen complexes may also contribute by improving the minority carrier lifetime in compensated silicon relative non-compensated. Additional sub-bandgap absorption of photons in compensated silicon is unlikely as the quantum efficiencies converge towards high wavelengths.

Acknowledgements

Funding was provided by the Norwegian Research Council and Elkem Solar AS through the EnergiX programme.

References

[1] Søiland AK, Odden JO, Sandberg B, Friestad K, Håkedal J, Enebakk E, Braathen S. Solar silicon from a metallurgical route by Elkem Solar: A viable alternative to virgin polysilicon. Proc. CSSC-6, Aix-les-Bains, France, 2012.
[2] Odden JO, Lommasson TC, Tayyib M, Vedde J, Buseth T, Friestad K, Date H, Tronstad R. Results on performance and ageing of solar modules based on Elkem Solar Silicon (ESS™) from installations at various locations. Sol. En. Mat. Sol. Cells. 2014;130:673-678.
[3] Glöckner R, De Wild-Scholten M. Energy payback time and carbon footprint of Elkem Solar Silicon®. Proc. 27th EUPVSEC, Frankfurt, Germany, 2012.
[4] Preis P, Díaz-Pérez P, Rudolph D, Peter K, Søiland AK. High efficiency potential of Cz silicon solar cells from metallurgical process route. Proc. 27th EUPVSEC, Frankfurt, Germany, 2012.
[5] Xiao C, Yang D, Yu X, Wang P, Chen P, Que D. Effect of dopant compensation on the performance of Czochralski silicon solar cells. Sol. En. Mat. Sol. Cells. 2012;101:102-106.
[6] Modanese C, Acciarri M, Binetti S, Søiland AK, Di Sabatino M, Arnberg L. Temperature-dependent Hall-effect measurements of p-type multicrystalline compensated solar grade silicon. Prog. Photovolt. 2013;21:1469-1477.
[7] Rougieux FE, Macdonald D, Cuevas A, Ruffell S, Schmidt J, Lim B, Knights AP. Electron and hole mobility reduction and Hall factor in phosphorus-compensated p-type silicon. J. Appl. Phys. 2010;108:013706.
[8] Schindler F, Forster M, Broisch J, Schön J, Giesecke J, Rein S, Warta W, Schubert MC. Towards a unified low-field model for carrier mobilities in crystalline silicon. Sol. En. Mat. Sol. Cells. 2014;131:92-99.
[9] Dubois S, Enjalbert N, Garandet JP. Effects of the compensation level on the carrier lifetime of crystalline silicon. Appl. Phys. Lett. 2008;93:032114.
[10] Sánchez E, Torreblanca J, Carballo T, Parra V, Bullón J, Míguez JM, Gutiérrez J, García J, Guerrero I, Ordás R, Izard J. Outdoor monitoring of the energy yield and electrical parameters of standard polysilicon based and new umg-Si PV modules. Energy Procedia. 2011;8:503.
[11] Tayyib M, Odden JO, Ramchander N, Prakash MB, Surendra TS, Muneeshwar R, Sarma AV, Ramanjaneyulu M, Sætre TO. A materials perspective on one full years performance of multicrystalline Si PV modules in a grid-connected system. Proc. 28th EUPVSEC, Paris, France, 2013.
[12] Tayyib M, Odden JO, Ramchander N, Prakash MB, Surendra TS, Muneeshwar R, Sarma AV, Ramanjaneyulu M, Sætre TO. Performance assessment of a grid-connected mc-Si PV system made up of silicon material from different manufacturing routes. Proc. 39th IEEE PVSC, Tampa Bay, Florida, 2013.
[13] Tayyib M, Odden JO, Sætre TO. Effect of temperature and sun intensity on multicrystalline silicon solar cells. Proc. 28th EUPVSEC, Paris, France, 2013.
[14] Tayyib M, Odden JO, Sætre TO. Irradiance dependent temperature coefficients for MC solar cells from Elkem solar grade silicon in comparison with reference polysilicon. Energy Procedia. 2014;55:602-607.
[15] Tayyib M, Odden JO, Dahl EH, Baggethun P, Sætre TO. Elkem silicon vs polysilicon: A quantitative impurity element analyses. Proc. 28th EUPVSEC, Paris, France, 2013.
[16] Tanay F, Dubois S, Enjalbert N, Veirman J. Low temperature-coefficient for solar cells processed from solar-grade silicon purified by metallurgical route. Prog. Photovolt. 2011;19:966-972.
[17] Rein S, Glunz SW. Electronic properties of the metastable defect in boron-doped Czochralski silicon: Unambiguous determination by advanced lifetime spectroscopy. Appl. Phys. Lett. 2003;82:1054-1056.
[18] Tayyib M, Odden JO, Preis P, Sætre TO. Impurity analyses of silicon wafers from different manufacturing routes and their impact on LID of finished solar cells. Proc. 39th IEEE PVSC, Tampa Bay, Florida, 2013.
[19] Macdonald D, Rougieux F, Cuevas A, Lim B, Schmidt J, Di Sabatino M, Geerligs LJ. Light-induced boron-oxygen defect generation in compensated p-type Czochralski silicon. J. Appl. Phys. 2009;105:093704.
[20] Lim B, Rougieux F, Macdonald D, Bothe K, Schmidt J. Generation and annihilation of boron-oxygen-related recombination centers in compensated p- and n-type silicon. J. Appl. Phys. 2010;108:103722.

[21] Geilker J, Kwapil W, Rein S. Light-induced degradation in compensated p- and n-type Czochralski silicon wafers. J. Appl. Phys. 2011;109:053718.
[22] Tayyib M, Rao YH, Ramanjaneyulu M, Surendra TS, Odden JO, Sætre TO. Initial light-induced degradation study of multicrystalline modules made from silicon material processed through different manufacturing routes. Proc. 38th IEEE PVSC, Austin, Texas, 2012.
[23] Peter K, Preis P, Díaz-Pérez P, Theobald J, Enebakk E, Søiland AK, Savtchouk A, Wilson M, Lagowski J. Light induced degradation in multicrystalline solar grade silicon solar cells evaluated using accelerated LID. Proc. 26th EUPVSEC, Hamburg, Germany, 2011.
[24] Macdonald D, Cuevas A. Recombination in compensated crystalline silicon for solar cells. J. Appl. Phys. 2011;109:043704.
[25] Macdonald D, Tan J, Trupke T. Imaging interstitial iron concentrations in boron-doped crystalline silicon using photoluminescence. J. Appl. Phys. 2008;103:073710.
[26] Xiao C, Yu X, Yang D, Que D. Impact of solar irradiance intensity and temperature on the performance of compensated crystalline silicon solar cells. Sol. En. Mat. Sol. Cells. 2014;128:427-434.
[27] Pavel AA, Khan MR, Islam NE. On the possibility of improving silicon solar cell efficiency through impurity photovoltaic effect and compensation. Solid-State Electron. 2010;54:1278-1283.
[28] Yan D, Cuevas A. Empirical determination of the energy band gap narrowing in p^+ silicon heavily doped with boron. J. Appl. Phys. 2014;116:194505.

Paper C

Reduced temperature sensitivity of multicrystalline silicon solar cells with low ingot resistivity

Charly Berthod, Rune Strandberg, Jan Ove Odden, and Tor Oskar Saetre

This paper has been published as:

Berthod, C., Strandberg, R., Odden, J.O. and Saetre, T.O. *Photovoltaic Specialist Conference (PVSC), 2016 IEEE 43rd* Portland, Oregon, USA.

Reduced Temperature Sensitivity of Multicrystalline Silicon Solar Cells with Low Ingot Resistivity

Charly Berthod[1], Rune Strandberg[1], Jan Ove Odden[2], and Tor Oskar Saetre[1]

[1]University of Agder, Department of Engineering Sciences, P.O. Box 509, NO-4898 Grimstad, Norway,

[2]Elkem Solar AS, P.O. Box 8040 Vaagsbygd, NO-4675 Kristiansand S, Norway

***Abstract* — This study presents experimental data on the reduction of temperature sensitivity of multicrystalline silicon solar cells made from low resistivity ingot. The temperature coefficients of solar cells produced from different ingot resistivities are compared, and the advantages of increasing the net doping are explained.**

***Index Terms* — compensated silicon, temperature coefficients, resistivity, multicrystalline silicon solar cells.**

I. Introduction

Solar cells and PV modules are systematically characterized at standard test conditions STC (1000 W/m^2, 25°C, AM 1.5) fulfilling the ASTM norms. Yet usual operating conditions deviate from these conditions. To take into account the temperature variations the general parameter "temperature coefficient" is introduced to describe how the power output varies with temperature under maximum power point operation of a solar cell. Temperature coefficients for every cell parameter can be derived and they are often presented as relative temperature coefficients. Silicon solar cells have a negative relative temperature coefficient of the efficiency which arises principally from a decrease in the open-circuit voltage at high temperature. In the case of multicrystalline silicon solar cells a common value for this temperature coefficient is -0.45%/°C. This means that a cell with a 20% efficiency at 25°C would have an efficiency of less than 17% at 60°C, which is a very common operating temperature.

Reduced temperature coefficients have been demonstrated on compensated silicon [1]-[4]. In addition, production methods yielding compensated silicon often offer advantages such as a reduction in the energy consumption and a lower carbon-footprint [5]. Another distinction between compensated silicon and non-compensated silicon is the production of ingots with a lower resistivity due to the presence of both boron and phosphorus. Indeed, since phosphorus has a lower segregation coefficient (0.35) than boron (0.8), their respective concentrations vary differently throughout the height of the ingot, which induces a resistivity increase along the ingot until a p/n changeover near the top part of the ingot. When using compensated material, a lower yield could therefore be obtained owing to the unusable n-doped part. A way to avoid this p/n changeover is to dope with gallium which has a segregation coefficient of 0.008. The ingot is thus fully p-type with a flatter resistivity profile.

On the contrary, non-compensated silicon is doped with only one type of dopant and has therefore a resistivity profile continuously decreasing along the ingot. To cope with solar cell processing, resistivity requirements are made with an upper and a lower resistivity limit which involve a low starting resistivity for compensated silicon and a higher starting resistivity for non-compensated silicon.

In most of the studies comparing the temperature sensitivity of compensated and non-compensated silicon solar cells [1]-[3], no specific attention is paid to the bulk resistivity of the samples. Yet the effect of resistivity on the solar cell temperature sensitivity has been demonstrated [4], thus questioning the impact of wafer resistivity in previous studies. In this paper an experimental investigation is carried out on the role of the wafer resistivity on the temperature coefficients.

II. Experimental Setup

Three compensated silicon ingots made of Elkem Solar Silicon® (ESS®) with targeted resistivities of 0.5 Ω.cm, 0.9 Ω.cm and 1.3 Ω.cm, and a non-compensated silicon reference ingot with a targeted resistivity of 1.3 Ω.cm made from a fluidized-bed reactor were used in this study. The compensated silicon ingots contain gallium. General ingot properties are summarized in Table I. Bricks of center positions of industrial G5 sized ingots were wafered and then processed into PERC (Passivated Emitter and Rear Cell) cells by REC Solar. The cells are high performance multicrystalline silicon solar cells measuring 15.6x15.6cm^2.

Table I. Ingot Description

Ingot name	Target Resistivity (Ω.cm)	Dopants
Comp1	0.5	B/P/Ga
Comp2	0.9	B/P/Ga
Comp3	1.3	B/P/Ga
Ref	1.3	B

The resistivity profiles of the four ingots are plotted in Fig. 1. The resistivities were measured by Semilab Eddy current. Flat resistivity profiles up to 0.8 in relative height were

obtained for the compensated ingots. The reference ingot which is only doped with boron has a resistivity starting higher than ingot Comp3, and crossing it at 0.6. The reference ingot even crosses ingot Comp2 but the solar cells used in this study stop just before this point.

The IV-characteristics were measured under a standard AM 1.5 G spectrum with a NeonSee™ AAA sun simulator. The temperature coefficients of the open-circuit voltage (β_{Voc}), of the short-circuit current (β_{Isc}), of the fill factor (β_{FF}) and of the efficiency (β_{η}) were obtained by measuring the IV characteristics of a cell from 25°C to 70°C with five-degree steps followed by a linear fitting of each parameter to get the coefficients. The coefficients are then divided by the value of the corresponding parameter at 25°C to get the relative temperature coefficients.

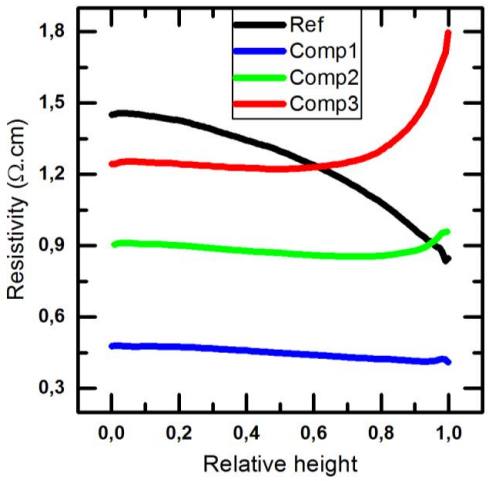

Fig. 1. Resistivity profiles of solar cells from the four ingots.

III. Results

The efficiency of the solar cells from different brick height is presented in Fig. 2. The highest efficiencies are located near the middle (here around 0.4 in relative height) of the ingot where the lowest defect concentration is expected. At the very bottom the cells have a higher oxygen concentration in general due to diffusion from the crucible which causes low efficiencies, and the dislocation concentration is increasing towards the top. The ingots were made with a high performance multicrystalline process allowing a low dislocation density growth along the ingot height, which can be seen as the efficiency decreases slowly along the ingot height. The ingots Ref and Comp3 have the same resistivities. However the compensated ingot shows slightly higher efficiencies. Compensated silicon generally has a lower lifetime and carrier mobilities [6-11], thus lower efficiencies are expected. In this case the better efficiencies for the compensated material may indicate fluctuations in cell processing predominate the performance differences between compensated and non-compensated silicon solar cells for this cell type. More advanced cell types such as heterojunction or PERL are more sensitive to lifetime, and it is expected that the difference between compensated and non-compensated would appear. The ingot Comp1 with an ingot resistivity of 0.5 Ω.cm shows a good efficiency profile even with its high doping. The best efficiencies were obtained with the 0.9 Ω.cm ingot (Comp2) with the best cell having an efficiency of 18.86% (not externally validated).

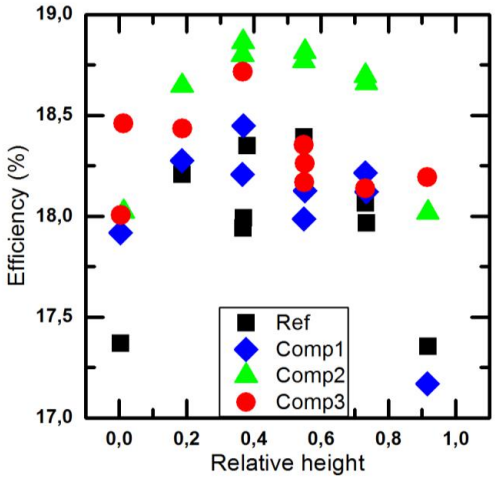

Fig. 2. Efficiency of solar cells from the four ingots as a function of the relative height.

The relative temperature coefficients of main cell parameters are shown in Fig. 3. The temperature sensitivity of the lowest resistivity ingot (Comp1) is reduced as shown in Fig. 3d. This ingot presents better β_{Isc} and β_{FF} (Fig.3 a,c) and a good β_{Voc} (Fig. 3b). Ingot Comp2 with a targeted wafer resistivity of 0.9 Ω.cm shows a temperature sensitivity similar to ingot Comp3. The reference ingot which is lightly compensated with a slightly lower efficiency profile than ingot Comp3 (Fig 2) has the worst temperature coefficients. This doesn't come from a usual benefit of compensated material in the β_{Isc} [1-4], where actually the reference ingot is better than the ingot Comp3 with the same resistivity. The low β_{Voc} and β_{FF} (Fig 2b,c) are the reasons for the worse β_{η}.

The improvement of the temperature coefficient of the low resistivity ingot is partially explained by the higher net doping, which is increasing the open-circuit voltage. This gain causes a direct increase of the β_{Voc} as can be seen from the equation [12,13]:

$$\beta_{V_{oc}} = \frac{1}{V_{oc}}\frac{dV_{oc}}{dT} = -\frac{1}{V_{oc}T_c}\left[\frac{E_{g0}}{q} - V_{oc} + \gamma\frac{kT_c}{q}\right] \quad (1)$$

where k, q, T_c and E_{g0} are the electron charge, Boltzmann's constant, the cell temperature and the linearly extrapolated bandgap of the relevant recombination process at 0 K, respectively. γ is a parameter corresponding to the temperature sensitivity of the mechanism determining the open-circuit voltage. Therefore a high open-circuit voltage implies a reduction of the temperature sensitivity of the solar cell [9].

The second cause of the better low resistivity ingot temperature sensitivities is the reduced β_{FF} (Fig. 2c). This coefficient can be expressed as [12,13]:

$$\beta_{FF} = \frac{1}{FF}\frac{dFF}{dT} = \left(1-1.02FF_0\right)\left(\frac{1}{V_{oc}}\frac{dV_{oc}}{dT}-\frac{1}{T}\right) - \frac{R_s}{\left(V_{oc}/J_{sc}-R_s\right)}\left(\frac{1}{R_s}\frac{dR_s}{dT}\right) \quad (2)$$

where R_s is the series resistance, FF_0 the ideal fill factor (free of series and shunt resistances effects), and v_{oc} is the normalized open-circuit voltage.

An increase of the open-circuit voltage will increase the ideal fill factor and reduce the β_{Voc} which both increase the β_{FF}. Therefore the low resistivity ingot (Comp1) with its higher open-circuit voltage shows the best β_{FF}.

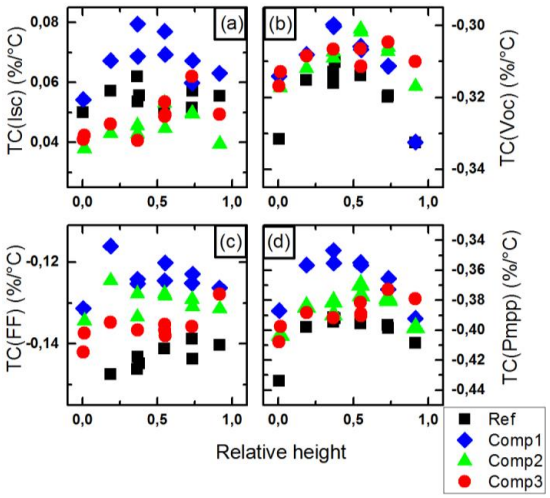

Fig. 3. Relative temperature coefficients of (a) the short-circuit current, (b) the open-circuit voltage, (c) the fill factor and (d) the power at maximum power point (equivalent to efficiency) as a function of the relative height for the same solar cells as in Fig. 2.

Another reason for the reduced temperature sensitivity of the low resistivity ingot (Comp1) is a larger β_{Isc}. The differences observed over the entire brick height (Fig. 3a) can only be explained by an improved temperature coefficient of the collection fraction. This is the second term of the following equation describing β_{Isc} [12,13]:

$$\beta_{J_{sc}} = \frac{1}{J_{sc}}\frac{dJ_{sc}}{dT} = \frac{1}{J_{sc,1sun}}\frac{dJ_{sc,1sun}}{dE_g}\frac{dE_g}{dT} + \frac{1}{f_c}\frac{df_c}{dT} \quad (3)$$

where E_g is the bandgap of the semiconductor. The first right-hand term is fixed for a certain semiconductor and arises from the bandgap dependency on the temperature.

IV. Discussion

The low resistivity ingot has the lowest short-circuit current due to the lowered lifetime expected with more doping and at the same time the best β_{Isc}. In Fig. 4 the β_{Isc} is plotted as a function of the short-circuit current. It can be observed that the cells with the highest current have the worst β_{Isc}. Indeed Comp1 with the highest doping concentration has the lowest currents and the best temperature coefficients. Ingot Ref should have had the best currents but due to processing fluctuations this ingot is below Comp2 and Comp3. Furthermore this ingot was expected to have the worst β_{Isc} [1-4], but possibly due to its lower currents this ingot shows better β_{Isc} than Comp2 and Comp3. We suggest that this might come from a larger improvement of the collection fraction with temperature. This may explain why cells with poor material qualities achieve higher β_{Isc} than good-quality cells.

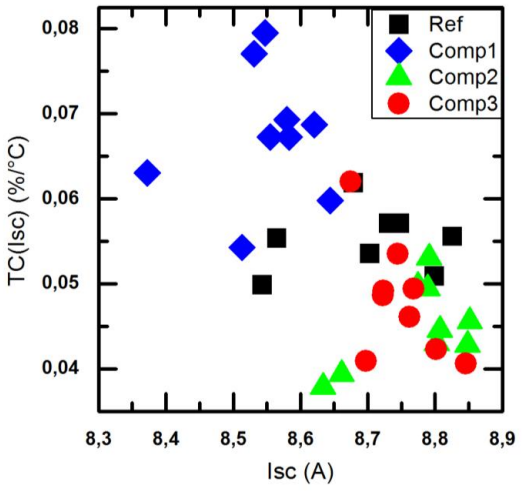

Fig. 4. Relative temperature coefficients of the short-circuit current as a function of the short-circuit current.

To estimate the impact of increasing the open-circuit voltage by decreasing the resistivity on the β_{Voc}, the latter parameter is plotted in Fig. 5 as a function of the open-circuit voltage. The curve is quasi-linear because of the small open-circuit voltage range with these cells. The ingots with the lowest resistivities (Comp1 and Comp2) have the best open-circuit voltages thanks to the higher net doping and thus a better temperature coefficient. Comp3 is slightly better than

Ref due to a slightly higher net doping. The resistivity of ingot Comp3 is mainly lower than Ref, therefore the net doping is higher. Furthermore the mobility is decreased in compensated material thus one has to increase the net doping to obtain the same resistivity as non-compensated silicon. These combined factors explain the better open-circuit voltage for Comp3 and as a result the better β_{Voc}.

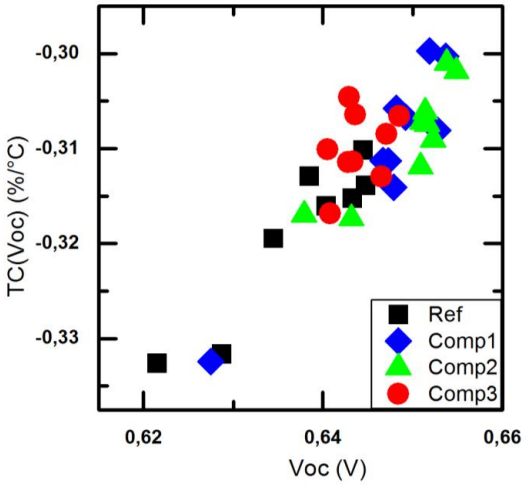

Fig. 5. Relative temperature coefficients of the open-circuit voltage as a function of the open-circuit voltage.

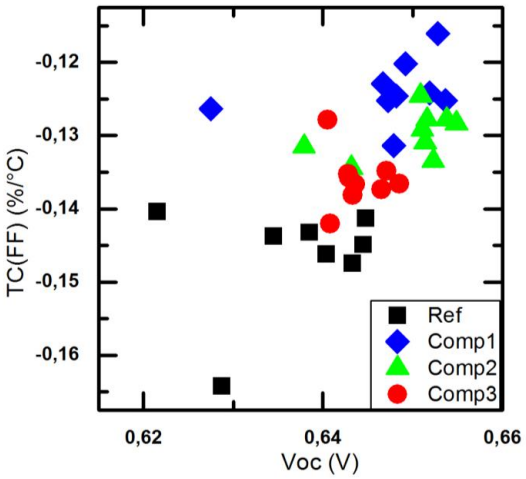

Fig. 6. Relative temperature coefficients of the fill factor as a function of the open-circuit voltage.

The β_{FF} also depends on the open-circuit voltage, present in the ideal fill factor and in β_{Voc}, as shown in (2). This dependency is plotted in Fig. 6. The β_{FF} clearly increases with the open-circuit voltage. Ingot Comp3 present better β_{FF} than the reference ingot due the higher net doping. And ingot Comp1 with the largest open-circuit voltages has the best results for this coefficient.

Hence a large open-circuit voltage caused by a high net doping enhances both β_{Voc} and β_{FF}.

V. Conclusion

We compared the temperature coefficients of silicon solar cells made from ingots with different resistivities and we have shown that a lowering of the wafer resistivity could lead to a great reduction of the temperature sensitivity of the solar cell.

This improvement comes from three distinct factors. First a high net doping decreases the lifetime which reduces the short-circuit current. This lower short-circuit current gives an enhanced temperature coefficient of the short-circuit current caused by unknown mechanisms. Secondly the higher net doping increases the open-circuit voltage which improves directly the temperature coefficient of the open-circuit voltage. And finally this higher open-circuit voltage also improves the temperature coefficient of the fill factor. The improvement of the temperature coefficient of the efficiency results from the enhancement of the three previous temperature coefficients.

References

[1] F. Tanay, et al., “Low temperature-coefficient for solar cells processed from solar-grade silicon purified by metallurgical route.” *Progress in Photovoltaics: Research and Applications*, 2011. 19(8): p. 966-972.

[2] M. Tayyib, J. O. Odden, N. Ramchander, M. B. Prakash, T. S. Surendra, R. Muneeshwar,... and T. O. Saetre. "Two years performance comparison of Elkem Solar multicrystalline silicon with polysilicon in a PV grid-connected system." In *40th IEEE Photovoltaic Specialist Conference*, Denver, Colorado, USA, 2014, pp. 3230-3233.

[3] M. Tayyib, J.O. Odden, N. Ramchander, M.B. Prakash, T.S. Surendra, R. Muneeshwar, A.V. Sarma, M. Ramanjaneyulu, and T.O. Sætre, "Performance assessment of a grid-connected mc-Si PV system made up of silicon material from different manufacturing routes", in *39th IEEE Photovoltaic Specialist Conference*, Tampa Bay, Florida, 2013.

[4] S. Ponce-Alcántara, J. P. Connolly, G. Sánchez, J. M. Míguez, V. Hoffmann, and R. Ordás. "A Statistical Analysis of the Temperature Coefficients of Industrial Silicon Solar Cells." *Energy Procedia* 55 (2014), 578-588.

[5] R. Gløckner, and M. De Wild-Scholten, "Energy payback time and carbon footprint of Elkem Solar Silicon®", in *27th EUPVSEC*, Frankfurt, Germany, 2012.

[6] Forster, M., et al., *Impact of incomplete ionization of dopants on the electrical properties of compensated p-type silicon.* Journal of Applied Physics, 2012. **111**(4): p. 043701.

[7] Rougieux, F., et al., *High efficiency UMG silicon solar cells: impact of compensation on cell parameters.* Progress in Photovoltaics: Research and Applications, 2016. **24**(5): p. 725-734.

[8] Schindler, F., et al., *Towards a unified low-field model for carrier mobilities in crystalline silicon.* Solar Energy Materials and Solar Cells, 2014. **131**: p. 92-99.

[9] Rougieux, F.E., et al., *Electron and hole mobility reduction and Hall factor in phosphorus-compensated p-type silicon.* Journal of Applied Physics, 2010. **108**(1): p. 013706.
[10] Dubois, S., N. Enjalbert, and J.P. Garandet, *Effects of the compensation level on the carrier lifetime of crystalline silicon.* Applied Physics Letters, 2008. **93**(3): p. 032114.
[11] Veirman, J., et al., *Electronic properties of highly-doped and compensated solar-grade silicon wafers and solar cells.* Journal of Applied Physics, 2011. **109**(10): p. 103711.
[12] O. Dupre, R. Vaillon, and M. A. Green. "Experimental assessment of temperature coefficient theories for silicon solar cells."*Photovoltaics, IEEE Journal of*, 6.1 (2016): 56-60.
[13] Green, M.A., *General temperature dependence of solar cell performance and implications for device modelling.* Progress in Photovoltaics: Research and Applications, 2003. **11**(5): p. 333-340.

Paper D

Reduction of temperature coefficients in multicrystalline silicon solar cells after light-induced degradation

Charly Berthod, Rune Strandberg, Jan Ove Odden, and Tor Oskar Saetre

This paper has been published as:

Berthod, C., Strandberg, R., Odden, J.O. and Saetre, T.O. *Photovoltaic Specialist Conference (PVSC), 2015 IEEE 42nd* New Orleans, Louisiana, USA.

Reduction of Temperature Coefficients in Multicrystalline Silicon Solar Cells after Light-Induced Degradation

Charly Berthod[1], Rune Strandberg[1], Jan Ove Odden[2], and Tor Oskar Sætre[1]

[1]University of Agder, P.O. Box 509, NO-4898 Grimstad, Norway,
[2]Elkem Solar AS, P.O. Box 8040 Vaagsbygd, NO-4675 Kristiansand S, Norway

***Abstract* — This study focuses on the variations of the temperature coefficients after light-induced degradation (LID) of compensated multicrystalline silicon solar cells from three different ingots. The ingots have been chosen to see the effect of the compensation level, the resistivity and the impact of adding gallium to keep the resistivity as constant as possible along the ingot. The temperature coefficients of the efficiency experience a major decrease after LID on all ingots. We found that this decrease varies along the ingot height and does not correspond to the V_{OC} drop. Moreover, no direct correlation with the interstitial oxygen concentration profiles could be seen.**

***Index Terms* — compensated silicon, light-induced degradation, silicon solar cells, temperature coefficients.**

I. Introduction

Compensated silicon produced by metallurgical refining methods offers well-known advantages compared to silicon from the Siemens process [1] such as a reduction in the energy consumption and a lower carbon-footprint [2]. Moreover, the solar cells/modules made of this material appear to behave better at high temperature [3]-[6] and have a higher open-circuit voltage [7]. However, a recent study indicates that the better temperature coefficient (TC) does not seem to come from the compensation level [8]. Instead, the ingot height seems to play a very important role for this parameter. The compensated material used in this study was Elkem Solar Silicon® (ESS®). It contains both phosphorus and boron, because of the difficulty of removing these elements fully in metallurgical processes.

Understanding the variation of the efficiency of solar cells with temperature is an important issue due to the elevated working temperature of the cells in modules under normal operating conditions. No comprehensive and general model has been developed that describes the TCs according to cell characteristics such as bulk resistivity, dopants concentrations, compensation level or recombination centers. Since variations in the TCs are observed between different cells [6], it seems logical that a modification or an improvement of the temperature coefficients is possible if the right measures are taken. To do so, a deeper understanding of how TCs depend on material properties needs to be developed.

In the present study, the TCs of the short-circuit current (J_{SC}), the open-circuit voltage (V_{OC}), the fill factor (FF) and the efficiency (η) of solar cells were measured on cells made of material taken from various heights in three different ingots made from three different blends of compensated silicon and conventional uncompensated silicon made by the Siemens process. The measurements of the cell characteristics were performed before and after LID.

II. Experimental Setup

The ingots consist of: 25%, 73% and 100 % compensated silicon. The mean resistivities of the ingots are 1.22 Ω.cm, 1.27 Ω.cm and 0.45 Ω.cm, respectively. The 73% blended ingot contains gallium. These values are summarized in Table I. Bricks of center positions of industrial G5 sized ingots were wafered. Wafers were picked from eight different locations distributed along the ingot height from the ingots with 25 % and 73 % compensated material. The low resistivity (LR) ingot with 100 % compensated material was made in a G5 sized research furnace. Six wafers were selected at varying heights from the LR ingot. The wafers from all three ingots were processed into cells by the same producer, which is a research institute, but the LR ingot was processed at a different period. This enables position tracking, but gives lower efficiencies than industrial processing of the same wafers. The cells are multicrystalline silicon solar cells (15.6x15.6cm2) with a conventional aluminium back surface field (Al-BSF).

The IV-characteristics were measured under a standard AM1.5G spectrum with a NeonSee™ AAA sun simulator at STC. The TCs were obtained by measuring the IV characteristics of a cell from 25°C to 70°C with two degrees steps followed by a linear fitting of each parameter to get the coefficients. As shown by Martin Green [9], the four IV parameters vary linearly with temperature over a limited temperature range. The TCs as well as the IV-curves were first measured on as-processed cells, and then after a 48h light-soaking under halogen lamps.

TABLE I. Ingot Description

Name	Blend-in ratio (% ESS®)	Mean resistivity (Ω.cm)	Dopants
BIR1	25	1.22	B-P
BIR4	73	1.27	B/Ga-P
LR	100	0.45	B-P

978-1-4799-7944-8/15/$31.00 ©2015 IEEE

The interstitial oxygen concentration of wafers taken along the three ingot heights was measured by Fourier transform infrared spectroscopy (FTIR).

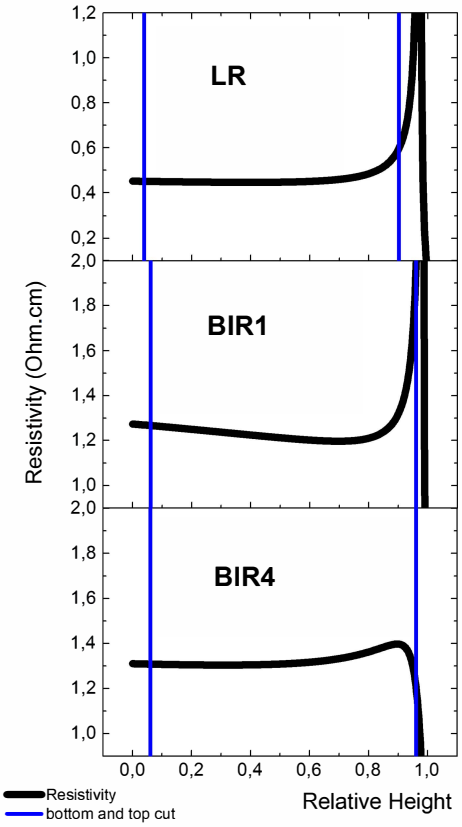

Fig. 1. Resistivity profiles of the ingots LR, BIR1 and BIR4. The blue lines represent the bottom and top cut positions, which are the same for the BIR1 and BIR4 ingots.

III. Results

The LR and BIR1 ingots have resistivity profiles, which are typical of compensated silicon, and have a p/n changeover at about 95% height of the ingot. The changeover corresponds to the resistivity peaks visible in Fig. 1. The BIR4 ingot contains gallium and has a more stable resistivity profile; almost flat on the total useable block length and without the p/n changeover. The blue bars represent the bottom and top cut positions set to fulfill lifetime and/or resistivity specifications. It should be noted that in the following graphs the relative height corresponds to the useable block length, i.e. the part in between the blue bars.

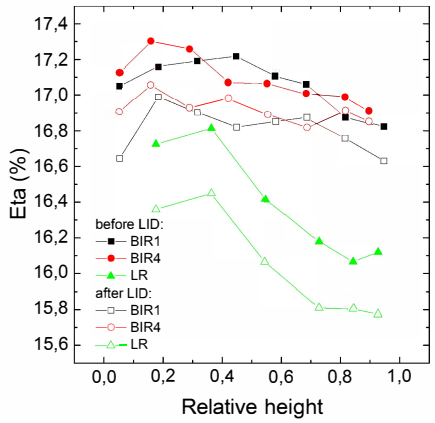

Fig. 2. Efficiency profiles along the three ingots. Filled symbols represent measurements before light-soaking while open symbols represent measurements after light-soaking.

The efficiencies of the cells before and after LID are presented in Fig. 2. The ingots BIR1 and BIR4 give cells with higher efficiencies than the LR research ingot. The reason for this is the quality of the solidification in the research furnace together with the non-optimal bulk resistivity. The LR ingot will contain a higher dislocation density as well as larger impurity concentrations. This is confirmed by the efficiency profile of the LR ingot which shows a larger decrease toward the top than the other two ingots in Fig. 2.

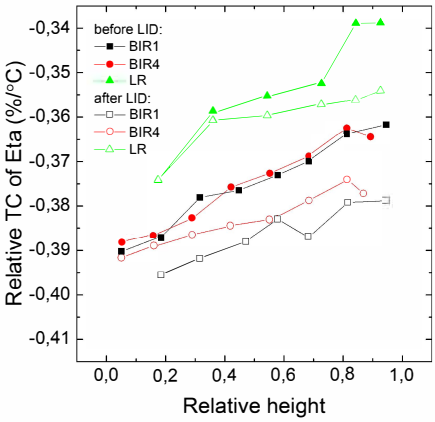

Fig. 3. Profiles of the relative TCs of the efficiency along the three ingots. Filled symbols are cells measured before light-soaking while open symbols are after light-soaking.

978-1-4799-7944-8/15/$31.00 ©2015 IEEE

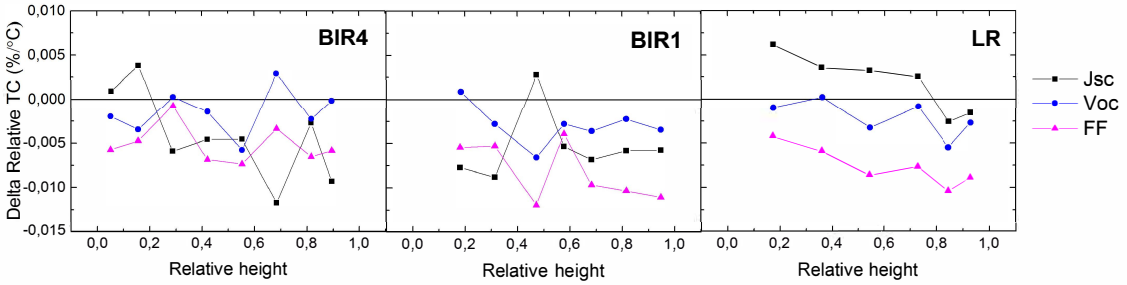

Fig. 4. The difference in relative TC for the Isc, Voc and FF of the three ingots.

The efficiency profiles remain similar after the LID with an approximate average loss in efficiency below 1.5% for the two industrial scale ingots, and slightly larger than 2% for the LR ingot. These average losses are just estimations based on a small number of cells.

As shown in two recent studies [8] [13], the TCs of compensated silicon solar cells depend on the position in the ingot. This is also seen clearly in figure 3. Moreover the difference between top cells and bottom cells is substantial before LID: approximately 10 % relative is gained on the top part of the ingot. The LR ingot gives cells with higher TCs than the two other ingots, but the increase along the ingot is similar in all three ingots.

The 48h light-soaking has reduced the TCs of the efficiency significantly. However, this TC drop is less pronounced for the LR ingot. In the next part we will suggest possible reasons for this decrease.

IV. Discussion

The pertinence of measuring temperature coefficients of solar cells before LID can be questionable because the cells are under illumination for 20min. The performance of the cells decreases because of this unavoidable light-soaking, meaning that the actual value of the temperature coefficients before LID should be slightly higher than measured.

As previously mentioned, the TCs of the J_{SC}, the V_{OC}, the *FF* and the efficiency are all increasing with ingot height. The TCs of the efficiency are shown in Fig. 3 (for the other parameters, before LID, please refer to [9]). The cause of this is still unclear, but Ref. [9] suggests that the increase of the TCs along the ingot height is not caused by the rise of the compensation level. The dislocation density and the impurity concentrations are varying along the ingot, and a lifetime limited by a recombination mechanism with a capture cross-section decreasing with temperature could explain this effect. The present study focuses on the role of the LID on the TCs. Multicrystalline silicon solar cells have a low concentration of oxygen (typically ~10^{17} cm^{-3}) and should not show a LID behavior due to the formation of B-O complexes [10]. Contrary to this, researchers have reported LID on multicrystalline cells as well [11], and particularly on highly compensated silicon solar cells [12], that exhibited a different degradation kinetic to standard cells. The interstitial oxygen concentration along the ingots is shown in Fig. 5. The measured wafers do not correspond to the cells displayed in Fig. 2, 3, 4 and 6. The segregation coefficient of oxygen is close to 1 so the main cause of the oxygen concentration profile is diffusion from the crucible to the silicon melt. As a result, the concentrations at the bottom and on the sides of the silicon slab are the largest. The ingots used in this study come from the center of the ingot and only the large concentration of interstitial oxygen at the bottom is observable in Fig. 5. The largest concentration of oxygen at the bottom of the ingot should induce a larger drop in efficiency in this part, but such a thing was not observed experimentally in Fig. 2.

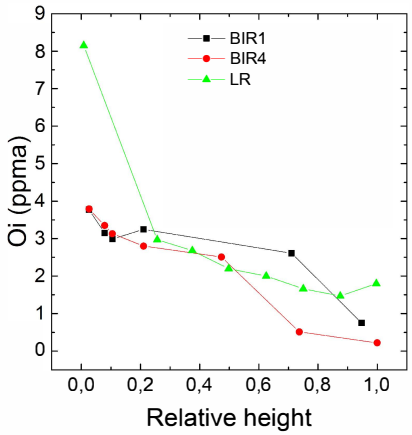

Fig. 5. Interstitial oxygen concentration measured by FTIR on wafers distributed along the ingots.

978-1-4799-7944-8/15/$31.00 ©2015 IEEE

The light-soaking has reduced the TC of the efficiency significantly. This is also seen for the relative TCs of the J_{SC}, the V_{OC} and the *FF* for the ingots BIR1 and BIR4 as shown in Fig. 4. On the LR ingot the *FF* is the main contribution in the reduction of the relative TC of the efficiency. The relative TC of the J_{SC} has even improved for the bottom and the middle part of the ingot. The variability from cell to cell in the LR ingot shows a steady trend whereas in the two other ingots some deviating measurements were observed. This can be due to non-optimized cell processing as the cells from the LR ingot were not fabricated at the same time as the cells from the ingots BIR1 and BIR4.

The V_{OC} has decreased because of the lowering of the lifetime after LID. The TC of the V_{OC} can be expressed as [9]:

$$\frac{1}{V_{OC}}\frac{dV_{OC}}{dT} = \frac{1}{T} - \frac{\frac{E_{g0}}{T} + k\gamma}{qV_{OC}} \quad (1)$$

where E_{g0} is the bandgap extrapolated linearly from the temperature of interest to 0 K, k is the Boltzmann's constant, γ is a constant equal to 3 and q is the elementary charge. The decrease of the V_{OC} itself induces a reduction of the TC of the V_{OC}.

The relative TC of the *FF* can be expressed as [9]:

$$\frac{1}{FF}\frac{dFF}{dT} = \left(1 - 1,02FF_0\right)\left(\frac{1}{V_{OC}}\frac{dV_{OC}}{dT} - \frac{1}{T}\right) \quad (2)$$

with FF_0 the ideal value of the *FF* for a cell free of series and shunt resistances. This expression depends on the V_{OC} in the relative TC of the V_{OC} as well as in the FF_0. The decrease of the V_{OC} due to LID reduces both the relative TC of the V_{OC} and the FF_0.

The mechanism causing the LID after 48h light-soaking has a negative impact on the TCs. The difference between the TCs of the efficiency before and after LID is presented in Fig. 6. The decrease in TC is larger on the top part of the ingot. Interestingly this is where the concentration of oxygen is the smallest. It is therefore unlikely that B-O complexes are responsible for the decrease of the TCs. Surface effects are believed to be part of the LID in cells with a low concentration of oxygen, but with a SiN:H/Si interface [10]. Moreover, the surface passivation plays an important role in the TC as observed in [14] and [15] where a relative TC of the efficiency up to *-0.1%/K* was measured on a silicon heterojunction cell with an a-SiO_x window layer compared to the usual *-0.3%/K* observed on this kind of solar cell. Then the decrease in TC observed after light-soaking could be due to differences in the surface passivation. However the larger drop on top of the ingot is not yet explained.

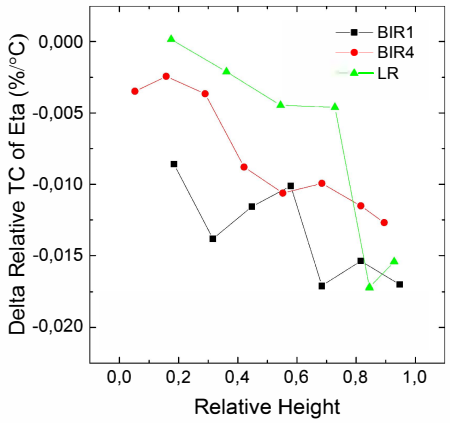

Fig. 6. Difference between the relative TCs of the efficiency before and after LID along the three ingots.

V. Conclusion

We have carried out an analysis of the effect of LID on the TCs in order to better understand the dependency of these parameters on the ingot height. It has been shown that:

1. LID has decreased the performance of the solar cells chosen in this study as predicted by other studies.
2. LID has also significantly decreased the TCs of the efficiency particularly at the top part of the ingot.
3. This reduction comes from the decrease of the TCs of the J_{SC}, the V_{OC} and the *FF* for the ingots with the mean resistivities around 1.25Ω.cm while for the LR ingot it comes mainly from the drop of the TC of the *FF*.

The reduction in the TCs of the V_{OC} and the *FF* is explained by the performance decrease of the cells. However the largest decrease of the TC of the efficiency at the top part of the ingot is not explained by the creation of B-O complexes because of the decreasing oxygen concentration toward the top of the ingot. The LID due to B-O complexes formation should increase along the ingot height, whereas the drop in the TC of the efficiency follows the opposite trend.

We believe that the lowering of the lifetime due to the B-O complexes formation only slightly reduces the TCs. However the largest variation in TCs has to originate from interface interactions and the possible rise of recombination at the surface because of LID.

References

[1] A.K. Søiland, J.O. Odden, B. Sandberg, K. Friestad, J. Håkedal, E. Enebakk, and S. Braathen, "Solar silicon from a metallurgical

978-1-4799-7944-8/15/$31.00 ©2015 IEEE

route by Elkem Solar: A viable alternative to virgin polysilicon", in *CSSC 6*, Aix-les-bains, France, 2012.

[2] R. Gløckner, and M. De Wild-Scholten, "Energy payback time and carbon footprint of Elkem Solar Silicon®", in *27th EUPVSEC*, Frankfurt, Germany, 2012.

[3] M. Tayyib, J. O. Odden, N. Ramchander, M. B. Prakash, T. S. Surendra, R. Muneeshwar,... and T. O. Saetre. "Two years performance comparison of Elkem Solar multicrystalline silicon with polysilicon in a PV grid-connected system." In *40th IEEE Photovoltaic Specialist Conference*, Denver, Colorado, USA, 2014, pp. 3230-3233.

[4] M. Tayyib, J.O. Odden, N. Ramchander, M.B. Prakash, T.S. Surendra, R. Muneeshwar, A.V. Sarma, M. Ramanjaneyulu, and T.O. Sætre, "Performance assessment of a grid-connected mc-Si PV system made up of silicon material from different manufacturing routes", in *39th IEEE Photovoltaic Specialist Conference*, Tampa Bay, Florida, 2013.

[5] F. Tanay, S. Dubois, N. Enjalbert, and J. Veirman. "Low temperature‐coefficient for solar cells processed from solar‐grade silicon purified by metallurgical route." *Progress in Photovoltaics: Research and Applications* 19.8 (2011): 966-972.

[6] S. Ponce-Alcántara, J. P. Connolly, G. Sánchez, J. M. Míguez, V. Hoffmann, and R. Ordás. "A Statistical Analysis of the Temperature Coefficients of Industrial Silicon Solar Cells." *Energy Procedia* 55 (2014), 578-588.

[7] A. Cuevas. "The paradox of compensated silicon." *Optoelectronic and Microelectronic Materials and Devices*, 2008. COMMAD 2008. Conference on. IEEE, 2008.

[8] C. Berthod, R. Strandberg, and J. O. Odden. "Temperature coefficients of compensated silicon solar cells – influence of ingot position and blend-in-ratio" To be published in *5th international conference on Silicon Photovoltaics*, March 23-25, 2015, Konstanz, Germany.

[9] M.A. Green. "General temperature dependence of solar cell performance and implications for device modelling." *Progress in Photovoltaics: Research and Applications* 11.5 (2003): 333-340.

[10] B. Sopori, P. Basnyat, S. Devayajanam, S. Shet, V. Mehta, J. Binns, and J. Appel. "Understanding light-induced degradation of c-Si solar cells." in *39th IEEE Photovoltaic Specialist Conference*, Austin, Texas, 2012.

[11] B. Damini, K. Nakayashiki, D. S. Kim, V. Yelundur, S. Ostapenko, I. Tarasov, and A. Rohatgi, "Light induced degradation in promising multi-crystalline silicon materials for solar cell fabrication," *3rd World Conference on Photovoltaic energy conversion*, pp. 927–930, 2003.

[12] S. Dubois, N. Enjalbert, and J. P. Garandet, "Slow down of the light-induced degradation in compensated solar grade multicrystalline silicon," *Applied Physics Letters* 93, pp. 103510, 2008.

[13] R. Søndenå, C. Berthod, J. O. Odden, A. K. Søiland, M. S. Wiig, and E. S. Marstein. "Temperature dependent quantum efficiency in multicrystalline silicon solar cells" To be published in *5th international conference on Silicon Photovoltaics*, March 23-25, 2015, Konstanz, Germany.

[14] J. P. Seif, A. Descoeudres, M. Filipič, F. Smole, M. Topič, Z. C. Holman, ... & C. Ballif. "Amorphous silicon oxide window layers for high-efficiency silicon heterojunction solar cells." *Journal of Applied Physics*, 2014, 115(2), 024502.

[15] J. P. Seif, G. Krishnamani, B. Demaurex, C. Ballif, & S. D. Wolf. "Amorphous/Crystalline Silicon Interface Passivation: Ambient-Temperature Dependence and Implications for Solar Cell Performance." *IEEE Journal of Photovoltaics*, 2015, 5(3), 718-724.

978-1-4799-7944-8/15/$31.00 ©2015 IEEE

Paper E

Temperature sensitivity of multicrystalline silicon solar cells

Charly Berthod, Rune Strandberg, Jan Ove Odden, and Tor Oskar Saetre

To be submitted:

Berthod, C., Strandberg, R., Odden, J.O. and Saetre, T.O.

TEMPERATURE SENSITIVITY OF MULTICRYSTALLINE SILICON SOLAR CELLS

Charly Berthod[1], Rune Strandberg[1], Jan Ove Odden[2], Tor Oskar Saetre[1].
[1]University of Agder, Department of Engineering Sciences, P.O. Box 509, NO-4898 Grimstad, Norway,
[2]Elkem Solar AS, P.O. Box 8040 Vaagsbygd, NO-4675 Kristiansand S, Norway

ABSTRACT

This paper presents measured temperature coefficients of multicrystalline solar cells. The impact on the temperature coefficients of different bulk resistivities, compensation levels, cell structures and relative heights along a brick were studied. It is shown that increasing the base net doping reduces the temperature sensitivity. The solar cells with the best temperature coefficients are situated at different heights of the ingot depending on the cell structure. This is explained to origin from a combination of the cell parameters variations along the ingot and changes of the recombination mechanisms which affect the temperature coefficients. Light-induced degradation has a negative effect on the cell performances as well as on the temperature coefficients. It is observed that solar cells which are lightly compensated (with a majority carrier concentration in the same order of magnitude as the dopants concentrations) do not show an advantageous temperature coefficient compared to solar cells made of non-compensated silicon.

1. INTRODUCTION

Solar cells are normally characterized under standard test conditions, although solar panels operating in the field exceed very often 25°C. Temperature increases have a negative effect on solar cell performances [1, 2]. At the highest irradiance point during a day, when the panel produces the most, the temperature of the panel is at its maximum. Hence, the loss of energy production due to the high cell temperature is also the highest. It is therefore important to account for the temperature sensitivity of a solar panel in order to predict accurately the actual production yield of an installation.

The temperature sensitivity of solar cells depends on many factors. The most well-known element is that a reduction of the temperature sensitivity can be achieved by increasing the open-circuit voltage thanks to the use of high-performance cell structures [3-6]. The base net doping is also an influencing parameter [7-9], the presence of compensating dopants in the feedstocks [7, 10, 11], and indirect effects such as the wafer position in the ingot [12] and light-induced degradation (LID)[13]. It is therefore important to identify and quantify the elements enabling an improvement of the temperature coefficients.

In the present paper a decorrelation is proposed to separate and identify the effect of each influencing parameter. Firstly, expressions of the temperature coefficients made by previous authors [1, 2, 4] are presented to give an overview of their main dependencies. Then, experimental temperature coefficients are displayed with their dependencies and correlated variables are isolated.

2. THEORY OF THE TEMPERATURE SENSITIVITY

The temperature sensitivity of a solar cell when operating at maximum power point is measured by the temperature coefficient of the efficiency. The efficiency of a PV device often varies linearly with the temperature on the operating temperature range [2]. Thus, the relative temperature coefficient of a

parameter (X), β_η, is the slope of this parameter as a function of the temperature on the considered temperature range divided by the value of the parameter at STC as shown in the next equation:

$$\beta_X = \frac{1}{X(25°\mathrm{C})} \frac{\mathrm{d}X(T)}{\mathrm{d}T}\bigg|_{T=25°\mathrm{C}} . \tag{1}$$

The efficiency can be expressed as the product of the open-circuit voltage, the short-circuit current and the fill factor, divided by the solar power. When deriving and dividing by the efficiency one gets:

$$\beta_\eta = \beta_{V\mathrm{oc}} + \beta_{I\mathrm{sc}} + \beta_{FF} \tag{2}$$

The first term is the relative temperature coefficient of the open-circuit voltage ($\beta_{V\mathrm{oc}}$) which can be expressed as [2]:

$$\beta_{V\mathrm{oc}} = \frac{1}{V_{\mathrm{OC}}} \frac{\mathrm{d}V_{\mathrm{OC}}}{\mathrm{d}T} = \frac{1}{V_{\mathrm{OC}} T_{\mathrm{c}}} \left(\frac{E_{\mathrm{g0}}}{q} - V_{\mathrm{OC}} + \frac{\gamma k T_{\mathrm{c}}}{q} \right) \tag{3}$$

where k, q, T_{c} and E_{g0} are Boltzmann's constant, the electron charge, the cell temperature and the linearly extrapolated bandgap of the relevant recombination process at 0 K, respectively. γ is a parameter depending on the recombination mechanisms and it can be expressed as a function of the External Radiative Efficiency (ERE) at the open-circuit voltage as follows [1]:

$$\gamma = 1 - \frac{\mathrm{d}\ln \mathrm{ERE}_{\mathrm{oc}}}{\mathrm{d}\ln T_{\mathrm{c}}} + \left(2\frac{\mathrm{d}\ln E_{\mathrm{g}}}{\mathrm{d}\ln T_{\mathrm{c}}} - \frac{\mathrm{d}\ln j_{\mathrm{sc}}}{\mathrm{d}\ln T_{\mathrm{c}}} \right). \tag{4}$$

E_{g} is the bandgap of the material and j_{sc} the short-circuit current density. ERE is defined as the fraction of the total dark current recombination that is emitted from the cell. Typical values for γ are in the range of ±3 [14]. The open-circuit voltage decreases with temperature due to the increase of the dark saturation current, so $\beta_{V\mathrm{oc}}$ is negative.

The second term of Eq. 2 is the relative temperature coefficient of the short-circuit current ($\beta_{J\mathrm{sc}}$). The short-circuit current can be written as the product of the ideal short-circuit current ($I_{\mathrm{sc,1sun}}$) and the collection fraction (f_{c}). The latter is the fraction of useful photons (with $E \geq E_{\mathrm{g}}$) collected as carriers. $\beta_{I\mathrm{sc}}$ can be expressed from the previous relation as [2]:

$$\beta_{I\mathrm{sc}} = \frac{1}{I_{\mathrm{SC}}} \frac{\mathrm{d}I_{\mathrm{SC}}}{\mathrm{d}T} = \frac{1}{I_{\mathrm{SC,1sun}}} \frac{\mathrm{d}I_{\mathrm{SC,1sun}}}{\mathrm{d}E_{\mathrm{g}}} \frac{\mathrm{d}E_{\mathrm{g}}}{\mathrm{d}T} + \frac{1}{f_{\mathrm{C}}} \frac{\mathrm{d}f_{\mathrm{C}}}{\mathrm{d}T} . \tag{5}$$

This temperature coefficient depends on the variation of f_{c} with the temperature, and on the increase of current due to the bandgap decreasing with temperature. Therefore this coefficient is positive, but with a smaller amplitude than $\beta_{V\mathrm{oc}}$.

The last term of Eq. (2) is the relative temperature coefficient of the fill factor (β_{FF}). This coefficient can be written as [4]:

$$\beta_{FF} = \frac{1}{FF} \frac{\mathrm{d}FF}{\mathrm{d}T} = \left(1 - 1.02 FF_0\right) \left(\frac{1}{V_{\mathrm{oc}}} \frac{\mathrm{d}V_{\mathrm{oc}}}{\mathrm{d}T} - \frac{1}{T} \right) - \frac{R_{\mathrm{s}}}{\left(V_{\mathrm{oc}} / J_{\mathrm{sc}} - R_{\mathrm{s}}\right)} \left(\frac{1}{R_{\mathrm{s}}} \frac{\mathrm{d}R_{\mathrm{s}}}{\mathrm{d}T} \right) \tag{6}$$

where R_s is the series resistance, FF_0 the ideal fill factor (free of series and shunt resistances effects), and v_{oc} is the normalized V_{oc}. The latter two parameters can be expressed as

$$FF_0 = \frac{v_{oc} - \ln(v_{oc} + 0.72)}{v_{oc} - 1} \text{ and } v_{oc} = \frac{q}{nkT} V_{oc}. \quad (7)$$

An increase in the open-circuit voltage will increase the FF_0 and reduce the β_{Voc} which both increase β_{FF}. The right-hand term in Eq. (6) is expected to have more variations with cells having large R_s.

3. EXPERIMENTAL PROCEDURE

In this study two types of multicrystalline silicon solar cells were investigated. The first type is Al-BSF cells made of wafers from the center brick of four different ingots with the same targeted resistivity made of a blend-in of compensated silicon (made of Elkem Solar Silicon®) and non-compensated silicon (material from a fluidized bed reactor). The wafers were processed in a laboratory production line. The other type is PERC solar cells. Wafers coming from the center brick of four different ingots were processed as PERC cells in an industrial production line. The ingots were made from the same feedstocks, one consisting entirely of non-compensated silicon and three with 70% compensated silicon. The compensated silicon ingots have different targeted resistivities of 0.5, 0.9 and 1.3 Ω·cm and the non-compensated silicon has a targeted resistivity of 1.3 Ω·cm as well. Each type of cell was then divided in two groups, as-processed cells, and cells which underwent a 48 hours light soaking treatment. All the values for the distinct ingots and the names for the different groups are summarized in Table 1.

Table 1: Ingots description

Cell structure	Groups	Ingot name	Targeted Resistivity (Ω·cm)	Dopants	Blend-in ratio (% ESS®)
Al-BSF	BIR BIR after LID	CL1	1.25	B-P	25
		CL2	1.25	B/Ga-P	40
		CL3	1.25	B/Ga-P	56
		CL4	1.25	B/Ga-P	73
PERC	Res Res after LID	Res.Noncomp	1.3	B	0
		Res1.Comp	0.5	B/Ga-P	70
		Res2.Comp	0.9	B/Ga-P	70
		Res3.Comp	1.3	B/Ga-P	70

The solar cells are standard 15.6x15.6 cm^2 cells which were selected at different locations along the center brick of each ingot. The current-voltage (IV) characteristics were measured under a standard AM1.5G spectrum with a NeonSee™ AAA sun simulator at STC. The temperature coefficients were obtained by measuring several IV characteristics of a cell from 25°C to 70°C, and a linear fitting over the temperature range was performed for each parameter.
The values for the open-circuit voltage, the short-circuit current and the fill factor were normalized with the maximum value of each parameter, and are called “relative” values, so that it is not confused with the normalized open-circuit voltage defined in Eq. (7).

4. RESULTS AND DISCUSSION

4.1. DECORRELATION

The cells parameters (open-circuit voltage, short-circuit current, fill factor and efficiency) vary with the bulk resistivity, the position of the cell along the brick height and the compensation level. And these parameters as well as LID were shown to affect the temperature coefficients [7-13]. However it is not clear if this is only due to the variations of the cell parameters with these parameters. As discussed in Ref. [12], β_{Voc} is improving toward the top of the ingot even though the open-circuit voltage is decreasing. This suggests a direct dependency of β_{Voc} with the relative height in the brick.

To distinguish between indirect effects of the variations of cell parameters and an actual dependency we used polynomial curve fitting. Then all experimental points were translated along the fitted curve to a single abscissa value. This way the observed dependency was suppressed and the new obtained data points could be plotted against another variable.

4.2. INTERDEPENDENCE OF THE CELL PARAMETERS WITH THE WAFER'S BRICK HEIGHT

Experimental temperature coefficients of the open-circuit voltage as a function of the wafer's brick height from which the cell was processed are shown in Fig. 1a. And the dependency of β_{Voc} with the open-circuit voltage is shown in Fig. 1b. Theoretical curves with γ values (from Eq. (4)) from 2 to 4 were calculated and displayed in Fig. 1b. β_{Voc} is depending on the open-circuit voltage as described in Eq. (3). Yet the spread in values is very large. The parameter γ has a significant impact on the variations as shown by the theoretical curves. This spread in β_{Voc} could be a consequence of important variations of γ.

The open-circuit voltage varies along the brick height and consequently a decorrelation is needed to estimate the impact of the relative height alone. The theoretical β_{Voc} with a given γ value (from Eq. (4)) were calculated. We can see in Fig. 1b that different γ give practically parallel curves. As the correction explained previously only considers the curvature, the choice of the value of γ doesn't affect the correction.

The experimental β_{Voc} was corrected according to the theoretical one, implying that each data point was shifted, parallel to the theoretical curves, to a common value of V_{oc}. The V_{oc}-corrected β_{Voc} was plotted as a function of the relative height in Fig. 2a. The experimental values were corrected for the open-circuit voltage, so the only dependence left is on γ. A second y-axis represents the corresponding γ values. The dependence of β_{Voc} on the relative height was corrected with a fitted curve and Fig. 2b was obtained. Note that correcting for the relative height is actually equivalent to correcting for the component of γ caused by the relative height.

The four groups of cells have their β_{Voc} increasing with the brick height, most likely due to the change in recombination mechanisms affecting the parameter γ. From Fig. 2b we can see that the data are less scattered after the decorrelation than the raw data in Fig. 1b. The remaining fluctuations are partly caused by measurements uncertainties. Furthermore a single correction was made on the height dependency of β_{Voc} for the four ingots. But γ might vary differently along the ingot height for each ingot.

The Al-BSF cells have a larger variation of their β_{Voc} owing to the position in the brick than to the changes of the open-circuit voltage. This is shown in the perpendicular trend of these two groups in Fig. 1b compared to the general increasing trend. We can see that this perpendicular trend is greatly reduced in Fig. 2b after the height correction. The cells of the two "Res" groups have the PERC design, and are more sensitive to the wafer quality (i.e carrier lifetime) due to the higher attainable open-circuit voltage offered by this cell type. This gives a larger spread in open-circuit voltage than the Al-BSF cells, as well as higher values (Fig. 1b). This spread of the open-circuit

voltage along the brick height cause a more pronounced variation of the temperature coefficient for the PERC type than what the γ -variation throughout the ingot does.

This is the opposite to the Al-BSF cells. And it explains why the best β_{Voc} of the Al-BSF cells are found at the top (where γ is the highest), while for PERC it is in the middle of the ingot (where the open-circuit voltage is the highest).

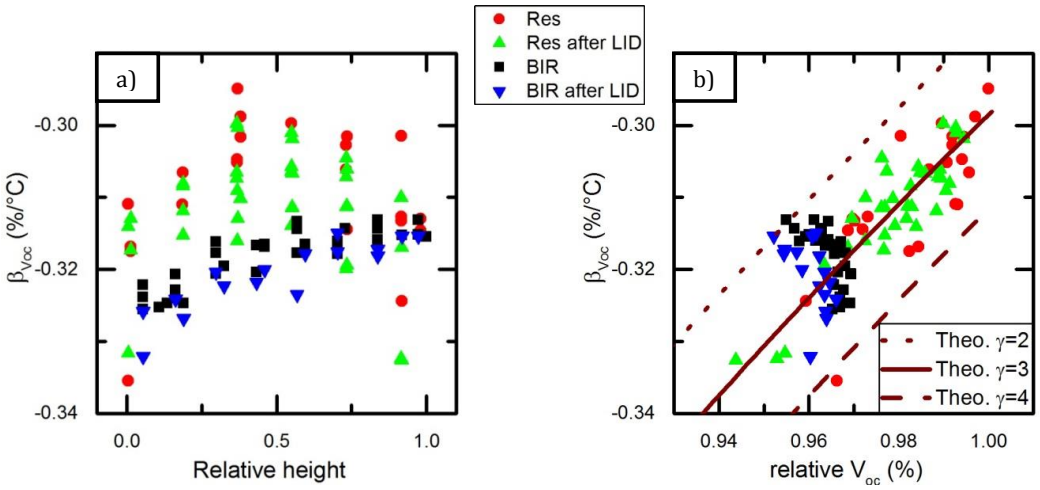

Fig. 1. β_{Voc} as a function of a) the relative height in the brick and b) of the relative open-circuit voltage with theoretical curves for three different γ values, for the four groups of ingots.

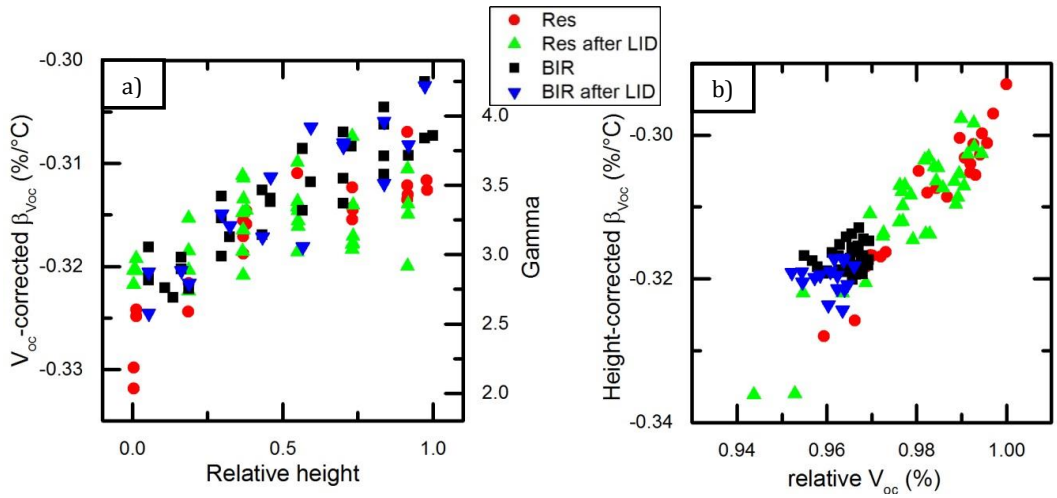

Fig. 2. a) Height-corrected β_{Voc} as a function of the relative height in the brick and of gamma, b) V_{oc}-corrected β_{Voc} as a function of the relative open-circuit voltage, for the four groups of ingots.

Fig. 3a displays experimental temperature coefficients of the short-circuit current as a function of the relative height. Apart from the group of cells "BIR after LID", all three groups have their temperature coefficients increasing with the relative height. Fig. 3b shows β_{Isc} as a function of the short-circuit current. Four different trends corresponding to the four groups of cells can de distinguished. In all cases a low short-circuit current gives an improved β_{Isc}. Yet, the short-circuit current just as the open-circuit voltage is varying along the brick height, therefore a decorrelation was made.

The correction was made on the first type of cells: the two "BIR" groups for a given current value; and to the second type of cells: the two "Res" groups with a second current value. Fig. 3c shows the results after correction. The shifts of the mean values of each group is due to the correction and should not be considered, therefore the y-axis is not shown. The increasing trend observed in Fig. 3a has vanished except for the group "BIR" where it has only been reduced. This means that the trends seen in Fig. 3a and 3b, i.e. the relation between the β_{Isc} and the wafers' position as well as the relation between β_{Isc} and the short-circuit current, are equivalent. We can deduce from Fig. 3b that cells of poor quality showing low short-circuit currents will see their currents increase more with temperature.

Two possible explanations for this phenomenon are proposed. A lower current can be caused by a reduced mobility or lifetime. If it is a reduced mobility (because of more ionized impurities for instance), the mobility dependency with temperature would be weaker [15, 16]. Another explanation is a lifetime limited by a defect with a positive temperature dependence. For example the capture cross sections of molybdenum, manganese and interstitial iron decrease with temperature [17, 18].

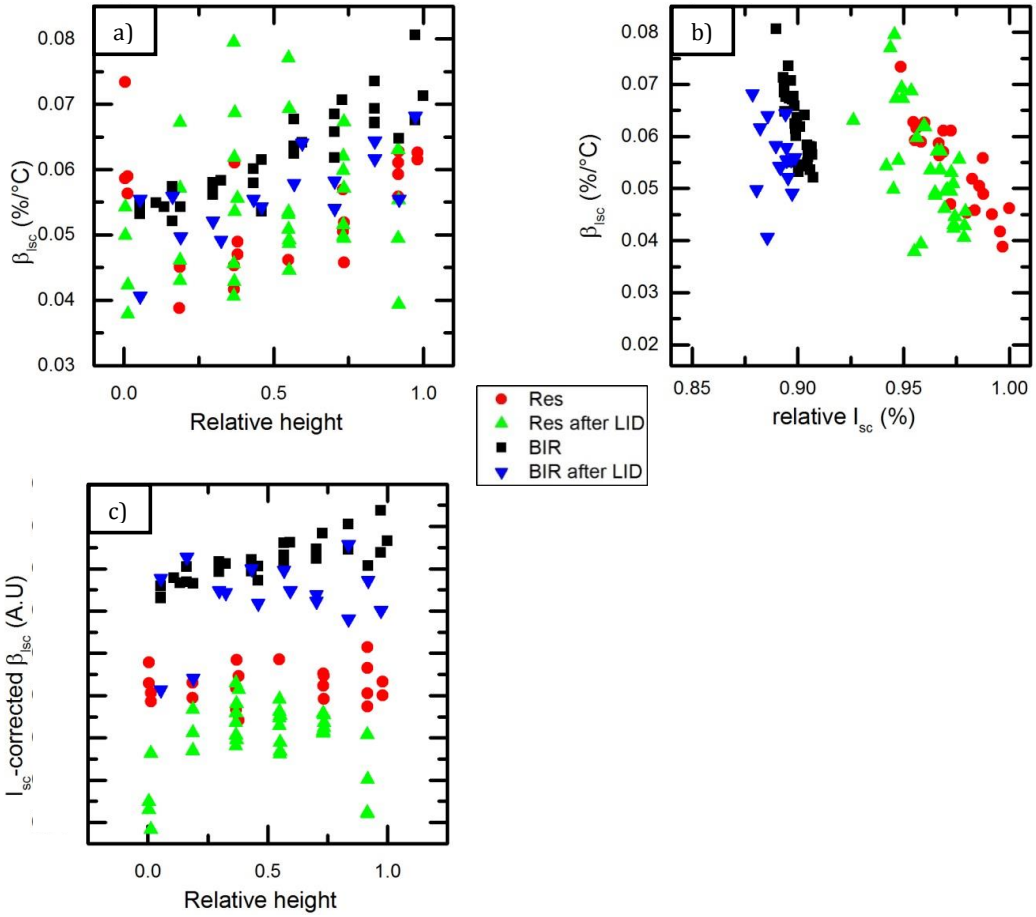

Fig. 3. β_{Isc} as a function of a) the relative height in the brick, b) of the relative short-circuit current for the four groups of ingots. c) I_{sc}-corrected β_{Isc} as a function of the relative height in the brick for the four groups of ingots. The correction was made separately for the two "BIR" groups and the two "Res" groups. The shift of the mean values of each group is due to the correction and should not be considered, only the presence or not of a trend should be examined.

It should be noticed that in Fig. 3b even though four different trends are observed, the slopes are relatively close. This can be explained by different collection fractions giving different short-circuit currents, but a similar dependence on the relative temperature coefficient of the collection fraction with the short-circuit current. Indeed the first summand of Eq. (5) does only depend on the absorbing material's bandgap and on the spectrum of the lamp.

The Al-BSF cells in this study possess a generally lower open-circuit voltage than PERC solar cells. This induces a lower ideal fill factor as described by Eq. (7). Yet PERC cells have higher series resistances due to their localized contacts and this is why their fill factor is lower than the Al-BSF cells. Experimental β_{FF} are plotted against the relative open-circuit voltage in Fig. 4a (where we see the lower open-circuit voltages of the Al-BSF cells), against the relative fill factor in Fig. 4b (where this time the higher fill factors for Al-BSF cells are visible) and against the relative height in Fig. 4c. The cells from the "BIR" groups show very dense clusters in Fig. 4a and 4b because of the smaller variations of the open-circuit voltage with the Al-BSF cell type, and thus of the fill factor. β_{FF} depends on the open-circuit voltage, so the linear trends visible in Fig. 1a for the Al-BSF cells appear as well in Fig. 4c.

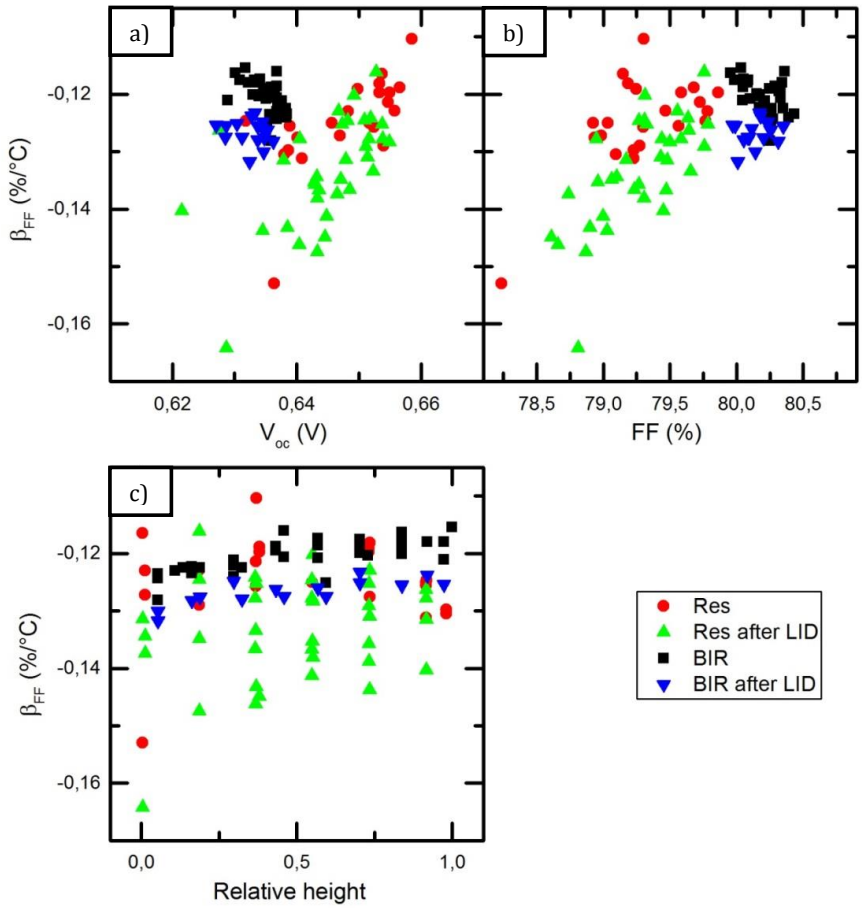

Fig. 4. β_{FF} as a function of a) the relative open-circuit voltage, b) the relative fill factor, and c) the relative height in the brick for the four groups of ingots.

The relative temperature coefficient of the efficiency is the sum of the three previous coefficients so the effects of each coefficient are added. β_η as a function of the relative height is shown in Fig. 5. We can observe that for the two "BIR" groups, there is an increasing trend. Thus the cells with the best

temperature coefficients will be found at the top of the ingot. This is explained by the improvement of β_{Voc} and β_{Isc} with the relative height (Fig. 2a and 3a respectively), combined with a small variation of the cell parameters along the ingot. As regards to the PERC cells, the data are more scattered due to the larger fluctuations of the open-circuit voltage and therefore of the temperature coefficients of β_{Voc} and β_{FF} (Fig. 1b and Fig. 4a respectively). The best temperature coefficients seem to be in the middle of the ingot. However the constant improvement of the solidification process in the industry tends to reduce the variations of the cell parameters along the ingot. This will probably cause PERC cells to have the best temperature coefficients at the top of the ingot like the Al-BSF cells.

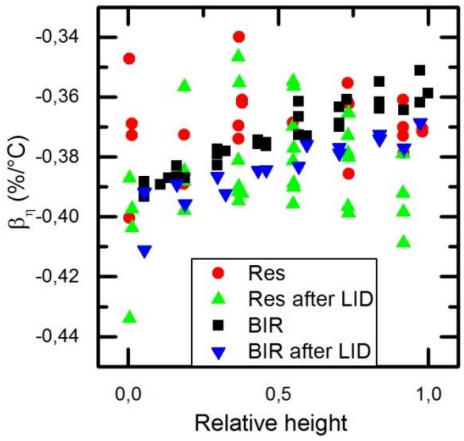

Fig. 5. β_η as a function of the relative height in the brick for the four groups of ingots.

4.3. EFFECTS OF THE RESISTIVITY

Reducing the ingot resistivity has been shown to have a beneficial effect on the temperature coefficients [7-9]. This improvement starts being significant below 1 Ω·cm for β_{Isc}, β_{Voc} and β_η according to Mueller et al. [8]. However the experimental results on β_{FF} do not seem to show an improvement. Ponce et al. [7] measured this beneficial impact of low resistivity on β_{FF} and β_η. However on β_{Isc} and β_{Voc} the effect is not clear.

In the following, the role of reducing bulk resistivity is assessed with a focus on the impact on the cell parameters. The influence of the type of cells, with different series resistance but similar bulk resistivities, is also investigated.

Decreasing the bulk resistivity, i.e. increasing the majority carrier concentration, can improve the open-circuit voltage and thereby the fill factor; however it reduces the minority carrier lifetime and thereby the short-circuit current. This decrease of the short-circuit current is displayed in Fig. 6 for the four ingots of the "Res after LID" group. The ingot Res1.Comp with the lowest resistivity has the lowest current. For the three other ingots no significant difference can be observed. And as discussed earlier, a reduced short-circuit current tends to show an improved β_{Isc}. Therefore the cells from the Res1.Comp ingot, show the best temperature coefficients.

Decreasing the resistivity enhances the open-circuit voltage which improves β_{Voc}, as described in Eqs. (3), (6) and (7). This is displayed in Fig. 6b where the ingots with the lowest resistivities Res1.Comp and Res2.Comp have the highest open-circuit voltages, and the highest β_{Voc}.

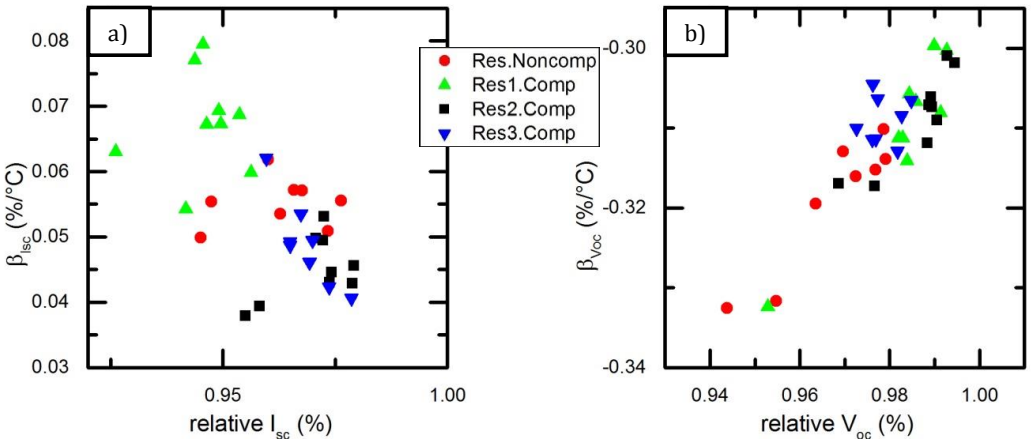

Fig. 6. a) β_{Isc} as a function of the short-circuit current and b) β_{Voc} as a function of the open-circuit voltage for the four ingots in the "Res after LID" group of cells.

The relative temperature coefficient of *FF* depends mainly on the V_{oc} (Fig. 3a) and the series resistance as seen in Eq. (6). To investigate the effects of the series resistance, we defined φ as follows:

$$\varphi = \beta_{FF,\exp} - (1.02FF_0)(\beta_{Voc,\exp} - 1/T_c). \tag{8}$$

The experimental values of β_{FF} and β_{Voc} were employed to calculate it. The series resistance term in Eq. (6) is the main part of φ. But shunt resistance effects not considered in the equation are also present in φ. This parameter was plotted against the resistivity in Fig. 7a. The BIR cells which have a lower series resistance, for a same bulk resistivity, show higher φ. This explains why Al-BSF cells have an increased β_{FF} compared to PERC (see Fig.4c). Decreasing the series resistance by reducing the bulk resistivity has a significant impact on φ. Ingot Res1.comp with a bulk resistivity around 0.5 Ω·cm exhibits the highest φ. The positive effect of a small series resistance on β_{FF} was observed in Ref. [14].

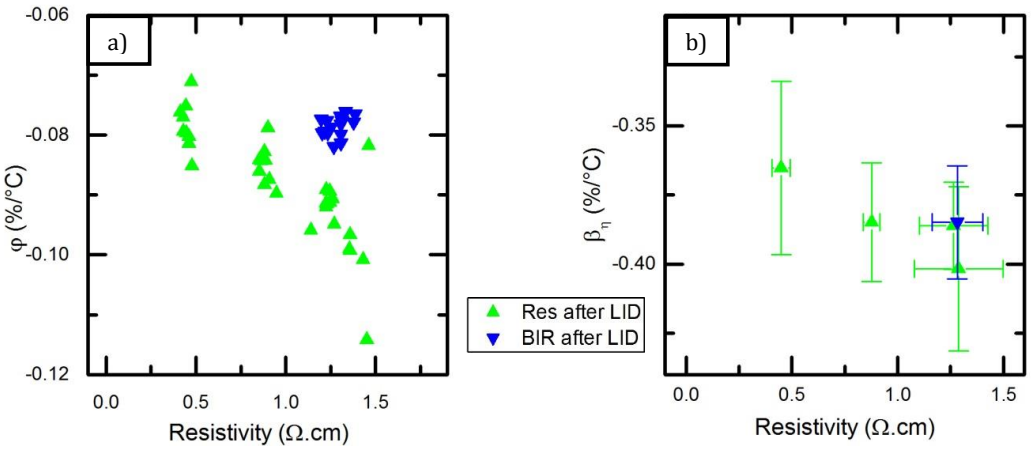

Fig. 7. a) φ (cf. Eq. (8)) as a function of the bulk resistivity and b) β_η as a function of the bulk resistivity for the two groups after LID. The error bars represent two times the standard deviation.

The temperature coefficient of the efficiency is plotted against the bulk resistivity in Fig. 7b. The error bars represent two times the standard deviation, i.e. ± 2SD. The group "BIR after LID" has a better average value of its temperature sensitivity compared to the two ingots Res.Noncomp and Res3.Comp which have similar bulk resistivities. However the overlapping of the error bars show it is not statistically significant. The average values of the cells from the ingots with different bulk resistivities are anticorrelated to the resistivity. This is explained by the improvement of all three temperature coefficients with a reduced bulk resistivity. The error bars are overlapping, which would mean that it is not statistically significant. This is caused by the large variations of the temperature coefficient along the ingot height, as shown in Fig. 8. The solar cells of the ingot Res1.Comp have distinctly improved β_η on the almost entire ingot height. We can conclude therefore that decreasing the resistivity should be of advantage for the temperature coefficients.

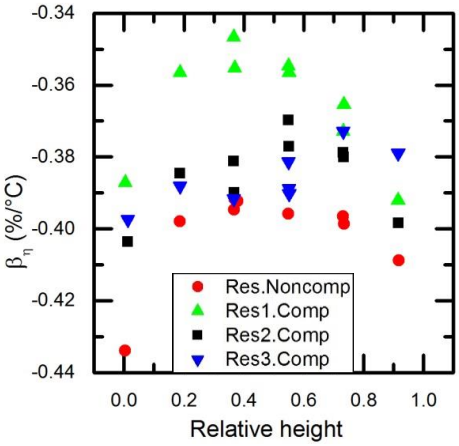

Fig. 8. β_η as a function of the relative height for the "Res after LID" group.

4.4. EFFECTS OF THE COMPENSATION LEVEL

In this part, the group of cells "BIR after LID" will be discussed. The four different ingots with distinct blend-in-ratios give varying compensation levels at the bottom of the ingots, from 1.4 for the lowest blend-in-ratio to 2.2 for the highest. The compensation level is defined as the total amount of dopants divided by the net doping:

$$C_l = \frac{[\mathrm{B}]+[\mathrm{Ga}]+[\mathrm{P}]}{\left([\mathrm{B}^-]+[\mathrm{Ga}^-]\right)-[\mathrm{P}^+]} \tag{9}$$

where [E] is the concentration of the element E, and [$E^{+/-}$] the concentration of the ionized element. The compensation level increases along the ingot height according to the different segregation coefficients of boron, phosphorus and gallium.

The relative temperature coefficient of the efficiency is plotted as a function of the compensation for the four different ingots in Fig. 9a. All four ingots have the same trend, an increasing temperature coefficient with an almost constant compensation level at the bottom of the figure. Then the compensation level starts increasing while the temperature coefficient keeps increasing steadily. This is an artefact of the effect of the relative height of the as cast ingots on the temperature coefficients as explained previously. The improvement of the temperature coefficient is only due to an increase of the relative height, which is correlated to the compensation level (especially at the end). This is further confirmed by the fact that all four ingots present the same trend only shifted along the compensation level axis.

To ensure the absence of correlation we plotted the mean values of the relative temperature coefficient of the efficiency shown in Fig. 9b with error bars which represent two times the standard deviation for the four ingots. And we observe that there is no statistically significant difference between the ingots with different blend-in-ratios.

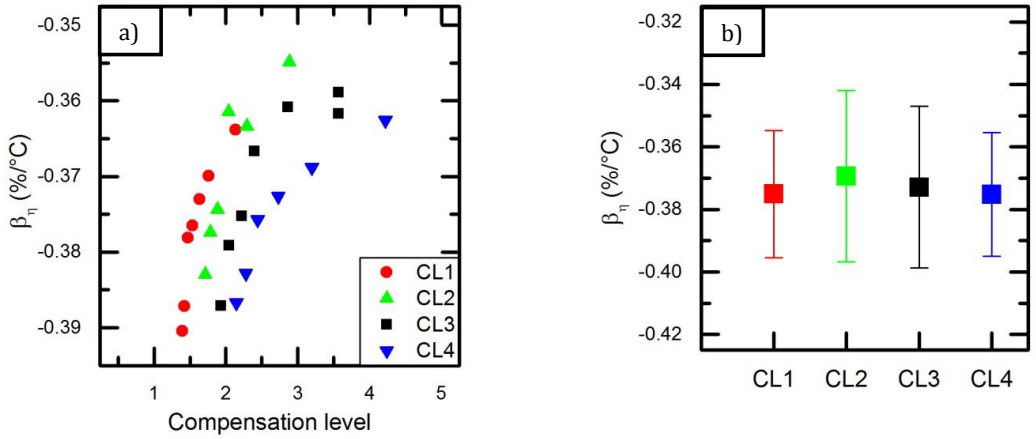

Fig. 9. a) β_η as a function of a) the compensation level and b) of the ingot for the cells of the "BIR" group. The error bars represent two times the standard deviation.

4.5. Effects of light-induced degradation (LID)

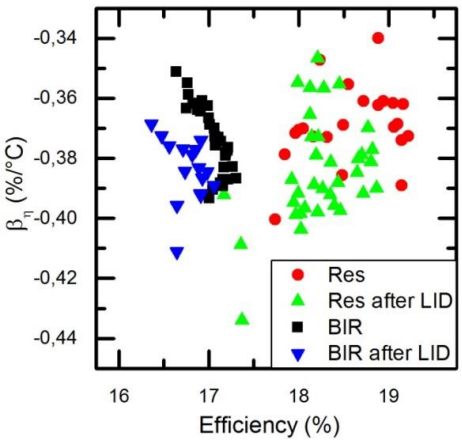

Fig. 10. β_η as a function of the efficiency for the four groups of cells.

The main effect of LID on the temperature coefficients is the decrease in the open-circuit voltage which worsens its temperature coefficient, as seen in Fig. 2b. The data points form a straight line meaning that no effect of LID on γ (in contrary of what was observed with the relative height) is visible. The decrease of the short-circuit current has little impact on its temperature coefficient as it seems it only "shifts" its trend to lower current (Fig. 3b). As regards to β_{FF}, we can observe that all the points are

translated diagonally in direction of the lower-left corner after LID in Fig. 4a. This is caused by the open-circuit voltage-dependence of this coefficient. Finally β_η is plotted as a function of the efficiency in Fig. 10. LID decreases the efficiency. And the temperature coefficient of the efficiency being the sum of the three previous coefficients cumulates the effects. Thus the temperature coefficients of solar cells after LID have declined, as was also observed in [13].

CONCLUSION

The relative temperature coefficients of multicrystalline silicon solar cells with different bulk resistivities, compensation level, cell structures, and positions along the center brick were measured. We have shown that no significant difference was observed on the temperature coefficients of cells with different compensation levels. The temperature sensitivity is reduced for cells with a low bulk resistivity thanks to the improvement of the temperature coefficients of the open-circuit voltage, the fill factor and the short-circuit current. The variations of the principal cell parameters along the brick height influence the temperature coefficients. And the temperature coefficient of the open-circuit voltage is a function of the relative height itself because of the changes in recombination mechanism. This is observed by the rise of the parameter gamma along the ingot height. Therefore a trade-off has to be found between the relative height and the values of cell parameters to get the best temperature coefficient of the efficiency. For the Al-BSF cells the cells with the best temperature sensitivities are at the top of the brick while for the PERC solar cells it is situated near the middle owing to the more important decrease of the open-circuit voltage near the top. We have also seen that LID has a slightly negative impact on the temperature sensitivity due to the deterioration of the cell parameters.

REFERENCES

1. Dupré, O., R. Vaillon, and M.A. Green, *Physics of the temperature coefficients of solar cells.* Solar Energy Materials and Solar Cells, 2015. **140**: p. 92-100.
2. Green, M.A., *General temperature dependence of solar cell performance and implications for device modelling.* Progress in Photovoltaics: Research and Applications, 2003. **11**(5): p. 333-340.
3. Green, M., K. Emery, and A. Blakers, *Silicon solar cells with reduced temperature sensitivity.* Electronics Letters, 1982. **18**(2): p. 97-98.
4. Zhao, J., et al., *Reduced temperature coefficients for recent high-performance silicon solar cells.* Progress in Photovoltaics: Research and Applications, 1994. **2**(3): p. 221-225.
5. Mishima, T., et al., *Development status of high-efficiency HIT solar cells.* Solar Energy Materials and Solar Cells, 2011. **95**(1): p. 18-21.
6. Lee, Y., et al., *High-efficiency Silicon Solar Cells: A Review.* Israel Journal of Chemistry, 2015. **55**(10): p. 1050-1063.
7. Ponce-Alcántara, S., et al., *A Statistical Analysis of the Temperature Coefficients of Industrial Silicon Solar Cells.* Energy Procedia, 2014. **55**: p. 578-588.
8. Mueller, M., et al. *Influence of the Wafer Resistivity on the Temperature Coefficients of industrial Silicon Solar Cells and on the Expected Performance Behaviour*. in *Prceeding of 25th EU PVSEC/WCPEC-5 conference*. 2010.
9. Berthod, C., et al. *Reduced temperature sensitivity of multicrystalline silicon solar cells with low ingot resistivity*. in *Photovoltaic Specialist Conference (PVSC), 2016 IEEE 43rd*. 2016. IEEE.
10. Tanay, F., et al., *Low temperature-coefficient for solar cells processed from solar-grade silicon purified by metallurgical route.* Progress in Photovoltaics: Research and Applications, 2011. **19**(8): p. 966-972.
11. Tayyib, M., J.O. Odden, and T.O. Saetre. *Effect of temperature and sun intensity on multicrystalline silicon solar cells*. in *European Photovoltaic Energy Solar Conference (EU PVSEC)*. 2013.
12. Berthod, C., R. Strandberg, and J.O. Odden, *Temperature coefficients of compensated silicon solar cells–influence of ingot position and blend-in-ratio.* Energy Procedia, 2015. **77**: p. 15-20.

13. Berthod, C., et al. *Reduction of temperature coefficients in multicrystalline silicon solar cells after light-induced degradation*. in *Photovoltaic Specialist Conference (PVSC), 2015 IEEE 42nd*. 2015. IEEE.
14. Dupre, O., R. Vaillon, and M.A. Green, *Experimental assessment of temperature coefficient theories for silicon solar cells.* Photovoltaics, IEEE Journal of, 2016. **6**(1): p. 56-60.
15. Rougieux, F.E., et al., *Electron and hole mobility reduction and Hall factor in phosphorus-compensated p-type silicon.* Journal of Applied Physics, 2010. **108**(1): p. 013706.
16. Schindler, F., et al., *Towards a unified low-field model for carrier mobilities in crystalline silicon.* Solar Energy Materials and Solar Cells, 2014. **131**: p. 92-99.
17. Paudyal, B.B., et al., *Temperature dependent carrier lifetime studies of Mo in crystalline silicon.* 2010.
18. Paudyal, B., K. McIntosh, and D. Macdonald. *Temperature dependent electron and hole capture cross sections of iron-contaminated borondoped silicon*. in *34th IEEE Photovoltaic Specialist Conference*. 2009.

Paper F

On the variability of the temperature coefficients of mc-Si solar cells with irradiance

Charly Berthod, Rune Strandberg, Georgi Hristov Yordanov, Hans Georg Beyer, and Jan Ove Odden

This paper has been published as:

Berthod, C., Strandberg, R., Yordanov, G.H., Beyer, H.G. and Odden, J.O. *6th International Conference on Silicon Photovoltaics, SiliconPV 2016* Chambery, France.

Available online at www.sciencedirect.com

ScienceDirect

Energy Procedia 00 (2016) 000–000

Energy Procedia

www.elsevier.com/locate/procedia

6th International Conference on Silicon Photovoltaics, SiliconPV 2016

On the variability of the temperature coefficients of mc-Si solar cells with irradiance

Charly Berthod[a]*, Rune Strandberg[a], Georgi H. Yordanov[a], Hans G. Beyer[a], and Jan O. Odden[b]

[a]*The University of Agder, Jon Lilletunsvei 9, 4879 Grimstad, Norway*
[b]*Elkem Solar AS, P.O. Box 8040 Vaagsbygd, NO-4675 Kristiansand S, Norway*

Abstract

The temperature sensitivity of silicon solar cells is in general assumed to be constant with irradiance in PV forecasting models, although it has been demonstrated experimentally that this is not true. In this study a theoretical model is established that describes the variation of the temperature coefficients of a silicon solar cell as a function of the irradiance. It is shown that the temperature sensitivity of the solar cell efficiency is decreasing with the irradiance and that the main reason for this behavior comes from the increase of the open-circuit voltage with light intensity. Moreover, a dependency of the cell´s ideality factor on the irradiance has to be assumed to receive good modelling results that can be confirmed experimentally.

Peer review by the scientific conference committee of SiliconPV 2016 under responsibility of PSE AG.

Keywords: Temperature coefficients; silicon solar cells; compensated silicon; irradiance; ideality factor.

1. Introduction

Solar cells and PV modules are systematically characterized at standard test conditions (STC) fulfilling the ASTM norms. However, only in rare occasions will the operating conditions correspond to STC. To cope with this fact the parameter “temperature coefficient” has been introduced to describe how the cell and module power output vary with temperature. Knowledge of this temperature coefficient is crucial for the prediction of PV energy production. The operating temperature of a solar panel depends on the environmental conditions (irradiance, ambient temperature, wind speed) and on material properties (absorptance and reflectivity, heat transfer coefficients to air

* Corresponding author. Tel.: +47 908 99 243.
E-mail address: charlyberthod@uia.no

Peer review by the scientific conference committee of SiliconPV 2016 under responsibility of PSE AG.

and support structure, etc.). Various models for forecasting the PV energy production depending on the above mentioned parameters are reviewed in [1].

As given in section 3 below, the temperature coefficient of the efficiency or equivalently of the power output (β_η) can be expressed as the sum of the temperature coefficients of open-circuit voltage (β_{Voc}), short-circuit current (β_{Jsc}) and fill factor (β_{FF}). In a recent paper [2], a theoretical model based on the work of Green [3] and Hirst and Ekins-Daukes [4] establishes the direct link between the temperature dependences and the losses in a solar cell. The temperature coefficient of the open-circuit voltage is strongly related to the open-circuit voltage itself, which is a function of the irradiance. Thus it is pertinent to assume that the temperature sensitivity of a solar cell varies with irradiance as well. This study addresses this question and proposes an expression of the temperature sensitivity of a solar cell as a function of the irradiance. This theoretical model is compared to experimental values for two different feedstocks: compensated silicon solar cells made from ESS® and uncompensated silicon solar cells. The experimental values used in this study as well as the technical procedure to measure them are presented in [5].

The averaged characteristics of the solar cells are summarized in Table 1. Both lifetime and carrier mobilities are generally lower in compensated material [6-11], resulting in a somewhat lower short-circuit current. The open-circuit voltage is slightly higher in this compensated silicon due to a lower ingot resistivity, meaning a higher net doping. This is visible in the series resistance which is lower for compensated silicon.

Table 1. Averaged characteristics of the solar cells

Feedstock	J_{sc} (mA.cm^{-2})	V_{oc} (mV)	*FF* (%)	η (%)	R_s (Ω.cm)
Compensated silicon	34.71	633	77.84	17.10	4.5
Uncompensated silicon	35.17	631	78.43	17.41	5.2

2. Irradiance dependence of the temperature coefficients

2.1. Temperature coefficient of the short-circuit current

The bandgap of silicon is decreasing with temperature causing the short-circuit current (J_{sc}) to increase. J_{sc} can be written as the product of an ideal current $J_{sc,1sun}$ taken at one sun intensity, a collection fraction f_c and the normalized irradiance *X (in suns)* [3]

$$J_{sc} = J_{sc,1sun} f_c X \ . \tag{1}$$

The temperature coefficient of J_{sc} can be expressed as:

$$\beta_{J_{sc}} = \frac{1}{J_{sc}} \frac{dJ_{sc}}{dT} = \frac{1}{J_{sc,1sun}} \frac{dJ_{sc,1sun}}{dE_g} \frac{dE_g}{dT} + \frac{1}{f_c} \frac{df_c}{dT} \ , \tag{2}$$

where E_g is the bandgap of the semiconductor. The first right-hand term is fixed for a certain semiconductor; its value is 167 ppm/°C for silicon [3]. The second right-hand term is the temperature sensitivity of the collection fraction, which depends on the design of the solar cell. Assuming that this parameter is independent of the irradiance gives a value for the temperature sensitivity of the short-circuit current which is independent of the irradiance as well.

Up to an irradiance of about 1 sun, the experimental values do not show a dependency on the irradiance, as shown in Fig. 1. For higher irradiances, a slight decrease in the temperature coefficients is observed, indicating that our assumptions give inaccuracies at higher irradiance. The constant temperature coefficients of the short-circuit current for both feedstocks was thus fitted for irradiances below 1 sun.

The benefit of compensated silicon is clear on this temperature coefficient and was already reported [12-14]. This advantage of compensated silicon could come from lifetime improvement in defect areas [10,15], or from the different mobility dependence with temperature [7,9,11,16].

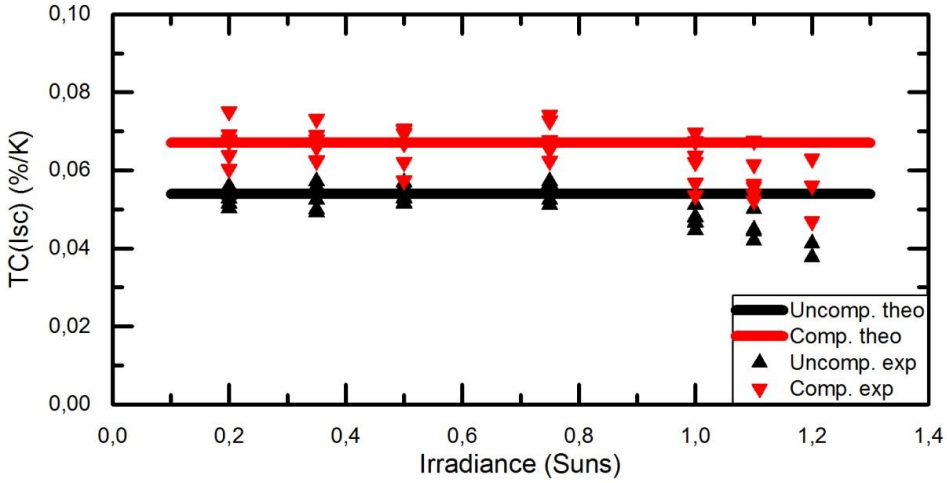

Fig. 1. Temperature sensitivity of the short-circuit current for compensated silicon (black) and uncompensated silicon (red). The triangles represent the experimental values and the lines the theoretical model.

2.2. Temperature coefficient of the open-circuit current

The relative variation of V_{oc} accounts for 80–90% of the overall temperature sensitivity for reasonably good silicon solar cells [2]. The temperature coefficient of the V_{oc} can be expressed as [3]:

$$\beta_{V_{oc}} = \frac{1}{V_{oc}}\frac{dV_{oc}}{dT} = -\frac{1}{V_{oc}T_c}\left[\frac{E_{g0}}{q} - V_{oc} + \gamma\frac{kT_c}{q}\right], \tag{3}$$

where k, q, T_c and E_{g0} are, respectively, the electron charge, Boltzmann's constant, the cell temperature and the linearly extrapolated bandgap of the relevant recombination process at 0 K. γ is a parameter corresponding to the temperature sensitivity of the recombination mechanism determining V_{oc}. An accurate way of calculating this parameter is described in [17]. Justified by the low sensitivity of β_{Voc} to γ (the dominant term on the right hand side of Eq. (3) is E_{g0}/q-V_{oc}), we confined ourselves to the use of an approximate value of $\gamma=3$ here. The only factor with an obvious dependency on the irradiance is V_{oc} itself. This can be described as:

$$V_{oc} = V_{oc,1sun} + \frac{nkT}{q}\ln(X), \tag{4}$$

where n is the ideality factor, X the irradiance in suns and $V_{oc,1sun}$ the V_{oc} at one sun intensity.

The temperature coefficient of V_{oc} is negative and can be increased by raising V_{oc}, which will decrease the temperature sensitivity of the solar cell. This means that decreasing the recombination currents in the bulk and on the surfaces of the cell greatly improves β_{Voc}. As a result, the solar cells with the highest V_{oc} will show good β_{η} [18].

The irradiance dependence of the β_{Voc} which is made by inserting Eq. (4) in (3) will now be compared to the experimental results from [5].

V_{oc} is increasing with irradiance and as a consequence the temperature sensitivity of V_{oc} is reduced. This can be seen in Fig. 2 where experimental values for β_{Voc} of both compensated and uncompensated silicon solar cells are plotted together with results from modelling. The green dashed and dotted lines show the temperature coefficient modelled with fixed values for the ideality factor (used here $n=1$ and $n=1.25$). It is clear that when assuming a

constant ideality factor, the model captures the general trend, but fails to match the experimental results across the entire range of irradiances. Therefore, an ideality factor varying linearly with the irradiance was introduced to the modelling. The relevance of assuming an ideality factor that depends linearly on the irradiance is discussed in subsection 2.4. Using a linear ideality factor for curve fitting improved the results to nicely fit the experimental values on the complete range of irradiances.

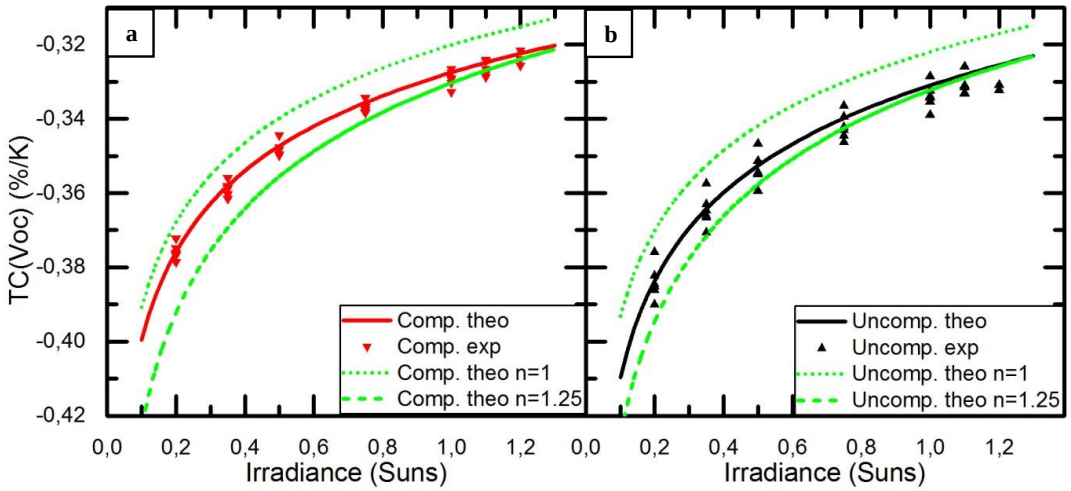

Fig. 2. Temperature sensitivity of the open-circuit voltage for a) compensated silicon and b) uncompensated silicon. The green dashed lines and dots represent the temperature sensitivity with a fixed ideality factor while the red and black lines show a linear-fitted ideality factor. Triangles are experimental values.

The temperature coefficient of compensated silicon is slightly better, which is mainly due to a smaller ideality factor compared to uncompensated silicon. The compensated silicon solar cells have a V_{oc} a few mV higher (2mV in average for these cells) than the uncompensated cells due to an increased doping level. This is explained by the use of lower resistivity ingots for compensated silicon. However this effect is rather small compared to the influence of the lower ideality factor.

2.3. Temperature coefficient of the fill factor

The fill factor is a parameter describing how much power you can extract from a cell given its J_{sc} and V_{oc}. It depends mainly on the V_{oc} and on the ideality factor which are related to the recombination mechanisms. On the other hand, parasitic series and shunt resistances decrease the fill factor and lower the maximum power that can be extracted from a device. For cells with a large shunt resistance, the temperature coefficient of the fill factor can be expressed as [3]:

$$\beta_{FF} = \frac{1}{FF}\frac{dFF}{dT} = \left(1-1.02FF_0\right)\left(\frac{1}{V_{oc}}\frac{dV_{oc}}{dT}-\frac{1}{T}\right)-\frac{R_s}{\left(V_{oc}/J_{sc}-R_s\right)}\left(\frac{1}{R_s}\frac{dR_s}{dT}\right), \tag{5}$$

where R_s is the series resistance, FF_0 the ideal fill factor (free of series and shunt resistances effects), and v_{oc} is the normalized V_{oc}. The latter two parameters can be expressed as

$$FF_0 = \frac{v_{oc}-\ln\left(v_{oc}+0.72\right)}{v_{oc}-1} \tag{6}$$

and

$$v_{oc} = \frac{q}{nkT} V_{oc} \ . \tag{7}$$

For good crystalline solar cells Eq. (5) can be simplified with $R_s=0$. Nevertheless, this assumption can be erroneous for solar cells with complex passivating layers where β_{FF} can be found positive for such device [19]. The charge transfer mechanisms (thermionic emission or tunneling) strongly depend on temperature affecting the series resistance, thus leading to potential improvement of the *FF* at higher temperature.

When inserting the irradiance dependency of V_{oc} from Eq. (4) into (7) and then into (5), and fitting the temperature coefficient of the series resistance we obtain the results in Fig. 3. This gives $\beta_{Rs}=0.15$ *%/K* for compensated silicon and *0.3 %/K* for uncompensated silicon which are typical values for multicrystalline silicon solar cells [20].

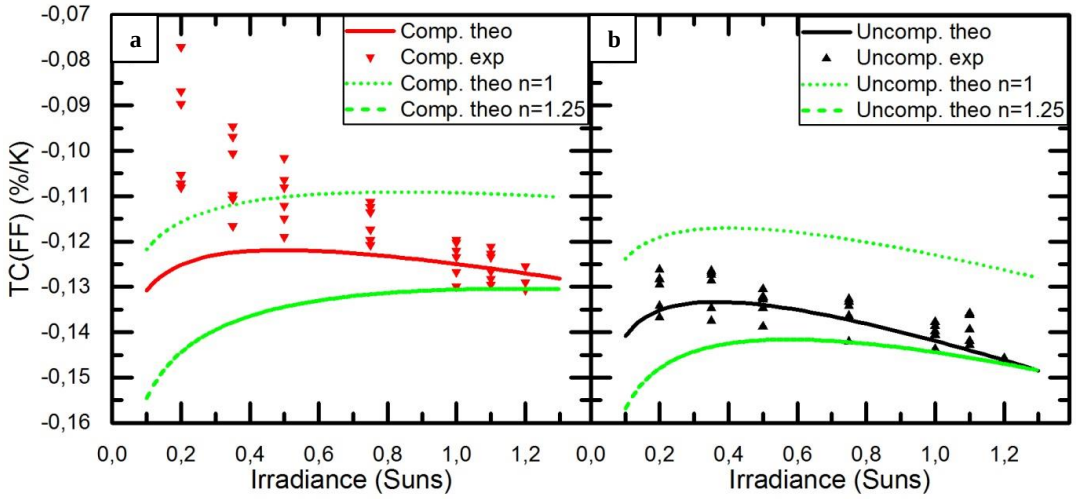

Fig. 3. Temperature sensitivity of the fill factor for a) compensated silicon and b) uncompensated silicon. The green dashed lines and dots represent the temperature sensitivity with a fixed ideality factor while the red and black lines show a linear-fitted ideality factor from Fig. 2. Triangles are experimental values.

A good fit is obtained for uncompensated silicon (Fig. 3b) whereas for compensated silicon (Fig. 3a) the theoretical curve matches experimental data for high irradiance (above 1 sun), while at low irradiance, the actual temperature sensitivity of the fill factor is higher than expected from the model. The ideality factor used to calculate this coefficient is the one fitted to the β_{Voc} of Fig.2. Small variations of the ideality factor (as shown by the green dashed lines and dots in Fig. 3) result in large variations of the temperature coefficient of the fill factor. However, the good agreement of the theoretical model with the measured β_{FF} for uncompensated silicon validates our method of fitting the ideality factor. The temperature coefficient of the *FF* is very sensitive to the ideality factor variations but less to the variations of the series resistance or to its temperature coefficient. The cause is the presence of the ideality factor in the dependence of V_{oc} on the irradiance, and in the definition of the normalized V_{oc}. The rise of β_{FF} at low irradiance for the compensated material could be due to shunt resistance effects that were not considered in Eq. (5).

2.4. Ideality factor varying with irradiance

The ideality factor used to achieve the values in Fig. 2 was modelled with a linear dependency on the irradiance. To verify this assumption we compared our fitted function with experimental data of the ideality factor in Fig. 4.

The local ideality factor along the *I-V* curve of two generic mc-Si PV modules is evaluated by the R_S-corrected *n-I* plot method [21]. First, the series resistance is estimated from classic *n-I* plot. The estimates are then fitted versus the equivalent cell temperature (ECT) determined from the open-circuit voltage. Then the R_s-corrected *n-I* plot is made which is supposed to be flat between open-circuit and the maximum power point. Finally, the module's local ideality factor at open-circuit for multiple *I-V* curves recorded outdoors at different illumination levels is plotted over irradiance. The results for the two multicrystalline modules called Multi1 and Multi2 are given in Fig. 4.

The two panels show a linear trend from 0.2 suns to 1.1 suns, however the slope is weaker compared to the ideality factors used in the fitting. And at low irradiance, below 0.2 suns, the experimental ideality factors increase rapidly. This behaviour is not taken into account in the model for the temperature coefficients. The linear model used in the fitting has, however, a trend and a magnitude comparable to that found experimentally for most of the relevant irradiance interval. Further experiments are needed to confirm if compensated silicon solar cells in general have a lower ideality factor than uncompensated silicon solar cells.

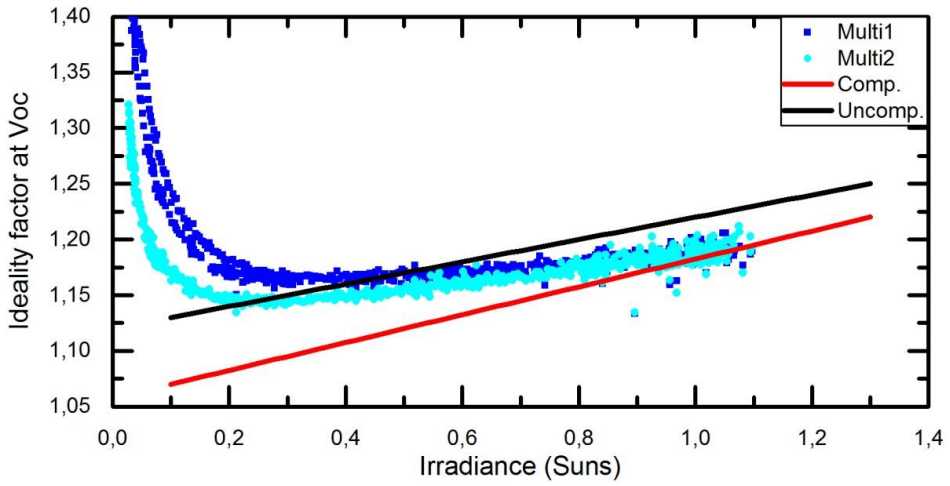

Fig. 4. The ideality factor as a function of irradiance. The red line is the fitted function described in section 2.2 for compensated silicon and the black line is the one for uncompensated silicon. The square blue and round cyan dots represent the ideality factor at V_{oc} of two multicrystalline silicon modules measured during one day.

3. Irradiance dependence of the temperature sensitivity of a solar cell

The temperature sensitivity of the power extracted from a solar cell at the maximum power point can be written as the sum of the temperature coefficients of the V_{oc}, J_{os}, and *FF* as follows:

$$\eta(T) = V_{oc}(T) \times J_{sc}(T) \times FF(T), \tag{8}$$

which, after differentiation gives:

$$\beta_{\eta} = \beta_{Voc} + \beta_{Jsc} + \beta_{FF} \tag{9}$$

When summing up the three theoretical models described by Eq. (2), (3) and (5), Fig. 5 is obtained. We can observe that the theoretical model in general overestimate the temperature sensitivity, although the model gives good predictions for cells made from uncompensated silicon. This overvaluation of the magnitude of β_{η} is also observed when the three experimental temperature coefficients (β_{Voc}, β_{Jsc}, and β_{FF}) from [5] are summed up. Therefore the model presented in this study gives good values for the three temperature coefficients of a solar cell, but when summed up it tends to overestimate the temperature sensitivity of the efficiency.

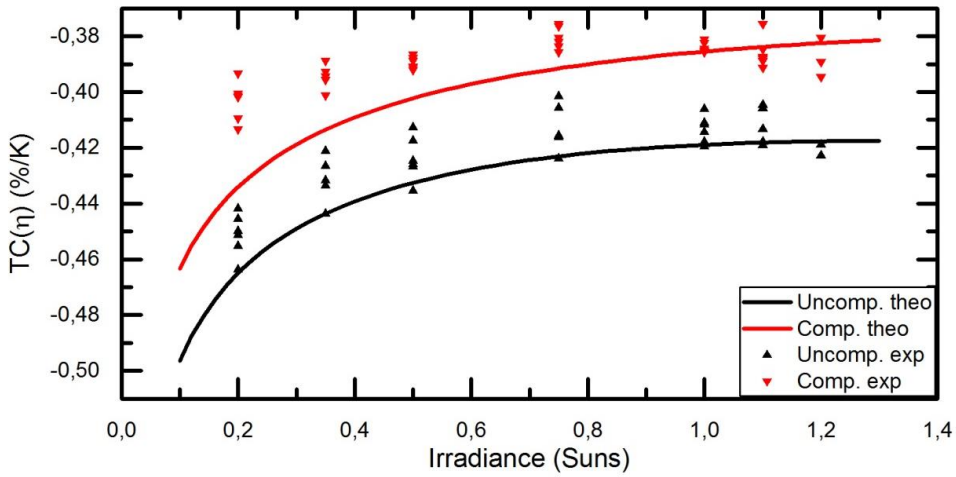

Fig. 5. Temperature sensitivity of the efficiency (or power output) for compensated silicon (black) and uncompensated silicon (red). The triangles represent the experimental values and the lines the theoretical model.

4. Conclusion

In this study, a theoretical model was developed that explains the increase of the temperature sensitivity of solar cells at low irradiance. This is shown to come mainly from a decrease of the open-circuit voltage and thus of its temperature coefficient. The model does not account for the decrease of the temperature coefficient of the short-circuit current at high irradiance, neither does it take into consideration the shunt resistances in the temperature coefficient of the fill factor which could explain the trend at low irradiance of compensated silicon. Finally, taking into account the irradiance dependency of the ideality factor is required to have a good fitting of the temperature coefficient of the open-circuit voltage, and this trend was subsequently confirmed on the module level.

Acknowledgements

The authors would like to thank Dr. Muhammad Tayyib for graciously providing his experimental data.

References

[1] Skoplaki E, Palyvos JA. On the temperature dependence of photovoltaic module electrical performance: A review of efficiency/power correlations. Solar Energy. 2009;83(5):614-24.
[2] Dupré O, Vaillon R, Green MA. Physics of the temperature coefficients of solar cells. Solar Energy Materials and Solar Cells. 2015;140:92-100.
[3] Green MA. General temperature dependence of solar cell performance and implications for device modelling. Progress in Photovoltaics: Research and Applications. 2003;11(5):333-40.
[4] Hirst LC, Ekins-Daukes NJ. Fundamental losses in solar cells. Progress in Photovoltaics: Research and Applications. 2011;19(3):286-93.
[5] Tayyib M, Odden JO, Saetre TO. Irradiance Dependent Temperature Coefficients for MC Solar Cells from Elkem Solar Grade Silicon in Comparison with Reference Polysilicon. Energy Procedia. 2014;55:602-7.
[6] Forster M, Cuevas A, Fourmond E, Rougieux FE, Lemiti M. Impact of incomplete ionization of dopants on the electrical properties of compensated p-type silicon. Journal of Applied Physics. 2012;111(4):043701.
[7] Rougieux FE, Macdonald D, Cuevas A, Ruffell S, Schmidt J, Lim B, et al. Electron and hole mobility reduction and Hall factor in phosphorus-compensated p-type silicon. Journal of Applied Physics. 2010;108(1):013706.
[8] Rougieux F, Samundsett C, Fong KC, Fell A, Zheng P, Macdonald D, et al. High efficiency UMG silicon solar cells: impact of compensation on cell parameters. Progress in Photovoltaics: Research and Applications. 2016;24(5):725-34.
[9] Schindler F, Forster M, Broisch J, Schön J, Giesecke J, Rein S, et al. Towards a unified low-field model for carrier mobilities in crystalline silicon. Solar Energy Materials and Solar Cells. 2014;131:92-9.
[10] Dubois S, Enjalbert N, Garandet JP. Effects of the compensation level on the carrier lifetime of crystalline silicon. Applied Physics Letters. 2008;93(3):032114.

[11] Veirman J, Dubois S, Enjalbert N, Garandet JP, Lemiti M. Electronic properties of highly-doped and compensated solar-grade silicon wafers and solar cells. Journal of Applied Physics. 2011;109(10):103711.
[12] Ponce-Alcántara S, Connolly JP, Sánchez G, Míguez JM, Hoffmann V, Ordás R. A Statistical Analysis of the Temperature Coefficients of Industrial Silicon Solar Cells. Energy Procedia. 2014;55:578-88.
[13] Tanay F, Dubois S, Enjalbert N, Veirman J. Low temperature-coefficient for solar cells processed from solar-grade silicon purified by metallurgical route. Progress in Photovoltaics: Research and Applications. 2011;19(8):966-72.
[14] Tayyib M, Odden JO, Saetre TO, editors. Effect of temperature and sun intensity on multicrystalline silicon solar cells. European Photovoltaic Energy Solar Conference (EU PVSEC); 2013.
[15] Macdonald D, Cuevas A. Recombination in compensated crystalline silicon for solar cells. Journal of Applied Physics. 2011;109(4):043704--8.
[16] Modanese C, Acciarri M, Binetti S, Søiland A-K, Di Sabatino M, Arnberg L. Temperature-dependent Hall-effect measurements of p-type multicrystalline compensated solar grade silicon. Progress in Photovoltaics: Research and Applications. 2013;21(7):1469-77.
[17] Dupre O, Vaillon R, Green MA. Experimental assessment of temperature coefficient theories for silicon solar cells. Photovoltaics, IEEE Journal of. 2016;6(1):56-60.
[18] Lee Y, Park C, Balaji N, Lee YJ, Dao VA. High-efficiency Silicon Solar Cells: A Review. Israel Journal of Chemistry. 2015;55(10):1050-63.
[19] Seif JP, Descoeudres A, Filipič M, Smole F, Topič M, Holman ZC, et al. Amorphous silicon oxide window layers for high-efficiency silicon heterojunction solar cells. Journal of Applied Physics. 2014;115(2):024502.
[20] Yordanov GH. The PVGIS relative efficiency model: equations for k1 through k6. Proc. 29th EU PVSEC, Amsterdam, the Netherlands, 2014, pp. 3297-3301.
[21] Yordanov GH, Saetre TO, Midtgård O-M. Differential analysis of PV module I-V curves. Proc. 28th EU PVSEC, Paris, France, 2013, pp. 3207-3211.